THE DEVELOPMENT OF UNIDIRECTIONAL AND MULTIDIRECTIONAL COMPOSITE MODELS USING A MODIFIED WEIBULL FAILURE DISTRIBUTION; THEORY, ANALYSIS AND APPLICATIONS

by

Juan Alfredo Erni

A Thesis Presented in Partial Fulfillment
Of the Requirements for the Degree
Master of Science

ARIZONA STATE UNIVERSITY

November 2007

THE DEVELOPMENT OF UNIDIRECTIONAL AND MULTIDIRECTIONAL COMPOSITE MODELS USING A MODIFIED WEIBULL FAILURE DISTRIBUTION; THEORY, ANALYSIS AND APPLICATIONS

by

Juan Alfredo Erni

has been approved

Month 2007

Graduate Supervisory Committee:

Barzin Mobasher, Chair
Subramanjam Rajan
Hanqing Jiang

ACCEPTED BY THE GRADUATE COLLEGE

ABSTRACT

The Weibull failure distribution is one of the most used and effective approaches to describe and model the particular behavior of Fiber Reinforced Composites (FRC). By using specific elements of orthotropic elastic materials (lamina or cell elements), where the constitutive behavior was based on the laminate theory for plane stress, several analytical models were developed for unidirectional and multidirectional composite materials. The unidirectional models were based on the Weibull Strength failure distribution, with the addition of a Simplified Load Sharing Rule. The multidirectional models used a modified Weibull failure distribution using the Tsai-Hill interactive failure criterion instead of the typical strength based criterion. The models were validated using several experimental data available in publications or experimental tests conducted in the structural laboratory at ASU. The results were shown to match closely with the experimental data, specially mimicking the characteristic pre-peak and post-peak non-linear behavior that characterizes FRC materials.

FRCs are starting to get widely used around the world as reinforcement for new concrete structural members or as a retrofit for old ones. A model, using elemental compression and tension tests data of both composites and plain concrete, was used to predict the moment-curvature curve of the retrofitted system for the three-point bending test. Finally, a simplified bilinear model developed on data of the moment-curvature curve is used to predict the load-deflection curves. Those curves were validated successfully using experimental data on three-point bending tests on plain concrete retrofitted with layers of Carbon Fiber – Epoxy composites.

To my Family, specially my Wife and Dad who supported and trusted me the most along all the way

ACKNOWLEDGMENTS

I would like to thank first and foremost, Dr. Barzin Mobasher, my advisor, mentor and chair of the committee, a man of almost limitless patience that gave me the opportunity to work on this project.

I would also like to thank Dr. Rajan and Dr. Jiang for making time in their busy schedules to serve in the committee.

Also I appreciate all the help and experience provided by Dr. Dallas Kingsbury for the experimental part. Thanks to him, Peter Goguen, Jeffrey Long and Danny Clevenger for their help, and patience in my learning period, in all the problems and misfortunes that usually happened with the Structural Lab equipment.

I would thank specially to all my peers in the Structural Group (past and present) for their help and support with anything that came in the way.

Last but not least, I would like to thank Mr. Brian Raji from KPFF Consulting Engineering for the support for this research.

TABLE OF CONTENTS

Page

CHAPTER Page

LIST OF TABLES

Table Page

LIST OF FIGURES

Figure Page

Figure Page

Figure Page

Figure Page

Figure Page

Figure Page

1. INTRODUCTION

1.1. Motivation for research and Overview

High strength and stiffness composites are ideal for use in structural elements where these characteristics are required for the most exigent conditions.

As the term indicates, composite material reveals a material that is different from common heterogeneous materials. Currently composite materials refer to materials having strong fibers – continuous or noncontinuous – surrounded by a weaker matrix material. The matrix serves to distribute the fibers and also to transmit the load to the fibers.

Composite materials are not new; they have been used since antiquity. Wood and cob have been everyday composites. Most notoriously Composites have also been used to optimize the performance of some conventional weapons. For example:

- In the Mongolian bows, the compressed parts are made of corn, and the stretched parts (tension) are made of wood and cow tendons glued together.
- Japanese swords have their blades made of steel and soft iron: the steel part is stratified like a sheet of paste, with orientation of defects and impurities in the long direction, then formed into a U shape into which the soft iron is placed. The sword then has good resistance for flexure and impact.

Nowadays, in structural engineering, bonding of steel plates to reinforced concrete (RC) structures has been a popular method for strengthening them. FRP composites have been used in other areas such as the aerospace industry for many years

and their superior properties are well known. The limited use of these materials in civil engineering applications has been due to their high cost. Their prices have, however, been coming down rapidly, enabling their wider applications in civil engineering. For application in the strengthening of structures, where the material cost is but one consideration and may be only a small portion of the total cost including labor cost and loss due to interruptions to services, FRP composites often provide the most cost effective solution overall [Hollaway and Leeming, 1999].

In recent years, there has been extensive research on the use of fiber-reinforced polymer (FRP) plates/laminates to replace steel plates in plate bonding. FRPs have also been used widely for column strengthening by external wrapping. One of the most effective FRPs, for structural reinforcing purposes, is the Carbon Fiber – Epoxy composites.

The origin of the Carbon Fibers (CF) was in the early 1960s at the Royal Aircraft Establishment at Farnborough, Hampshire (UK). There are manufactured in many forms, but the most popular form used in plate bonding is a cloth of woven (knitted) carbon filaments. Each carbon filament thread is a bundle of many thousand carbon filaments. A single such filament is a thin tube with a diameter of 5–8 micrometers and consists almost exclusively of carbon. The density of carbon fiber is 1750 kg/m3. It has high electrical and low thermal conductivity. When heated, a carbon filament becomes thicker and shorter. Carbon fiber thread or yarn is rated by the linear density (mass per unit length, with the unit 1 tex = 1 g/1000 m) or by number of filaments per yarn count, in thousands.

In this research, the CF knitted cloth that is used is shown in Figure 1.1. The main longitudinal direction contains 75% of all the fibers in the cloth, while the perpendicular direction will be taking the remaining 25%. There is no interaction between the perpendicular yarns, in the cloth configuration, because the joint is made by stitching the yarns together. That interaction will occur in Composite form, where the matrix, Epoxy Resin Polymer in our case, will transmit the load to all the yarns imbedded in it.

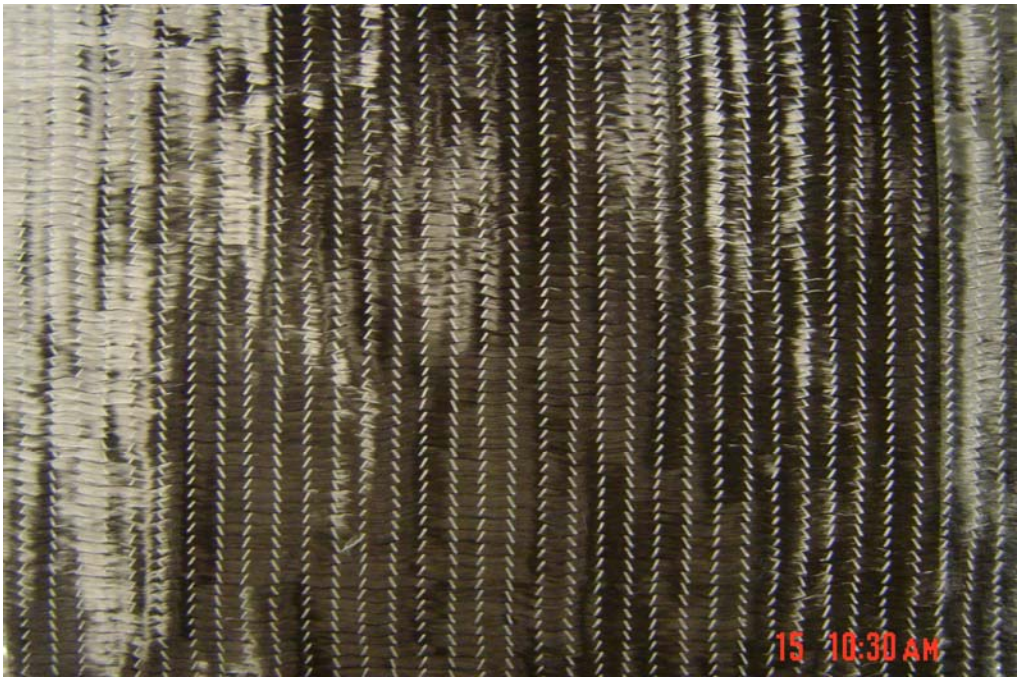

Figure 1.1. Carbon Fiber Knitted Cloth

The Composite material made of CF cloth and Epoxy resin, works well as a structural reinforcement not only because of its high strength and stiffness to weight ratio and corrosion resistance, but also for its long term and fatigue behavior. Rapid growth in recent years in both field application of and research on FRP composites for strengthening RC structures is testimony to the importance and popularity of this new technology.

Regarding the contents of the thesis, Chapter 2 will detail the experimental characterization work done with these CFRP materials. Those experimental tests presented are uniaxial tension tests, +/-45° shear tests, and compression tests for several laminate configurations. With that data we can get elastic properties for those specific laminate configurations such as principal and transversal elastic modulus (E_{11}, E_{22}), major and minor Poisson ratios (v_{12}, v_{21}), shear modulus (G_{12}), tensile strengths (S_{1T}, S_{2T}), shear strength (S_{12}), and compressive strengths (S_{1C}, S_{2C}).

The problem of designing with FRP lies in the lack of experience of most engineers to deal with non isotropic materials, where the engineer's job is more like a material selector than a true material designer. Orthotropic materials and its complex behavior, including its stress analysis, will be detailed later in Chapter 3. While in Chapter 4, the theory explained in Chapter 3 will be used to create the macroscopic stress-strain behavior models of these CFRP, and generally FRP, laminates. The modeling will deal, initially, with in simple and known engineering approaches and criteria, such as the Tsai-Hill and maximum stress criterion; and later it will include additional behaviors to explain the failure mechanisms, such as load sharing rules, Weibull statistical failure distribution, etc.

Chapter 5 will deal with the application of a simplified CFRP laminate model, based on the experimental work of Chapter 2, to model the behavior of a concrete beam retrofitted with this CFRP laminate. Experimental results, with one and two layers of the CFRP fabric, will be used to validate the analysis of the beam behavior.

1.2. Literature Review

1.2.1. Failure Criteria

The results from a coordinated study known as the World-Wide Failure exercise [Hinton, Kaddour, Soden, 2002], where 12 of the leading theories for predicting failure in composite laminates have been tested against experimental evidence, was conducted. The comparison has been effectuated through 14 carefully selected test cases, which include biaxial strength envelopes for a range of unidirectional and multi-directional laminates, and stress–strain curves for a range of multi-directional laminates, loaded under uniaxial or biaxial conditions. The exercise used the predictions and experimental data to identify the strengths and weaknesses of each theory, together with a ranking of the overall effectiveness of each theory, therefore giving the reader a good overview when selecting an appropriate failure theory for use in a given design situation.

From those results involving Tsai contributions to this 'exercise' [Hinton, Kaddour, Soden, 2002] utilizing his well known theory which has been made widely available. It employs the interactive Tsai–Wu failure criterion, which is arguably one of the best known and mathematically satisfying theories available. Tsai has advocated the theory for its simplicity and as a tool that can be applied under a wide range of conditions. It is not intended to capture the detailed physics associated with the various failure mechanisms. Starting with the failure envelopes for unidirectional laminate, in this exercise the Tsai theory has described the available experimental results better than any other theory. However it has been noted that the theory predicts enhancement of strength under compression-compression biaxial loading, which is not tested by the experimental

data. Also the predicted initial failure envelopes for the multidirectional laminates were in poor agreement with the experiments, while the predicted shapes of the final failure envelopes for the multi-directional laminates agreed quite well with the available experimental results. Like many of the theories featured in the 'exercise', the Tsai theory is linear-elastic and it could not predict the large non-linear strains observed in those test cases where high lamina shear was involved. Tsai's theories have been recommended for predicting the response of a lamina, according to Hinton, Kaddour, and Soden, ensuring reasonably conservative predictions of all lamina failure envelopes.

It is difficult to reach definitive conclusions on the applicability of the various theories based in comparison with the limited experimental data available, especially in the cases of FPF and under biaxial compression and compression and shear. Theories based on the maximum stress criterion, a partly interactive approach, or a totally interactive criterion (Tsai-Wu/Tsai-Hill), give reasonable predictions of ultimate failure in fiber dominated laminates if the First Fiber Failure (FFF) is used as a definition of Ultimate Laminate Failure (ULF) [Daniel, 2007].

In order to derive this linear-elastic theories to a non-linear constitutive behavior, the Monte Carlo simulation technique coupled with a stress analysis method was used as one of the most effective tools for understanding the tensile failure process [Zhou, Baseer, Mahfuz and Jeelani, 2006].

1.2.2. Statistical Analysis

Monte Carlo simulation techniques use primarily the Weibull failure distribution function to randomly generate the values of uncertain variables. Since fibers tend to be brittle solids and, due to flaws along their lengths, their strengths are statistical in nature. Fibers are customarily described using a Weibull distribution [Weibull, 1939; Weibull, 1951], where the cumulative probability of fiber failure $P_f(\sigma,L)$ in a length L at an applied tensile stress σ can be expressed using the Weibull distribution:

$$P_f(\sigma, L) = 1 - \exp\left(-\frac{L}{L_0}\left(\frac{\sigma}{\sigma_0}\right)^m\right) \tag{1.2.1}$$

Where σ_0 is the characteristic fiber strength at gauge L_0, and m is the Weibull modulus describing the variation in fiber strengths (high m indicates low variability in strength values).

Scatter in the experimental strength distribution may be attributable, however, to external factors such as overall composite homogeneity or volume fraction variations, and hence comparison of predicted and measured strength distributions must be approached cautiously [Curtin, 2007].

A Micro-Mechanical analysis was utilized to represent the effects of statistical distributions of micro parameters on global failure [Gao, 1993]. The analysis is combined with the Tsai-Hill failure criterion and models of structural reliability to study the reliability optimization and the influence of micro level parameters on the reliability of the composites. It is shown that the influence of those micro parameters, which are

directly related to the manufacturing of composites, is critical in tailoring and optimizing the global reliability of composite materials.

There is a considerably small body of literature that deals with the probability of failure or reliability of lamina under off-axis or general loadings. A proposed method [Miki, Murotsu, Tanaka, Shao, 1990], that deals with this issue, where the emphasis was placed on the fiber orientation angle, along where the maximum reliability is obtained, and it was found that the optimum angle varies with the variation of the applied stress in some cases.

The so called "chain of bundles" model has been a basis of most earlier statistical treatments of failure of unidirectional lamina under tension loads in fiber direction [Zweben, Rosen, 1970], [Harlow, Phoenix, 1981]. The recursion analysis proposed by Harlow and Phoenix gives the probability of the occurrence of a k-plet, the consecutive failure of k or more adjacent fibers in the material. The notion is that if k is chosen sufficiently large, the occurrence of a k-plet is equivalent to total failure. [Phoenix, Smith, 1983].

Various other numerical models of fiber damage accumulation have been developed, such as Global Load Sharing (GLS) [Curtin, 1991] and Local Load Sharing (LLS) [Curtin and Zhou, 1995]. The difference between the two models is in the way broken fibers transfer their load to the other fibers of the composite. Under GLS, broken fibers transfer the entire load to the remaining fibers of the cross section equally, while LLS transfer the bulk of the load to the fibers in a determined neighborhood around the

break. Stress concentrations are largely insensitive to the fiber and matrix constitutive properties [Xia and Curtin, 2000].

The GLS rule over predicts the strength of the composite, therefore an attempt to decrease the tensile strength associated with increasing fiber/matrix interfacial sliding was investigated [Xia and Curtin, 2000], and high Weibull modulus (m) fiber reinforced composites are particularly sensitive to local stress concentrations, while fiber reinforced composites with a low Weibull modulus are not very sensitive to such stress concentrations, therefore it has no significant influence on the strength of the composite. Low Weibull modulus fibers composites are preferably used, from a design perspective, for decreasing the composite sensibility to highly localized stresses.

1.2.3. Modeling of the Constitutive Behavior

The association between a finite-size GLS problem and the LLS problem that forms the basis of some analytical models is valuable and conceptually intriguing, but has not been derived from fundamental considerations for any type of fibers. Thus, the accuracy of the analytical models to composite failure in systems with, for instance, very high Weibull modulus, where localized damage progression may be driven more strongly than envisioned within the analytical model, may be limited. The limited experimental data had precluded an assessment of the accuracy of the composite strength distributions (i.e., the composite Weibull modulus) [Curtin, 2007].

Most of the studies using the Weibull distribution have been developed for ceramic matrices materials. Several models for predicting the uniaxial stress-strain

behavior of a unidirectional ceramic matrix composite [Curtin, Ahn, Takeda, 1998] considered the ceramic reinforcing fibers as brittle materials that can be described statistically by a flaw distribution. These models used, successfully, the two-parameter Weibull form for the number of flaws which can fail in length L at stress σ.

A physically based unit cell damage model, which incorporates two basic failure models, was developed to predict non-linear behavior of cross-ply ceramic matrix laminates due progressive failures [Yen and Jones, 1997].

The performance of those uniaxial fiber-reinforced ceramics and metals containing initial fiber damage or discontinuous reinforcements has been addressed within the context of a theory which has previously been successful in predicting the strength and toughness of undamaged fiber-reinforced materials. That theory is a general constitutive law relating stress and strain in terms of the number of breaks per unit length of fiber [Curtin, Zhou, 1995]. The specification of a damage evolution law, which can include both initial fiber breaks, the usual in situ Weibull flaw population of the fibers, and also residual stress distributions, then completes the model for the tensile constitutive behavior up to failure.

Specific predictions show that initial fiber damage is found to modify the entire stress-strain response of the composite [Curtin, Zhou, 1995], resulting in smaller elastic modulus, lower tensile strengths and smaller strains to failure. However, the strength reduction is shown to be small even at moderate levels of damage while the failure strains are essentially unchanged. The scale at which damage begins to have a substantial influence on strength is when the fiber break spacing is comparable to the relevant slip

length. The analytic results have also been confirmed by detailed numerical studies of composite failure in the presence of damage. A specific application of the analysis to the case of Nicalon-CAS suggests that premature fiber damage is responsible for the detailed stress-strain behavior and UTS observed in this system.

The possibility of decreasing ultimate tensile strength associated with increasing fiber/matrix interfacial sliding was investigated in ceramic-matrix composites [Xia, Curtin, 2000]. An axisymmetric finite-element model was used to calculate axial fiber stresses versus radial position within the slipping region around an impinging matrix crack as a function of applied stress and interfacial sliding stress.

According to Xia and Curtin, constitutive damage models for fiber-reinforced composite materials should take into account the occurrence of the different damage mechanisms, their interaction and their influence on the resulting mechanical properties. Fiber breakage has usually been considered in damage models by means of deterministic failure criteria which thus lead to non-progressive behavior or to a complete material collapse which is not realistic. Xia and Curtis work presents a progressive damage model for fiber-reinforced composites based on the fragmentation analysis of the fibers. The stiffness loss of a unidirectional composite comes from the parameters of the Weibull distribution of the fiber strength and the mechanical properties of the fiber, matrix and the interface. The model has been developed for the initial stages of damage and is formulated in the framework of the mechanics of the continuous media. The constitutive model can be employed to simulate the contribution of fibers in damage models based on the rule of mixtures.

Another model [Turon, Costa, Maimi, Trias, Mayugo, 2005], that does not include local load sharing effects, but it is able to account for the stiffness loss of unidirectional composites, is based on the consideration that the fibers are not a pure elastic constituent until a nominal strength is reached. Therefore, the non-linear behavior of fiber-dominated composites can be reproduced with the proposed model.

The formulation may be refined in several ways. For instance, stiffness loss due to the debonding near the fiber break could improve the accuracy of the model. However, the formulation presented is flexible enough to permit the introduction of other degradation processes such as the static fatigue of glass fibers in moist environments.

Other model that uses a specific interface elements of orthotropic elastic–perfect plastic materials incorporating the interfacial friction, a meso-Monte Carlo 2D finite element model with large-fine mesh, was built to simulate the deformation, damage, and failure process of unidirectional fiber reinforced ceramic matrix composites (FCRMC) under tensile loading [Cheng, Qiao, Xia, 2004]. The numerical simulation by ABAQUS/Standard can provide stress–strain curve and the meso-crack evolution process from deformation, damage to the ultimate failure of FRCMCs accompanied with damage mode of matrix crack saturation. The damage evolution process begins with the failure of low strength fiber or matrix elements, which is called ‘‘crack source’’, and then the ‘‘crack sources’’ extend to become the ‘‘matrix cracks’’ or ‘‘through matrix cracks’’. Because of interface sliding, there forms an exclusion zone in the vicinity of each matrix crack. When all these exclusion zones overlap, matrix crack saturation occurs. Then the fiber elements bear the subsequent loads. Catastrophic composite failure occurs when

there are enough failed fiber elements. Similar to the mechanical behavior of elastic–plastic materials, yielding segment, hardening segment can be found in the macro-stress–strain curve, which is in agreement with experiments qualitatively. The model can give stress–strain curve with small fluctuation error within the scale of model size and meso-crack evolution process of deformation, damage and ultimate failure of FRCMCs and simulate the damage mode of matrix crack saturation.

Another model based on CFRPs [Zhou, Baseer, Mahfuz, Jeelani, 2006], presents an analytical approach which combines the modified shear-lag model and Monte Carlo simulation technique to simulate the tensile failure process of unidirectional T700 carbon reinforced composite. Two kinds of matrix were investigated in the present paper, one is neat epoxy and the other one is SiC nano-particle filled epoxy. In the model, the strength of the fiber elements is randomly allocated by the Monte Carlo method; the elastic properties of the matrix elements and the friction after the interfaces breakage are definitely allocated. Using this model, the deformation, damage and failure process of the composite are simulated on the microscopic level, the tensile stress–strain relationship is well predicted.

1.2.4. Beam Modeling

The use of fiber-reinforced polymer (FRP) composites for the rehabilitation of beams and slabs started about 15 years ago with the pioneering research performed at the Swiss Federal Laboratories for Materials Testing and Research, or EMPA [Meier, 1987].

Most of the work since then has focused on timber and reinforced concrete structures, although some steel structures have been renovated with FRP as well. The high material cost of FRP might be a deterrent to its use, but upon a closer look, FRP can be quite competitive. In addition to their resistance to corrosion, FRP have high ratios of strength and stiffness to density. The light weight of FRP provides considerable cost savings in terms of labor: a worker can handle the FRP material, whereas a crane would be required for its steel equivalent. FRP laminates and fabric come in great lengths, which can be cut to size in the field, as compared with welding of steel plates. FRP laminates or fabric are thin, light and flexible enough to be inserted behind pipes, electrical cables, etc., further facilitating installation. With heat curing, epoxy can reach its design strength in a matter of hours, resulting in rapid bonding of FRP to the structure and consequently, minimum disruption to its use. The tensile strength of FRP can exceed 3000 MPa (compared to 400 MPa for reinforcing steel), and their stiffness ranges from slightly greater than that of steel for high-modulus carbon to about 1/3 that of steel for S-glass. FRP do not exhibit plastic yielding as steel does, however, and behave elastically up to an ultimate strain in the range of 1.5 % to 5 % (compared with a range of 15 % to 20 % for reinforcing steel). This brittle behavior must be accounted for in structural design.

Where FRP composites are used as external reinforcement in the rehabilitation of reinforced concrete (RC) beams and slabs, they increase the strength (ultimate limit state) and the stiffness (serviceability limit state) of the structure. Structural rehabilitation with FRP is thus motivated by requirements for earthquake strengthening, higher service

loads, smaller deflections or simply the need to complement deficient steel reinforcement. Care must be used to ensure that the concrete surface to which the strengthening is applied is sound, and the bonding between FRP and concrete is good.

The increase in strength and stiffness is sometimes realized at the expense of a loss in ductility, or capacity of the structure to deflect inelastically while sustaining a load close to its capacity. A number of issues still impede the routine use of FRP as a structural strengthening material. Chief among them is the absence of a long record of use, causing concern about durability with potential users. Another concern is fire resistance, especially as rehabilitation with FRP expands from highway bridges to buildings. The absence of standards is also an impediment, but this is being remedied through the efforts of various individuals and organizations such as the American Concrete Institute. At the time of this writing, ACI Committee 440 has produced a draft "Guide for the Design and Construction of Externally Bonded FRP Systems for Strengthening Concrete Structures". The Canadian Standards Association (2000), the (European) Federation Internationale du Beton (200l), the (British) Concrete Society (200l), and the Japan Building Disaster Prevention Association (1999) have published similar documents.

Naaman et al. [Naaman, Park, Lopez, Till, 2001, 1999] reported on a series of tests of RC beams strengthened in flexure or shear with carbon FRP and loaded under static or cyclic loads, at room or low temperatures. The test parameters included the amounts of reinforcing steel and FRP, concrete cover thickness and condition (with repair mortar used to simulate damaged concrete), and anchorage configurations. The work

includes a Substantial review of the literature, which is updated here. The authors found that, for a given reinforcement ratio, the ultimate load capacity increased but the ultimate deflection, and therefore ductility, decreased with the strengthening level. The three beams with various anchorage conditions (extended length, perpendicular wrap or normal condition, i.e., with no extra effort to enhance anchorage) had the same ultimate load and deflection. Naaman et al. recommended limiting the increase in strength due to FRP to 20% of the nominal flexural strength of the beam with the maximum steel reinforcement ratio allowed by the ACI 3 18 Code [American Concrete Institute, 1999].

The performance of fiber-reinforced cementitious composites are characterized by a high elastic limit, strain hardening, and toughness associated with multiple cracking mechanism [Mobasher, Shah, 1989; Mobasher, Li, 1996].

Soranakom and Mobasher developed a procedure to obtain closed-form solutions to generate moment-curvature diagrams for FRC [Soranakom and Mobasher, 2007]. The procedure uses two intrinsic material parameters at cracking and four nondimensional parameters yield moment-curvature responses which are a product of a nondimensional function and its geometrical dependant dimensioning scale. The moment-curvature relationship, further simplified to two bilinear models, may be used to represent deflection softening and deflection hardening for low and high post-peak tensile strength.

By applying the moment-area method, the curvature distribution along a beam was integrated up to the midspan of the beam to yield closed-form solutions for the midspan deflections of three- or four-point bending tests.

Use of uniaxial tensile response to generate moment-curvature diagram generally underpredicts the flexural response [Soranakom and Mobasher, 2007]. This discrepancy was explained by the nature of tensile stress distribution in the uniaxial and flexural test. The uniform stress in the uniaxial tension test has a higher probability of localizing at a defect to initiate cracks than the triangular stress in bending. The higher the post-peak tensile strength, the less pronounced of size effect between tension and flexure. It is also observed that the four-point bending test is more comparable to the uniaxial tension test than the three-point bending.

2. EXPERIMENTAL DATA

To determine the composite's stress-strain behavior in the principal material direction, experimental tests at Arizona State University (ASU) Structures laboratory were conducted.

We present a summary of tensile tests conducted in order to document the mechanical properties of carbon fiber-epoxy composites manufactured by KPFF Consulting Engineers during the field installation of the Carbon Fiber-Epoxy retrofit system. Also, laboratory manufactured samples were made using CF fabrics and epoxy provided by KPFF and tested later. The samples were cut from 17" by 13" sheets delivered to the Structural Engineering Laboratory of Arizona State University. Testing was conducted in accordance to the ASTM test guidelines. These test methods determine the in-plane properties of polymer matrix composite materials reinforced by high-modulus fibers. The test methods are applicable to composite materials with continuous fiber or discontinuous fiber-reinforced composites in which the laminate is balanced and symmetric with respect to the test direction. Different configurations were tested, each having 2 layers of carbon fibers cross ply fabrics.

2.1. Laminate Configurations

As defined in Chapter 1, the CF single fabric cloth contains 2 yarn directions. The main longitudinal direction contains 75% of all the fibers in the cloth, while the perpendicular direction takes the remaining 25%. There is no interaction between the perpendicular yarns, in the cloth configuration alone, because the joint is made by

stitching the yarns together. Therefore a 2 layer fabric cloth configuration contains 2 yarn directions in the 0° orientation and 2 in the 90° orientation (respect to the test direction). Because of the difference in the amount of fibers for each direction in the fabric, and for sake of simplicity, the configurations will have a subscript (p for the 75% contain fibers and t for the 25% contain fibers) denoting the type of yarns involved. For example, a $0_p/90_t\text{-}90_t/0_p$ configuration means that the first layer is in the 0° direction and contains 75% of the fibers of the cloth layer; the second layer is at 90° oriented with 25% of the fibers of the cloth layer, and so on. The detailed example is shown on Figure 2.1.1.

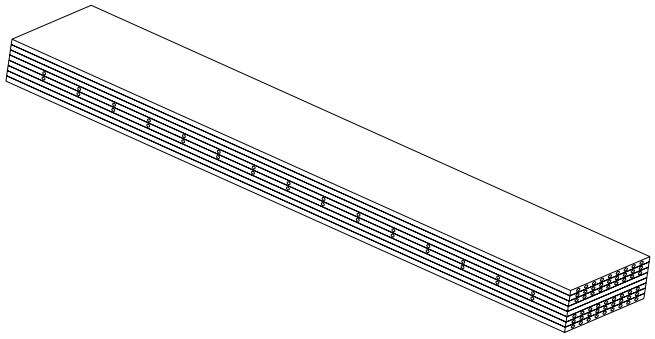

Figure 2.1.1. Schematic of the $0_p/90_t\text{-}90_t/0_p$ laminate configuration

Four different configurations were tested with at least three replicate samples for each series. The code for specimen identification of the samples in this series is as follows: #1#2 - #3

Where #1 is the Test code:

- T : Uniaxial Tension tests
- C : Uniaxial Compression tests

- S : +/- 45 Shear tests

Where #2 is the laminate configuration:

- A : 90_t / 0_p – 90_t / 0_p
- B : 90_t / 0_p – 0_p / 90_t
- C : 0_p / 90_t – 90_t / 0_p
- D : 0_p / 90_t – 90_p / 0_t

#3 is the identification number of the replicate sample.

2.2. Equipment

- A micrometer with a 4 to 5 mm [0.16 to 0.20 in] nominal diameter double ball interface was used to measure the thickness (Accuracy of +/-2.5um [+/-0.0001in]). Another micrometer with flat anvil interface was used to measure the width of the sample (Accuracy of +/-25um [+/-0.001in]).
- In accordance to ASTM E 4, an MTS servohydraulic testing machine with a capacity of 55 kips was used. All the testing procedures were developed using state of the art computer software. The test machine had the following characteristics:
- Testing machine heads: one stationary and one movable head.
- Drive mechanism: capable of imparting a controllable velocity with respect to the stationary head. The equipment was calibrated to 0.1% of the specifications by qualified and certified MTS technicians. All calibration files are on file in the Structural engineering laboratory.

- Load indicator: load range of interest of within +/- 0.1% of the indicated value.
- Grips: hydraulically controlled frictional grips which are rotationally self-aligning to minimize bending stresses in the coupon.
- Strain indicating device: An electronic extensometer calibrated by certified technicians were used. The extensometer gage length had a range of 10 to 50 mm [0.5 to 2.0 in]. Extensometer used satisfied Practice E83, class B-1 requirements for the strain range and should be calibrated in accordance to the practice E83.
- All tests were conducted in nominal room temperature of 73°F. The temperature was maintained within +/-3˚C [+/-5˚F].

2.3. Testing Procedures and Calculations

- Sampling: All the sampling methods, including dimensions and tabs, were in accordance with the proper documentation. The geometry and the sample type were recorded.
- The number of samples should be a minimum of 5. For statistically significant data the procedures outlined in Practice E122.
- Area measurement, A=w x h, where w is the average width, and h is the average thickness (both measured in 3 different places in the gage length).
- Speed of testing: nearly constant strain rate in the gage section, the strain rate was selected so as to produce failure within 1 to 10 min. For the constant head speed tests, the displacement rate was 2mm/min [0.05in/min].

Sample insertion, preparation and test

- The samples were stored in the conditioned environment (room temperature) until test time.
- The specimens were placed in the grips of the testing machine, taking care to align the long axis of the gripped specimen with the test direction. After tightening the grips, the pressure in the pressure controllable grips were recorded.
- Transducer was installed by attaching the strain indicator to the specimen, symmetrically about the mid-span, mid width location.
- Throughout the duration of the test, the load versus strain (or transducer displacement) continuously at a frequency of 2 samples per second. During the test, any transition region or initial ply failures were noted and the load, strain and mode of damage at such points were recorded.

Post Processing

- Data were tabulated and statistical properties of the test results were reported.
- Failure mode and location of failure of the sample was recorded.
- Additional checks for grip/tab failures were conducted and the results were reexamined for the means of load introduction into the material if a significant fraction of failures in a sample population occurs within one specimen width of the tab or grip.

Calculations

Tensile (compressive) stress/tensile (compressive) strength

- The ultimate tensile (compressive) strength was calculated using equation 2.3.2 and reported. The tensile stress at each required data point using equations listed below. Tensile modulus was calculated using the linear portion of the stress strain response and:

$$F_{tu} = \frac{P_{max}}{A} \tag{2.3.1}$$

$$\sigma_i = \frac{P_i}{A} \tag{2.3.2}$$

- The ultimate shear strength was calculated using equation 2.3.3

$$F_{SU} = \frac{P_{\max}}{2A} \tag{2.3.3}$$

$$\sigma_{sI} = \frac{P_I}{2A} \tag{2.3.4}$$

- Both tensile (compressive) modulus and ultimate tensile (compressive) strain were calculated using the response recorded by an extensometer. The tensile (compressive) strain was computed from the indicated displacement at each required data point using the following equation:

$$\varepsilon_i = \frac{\delta_i}{L_g} \tag{2.3.5}$$

- Both shear modulus and ultimate shear strain were calculated using the response recorded by the transducer (Strain gages). The shear strain was computed from

the indicated displacement at each required data point using the following equation:

$$\varepsilon_I = |\varepsilon_x| + |\varepsilon_y| \tag{2.3.6}$$

- The tensile (compressive) chord modulus was calculated from the following equation:

$$E^{chord} = \frac{\Delta\sigma}{\Delta\varepsilon} \tag{2.3.7}$$

- The shear modulus was calculated from the following equation:

$$G = \frac{\Delta\sigma}{\Delta\varepsilon} \tag{2.3.8}$$

2.4. Test Data

2.4.1. Uniaxial Tension Tests

We prepared the samples in dumbbell shape following dimensions used in ASTM D638-03. They start with a basic rectangular shape of 9.5” by 1.5”, and an average of 0.15” thickness. A typical sample is shown in Figure 2.4.1.1.

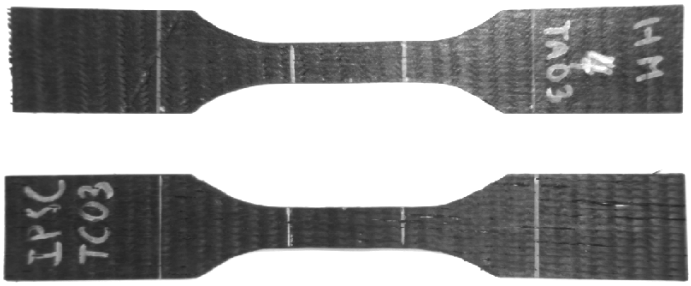

Figure 2.4.1.1. Typical Dumbbell CF samples (2 cloth layers)

The test conditions follow the ASTM D3039-00. We use a stroke control of 0.05 in/min and we measured force and axial displacement using the stroke and an extensometer with 2" gage, as shown in Figure 2.4.1.2. Figures 2.4.1.3, 2.4.1.4, 2.4.1.5 and 2.4.1.6 show the uniaxial stress-strain response for all 4 configurations.

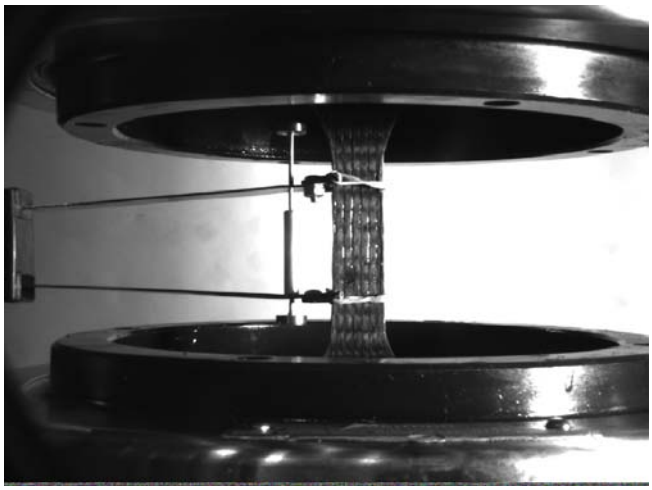

Figure 2.4.1.2. Typical Tension Test Setup

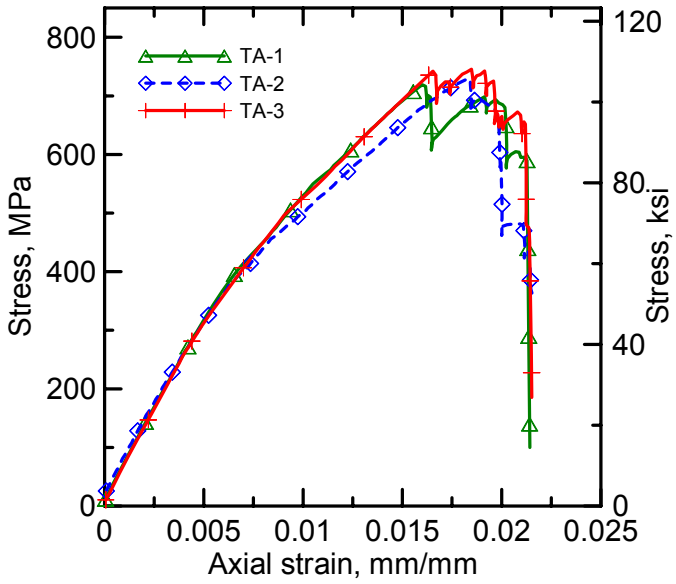

Figure 2.4.1.3. CFC uniaxial stress-strain response for configuration A

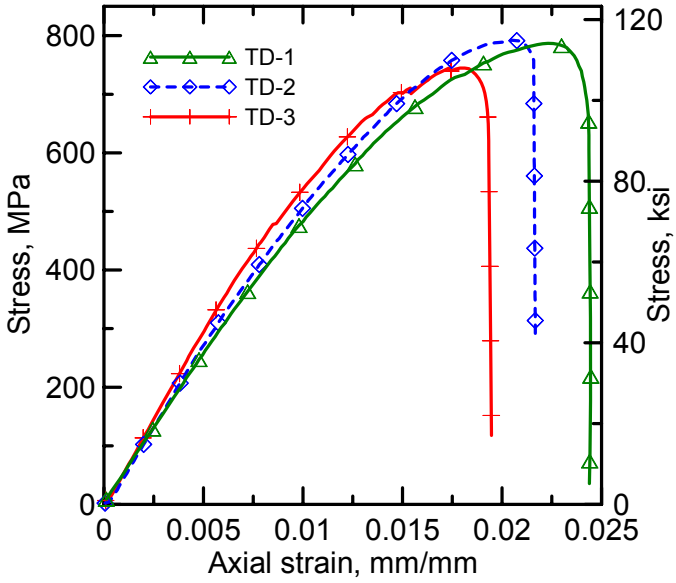

Figure 2.4.1.4. CFC uniaxial stress-strain response for configuration B

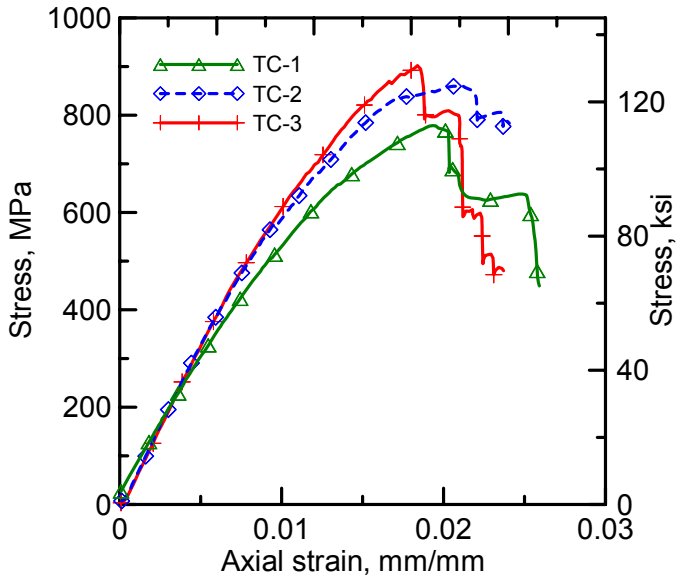

Figure 2.4.1.5. CFC uniaxial stress-strain response for configuration C

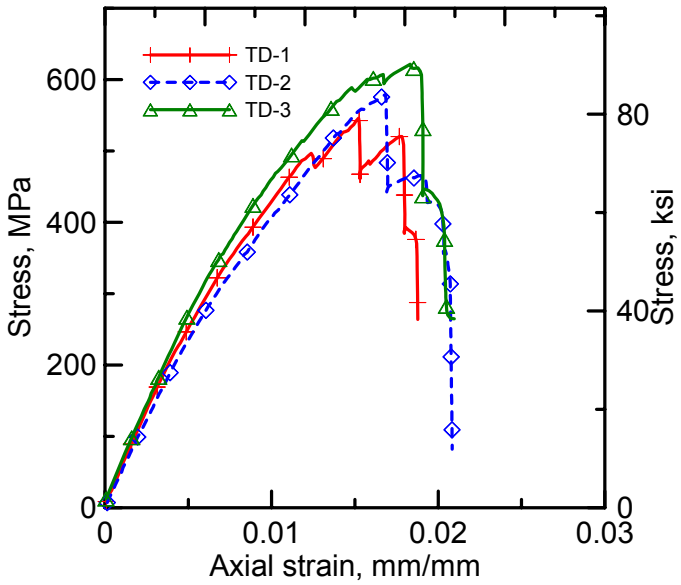

Figure 2.4.1.6. CFC uniaxial stress-strain response for configuration D

From the experimental tension tests it is clear that the CFC has three distinct regions during loading – an initial region of high stiffness where strain increases results in large stress increases (or elastic region), a second region of non-linear behavior where

the stiffness is constantly decreasing until it reaches the peak load/stress; this is due to the nature of the plies that compose the laminate, where their internal flaws will make them fail at different levels, I will speak of these particular behavior in chapter 3. Finally, the third region is governed by sudden drops of the load until the final failure of the CFC.

The failure patterns of the samples under the uniaxial tension test are shown on Figure 2.4.1.7 and 2.4.1.8.

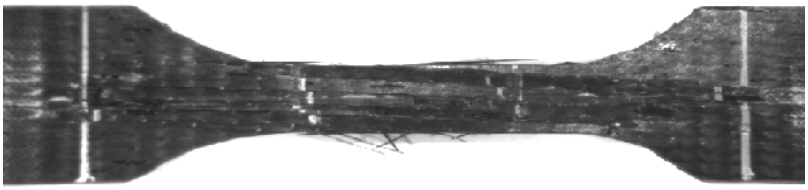

Figure 2.4.1.7. CFC failure pattern under uniaxial tension

Figure 2.4.1.8. CFC failure pattern under uniaxial tension

2.4.2. Uniaxial Compression Tests

We prepared the samples in rectangular shape following partially the ASTM D6641/D6641-01 guidelines. They start with a basic rectangular shape of 2.5” by 0.5”, and an average of 0.15” thickness. A typical sample is shown in Figure 2.4.2.1.

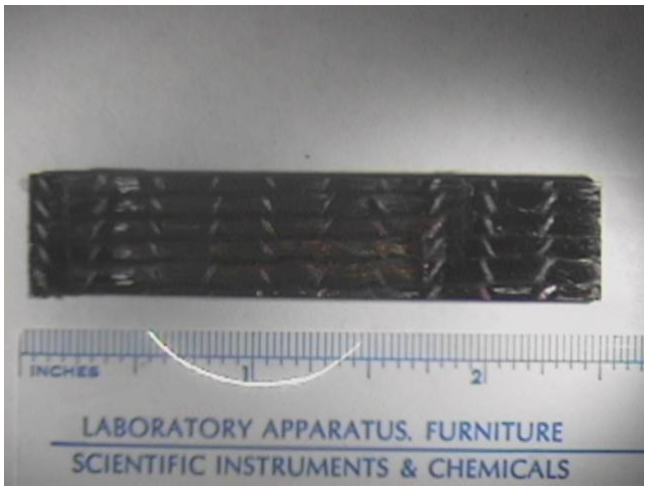

Figure 2.4.2.1. Typical Uniaxial Compression CF sample (2 cloth layers)

We use a stroke control of 0.05 in/min and we measured force and axial displacement using the stroke with a calibrated gage, as shown in Figure 2.4.2.2. Figures 2.4.2.3, 2.4.2.4, 2.4.2.5 and 2.4.2.6 show the uniaxial compression stress-strain response for all 4 configurations.

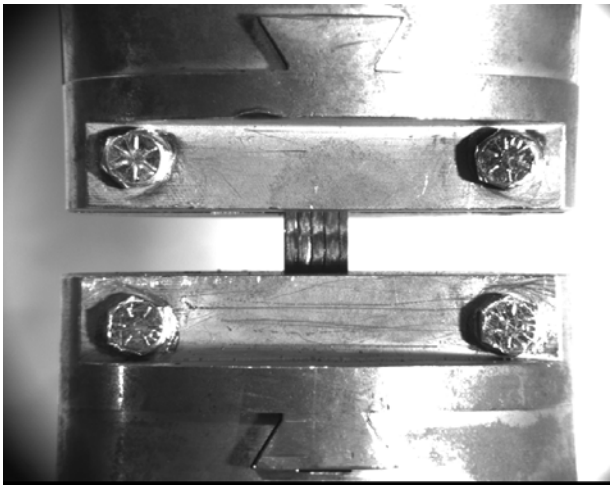

Figure 2.4.2.2. Typical Compression Test Setup

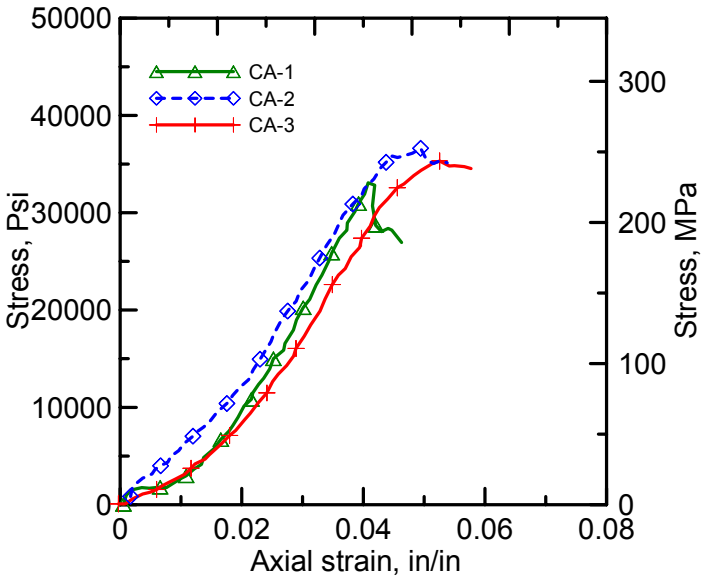

Figure 2.4.2.3. CFC compression stress-strain response for configuration A

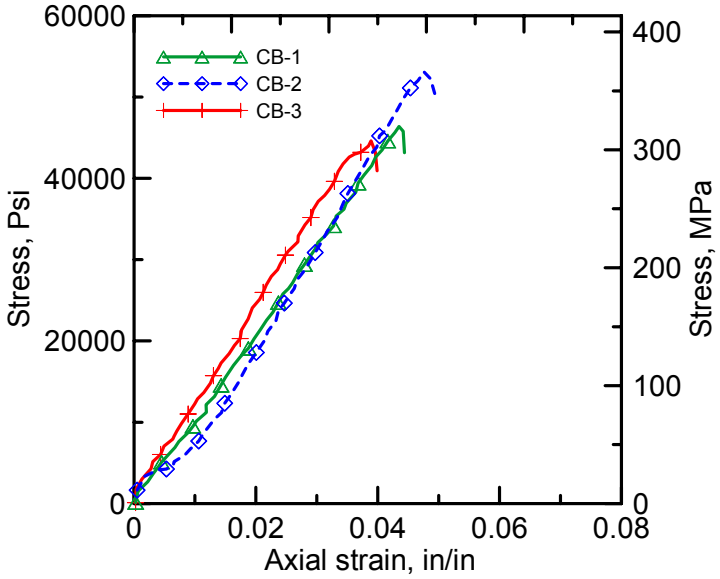

Figure 2.4.2.4. CFC compression stress-strain response for configuration B

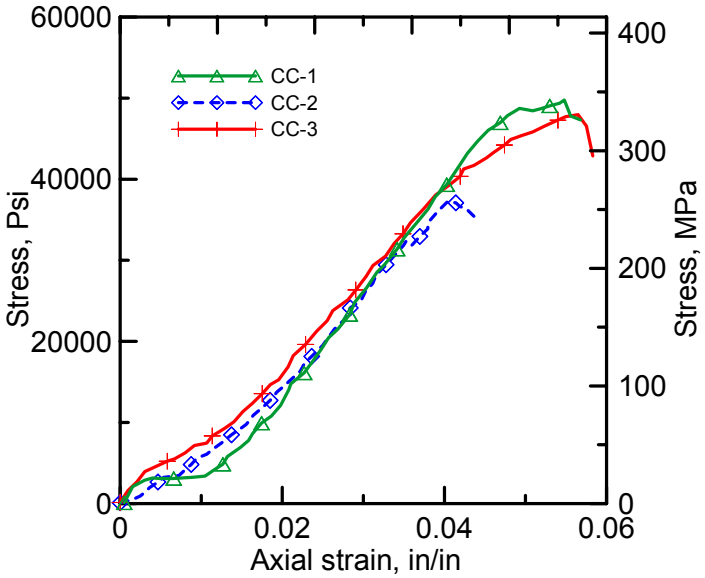

Figure 2.4.2.5. CFC compression stress-strain response for configuration C

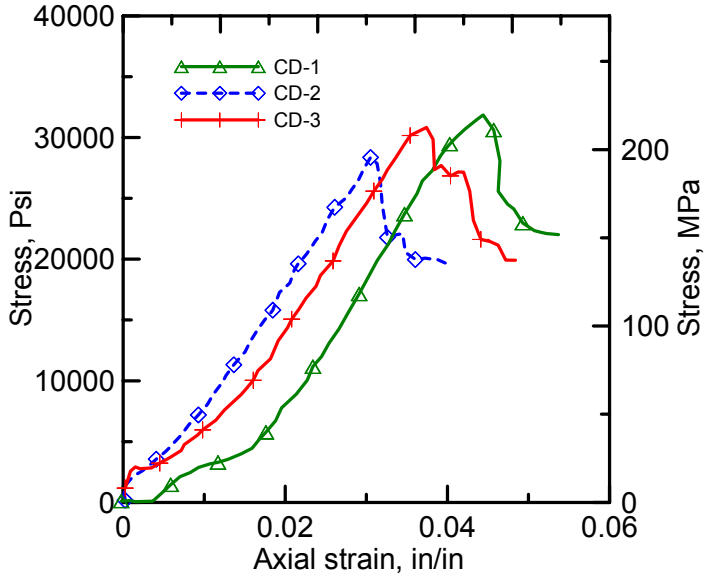

Figure 2.4.2.6. CFC compression stress-strain response for configuration D

From the experimental compression tests it is clear that the CFC has three distinct regions during loading – an initial low stiffness region, not always, where the contact on the sample is not uniform. The second region has high stiffness where strain increases results in large stress increases (or elastic region), the third region is defined by one or many load drops (final failure of the CFC).

The failure patterns of the samples under the uniaxial compression test are shown on Figure 2.4.2.7, 2.4.2.8 and 2.4.2.9. We can see the mechanism of kink zone formation on one, shear failure and the unexpected crushing.

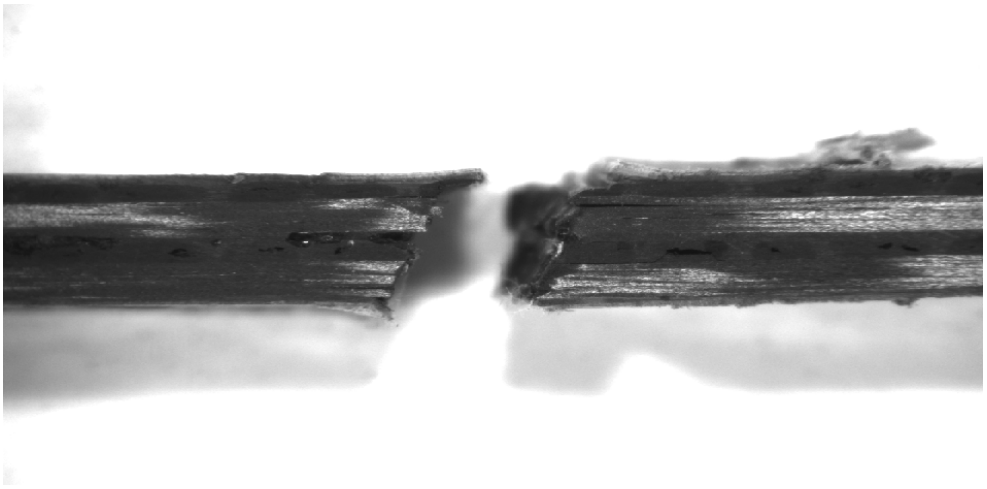

Figure 2.4.2.7. Shear failure under uniaxial compression

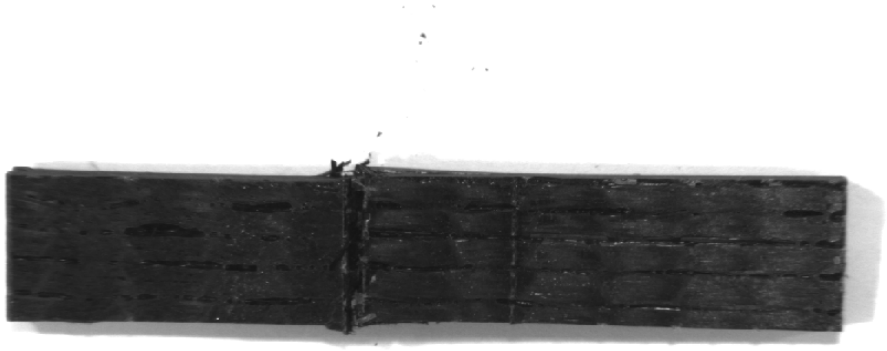

Figure 2.4.2.8. Kink zone formation under uniaxial compression

Figure 2.4.2.9. Crushing of the lower part under uniaxial compression

2.4.3. +/-45 Shear Tests

We prepared the rectangular samples according to the standard ASTM D 3039. They have basically a rectangular shape of 9" by 1.5". The typical test setup is shown in Figure 2.4.3.2. Another condition in the preparation of the sample, specified in the ASTM standard D 3518/D 3518M-01, is the orientation of the sample (as the name of the test states) where the composite material form is limited to a continuous-fiber-reinforced composite +/-45° laminate capable of being tension tested in the laminate x direction.

Figure 2.4.3.1. Typical rectangular CF sample Rosette arrangement (2 cloth layers)

We use a stroke control of 0.05 in/min (following ASTM D 3039) and we measured force, axial displacement using the load cell and stroke (LVDT). Also we measured the strains (X and Y directions) using a 90 degree rosette strain gage arrangement shown if Figure 2.4.3.2 and an alternative solution is also shown in Figure 2.4.3.3. Figures 2.4.2.3, 2.4.2.4, 2.4.2.5 and 2.4.2.6 show the uniaxial compression stress-strain response for all 4 configurations.

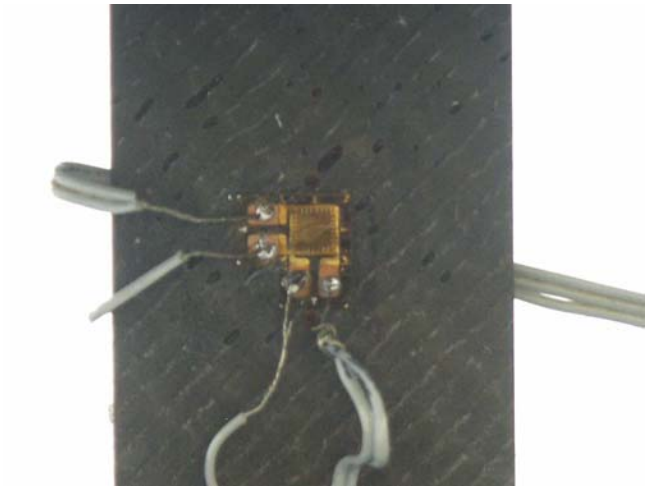

Figure 2.4.3.2. Typical Shear Test Setup

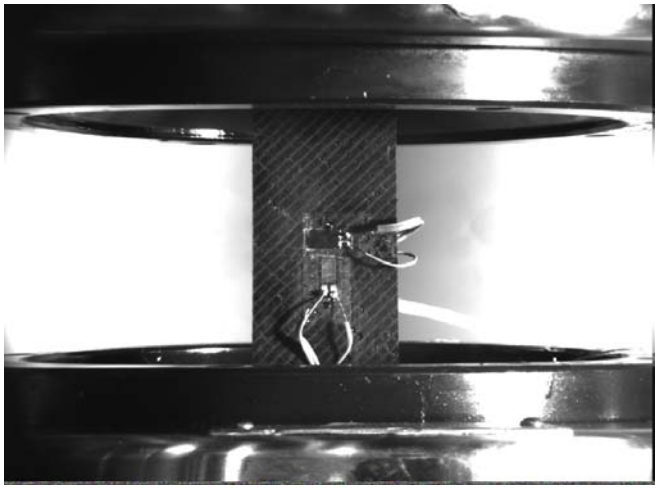

Figure 2.4.3.3. Alternative strain gage rosette

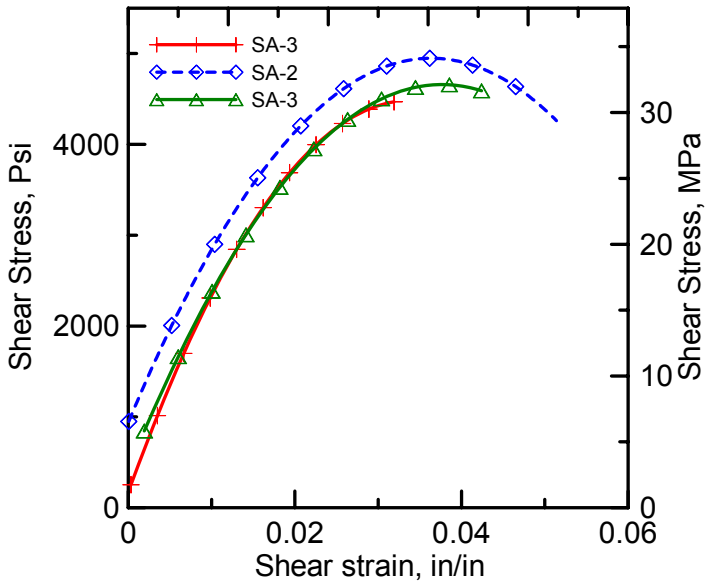

Figure 2.4.3.4. CFC shear stress- shear strain response for configuration A

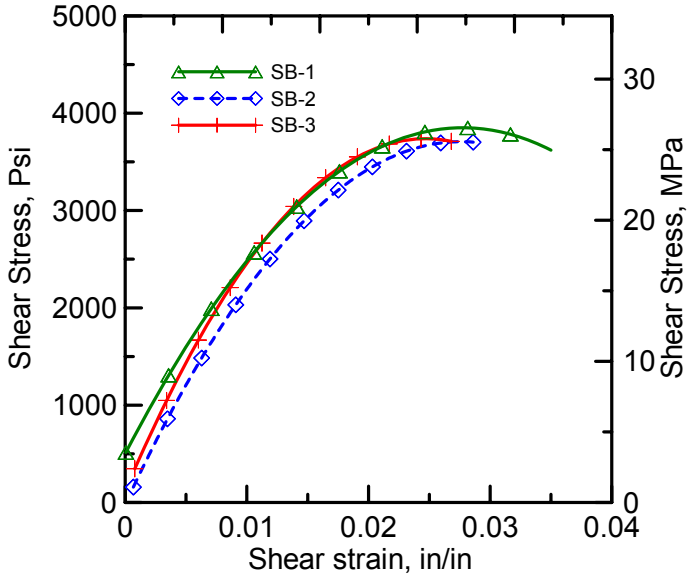

Figure 2.4.3.5. CFC shear stress- shear strain response for configuration B

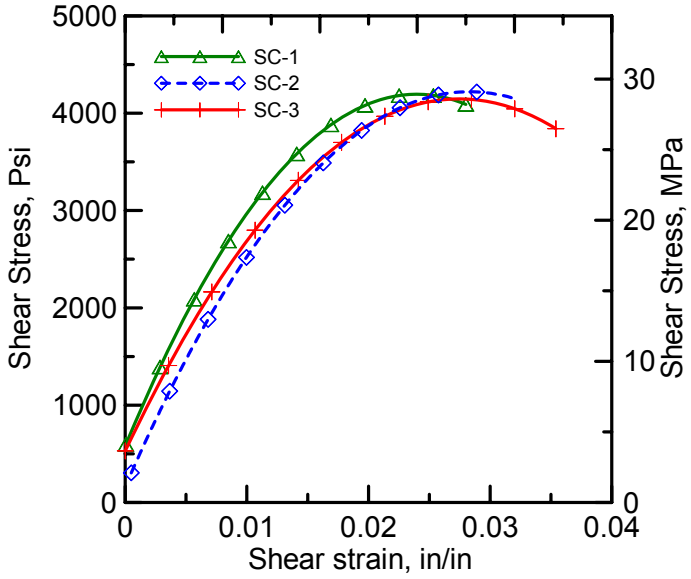

Figure 2.4.3.6. CFC shear stress- shear strain response for configuration C

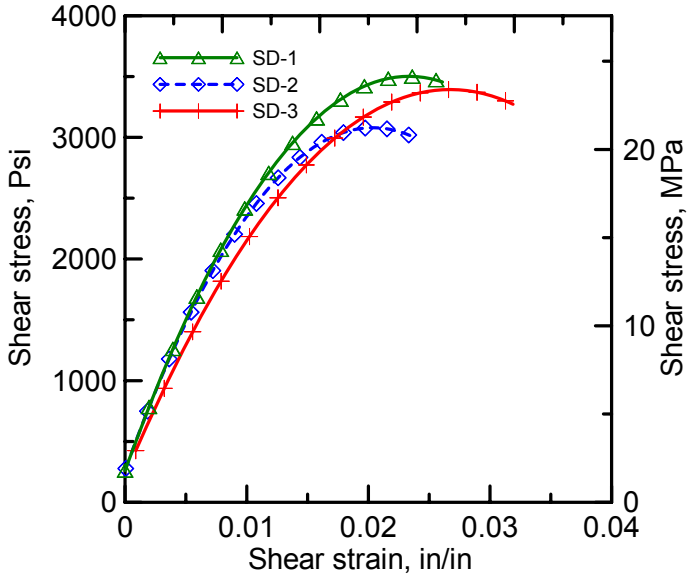

Figure 2.4.3.7. CFC shear stress- shear strain response for configuration D

It can be shown from laminate theory [Whitney and Daniel, 1984] that the state of shear stress and strain in the lamina coordinate system can be expressed in terms of the laminate axial stress σx, and the axial and transverse strain, εx and εy, respectively.

From the experimental shear tests it is clear that the CFC has two distinct regions during loading – an initial linear elastic region dies very quickly and is followed by a second region of non-linear behavior where the stiffness is constantly decreasing until it reaches the peak load/stress and fails.

The failure patterns of the samples under the +/-45 shear test are shown on Figure 2.4.3.8.

Figure 2.4.3.8. CFC failure pattern under +/-45 shear test

Finally, in Table 2.4.1 there is a summary of the properties for the four different configurations of CFE laminate.

Table 2.2.1. Summary of all CFE Test

Property\Configuration	Units	90/0-90/0 (Conf. A)	90/0-0/90 (Conf. B)	0/90-90/0 (Conf. C)	0/90-90/0 (Conf. D)
Tensile elastic Modulus	**(GPa)**	44	43	49	40
Tensile elastic Modulus	**(ksi)**	6383	6199	7046	5798
Tensile strength	**(MPa)**	780	758	820	592
Tensile strength	**(ksi)**	113	110	119	86
Tensile strain at max stress	**(%)**	2.08	2.14	1.98	1.8
Shear Modulus	**(MPa)**	1766	1628	1768	1485
Shear Modulus	**(ksi)**	256	236	256	215
Shear strength	**(MPa)**	33	27	30	24
Shear strength	**(psi)**	4713	3902	4289	3493
Shear strain at max stress	**(%)**	3.91	2.78	2.73	2.4
Compressive elastic Modulus	**(MPa)**	7495	7519	7614	6234
Compressive elastic Modulus	**(ksi)**	1087	1091	1104	904
Compressive strength	**(MPa)**	291	319	303	203
Compressive strength	**(ksi)**	42	46	44	29
Compressive strain at max stress	**(%)**	5.1	5.01	4.7	4.6

3. ORTHOTROPIC ELASTICITY AND LAMINATE THEORY

3.1. Introduction

An isotropic material is one that has identical mechanical, physical, thermal and electrical properties in every direction. Isotropic materials involve only four elastic constants, the modulus of elasticity, E, the shear modulus, G, the bulk modulus, K and the Poisson's ratio, v. However, only two are independent.

Most engineers and material scientists are well schooled in the behavior and design of isotropic materials, which include the family of most metals and pure polymers. The rapidly increasing use of anisotropic materials such as composite materials has resulted in a materials revolution and requires the knowledge base of anisotropic material behavior.

Fiber reinforced composite materials are unique in application because the use of long fibers results in a material which has a higher strength-to-density ratio and/or stiffness-to-density ratio than any other material system at moderate temperature, and there exists the opportunity to uniquely tailor the fiber orientations to a given geometry, applied load and environment. Therefore through the use of composite materials, the engineer is not only a material selector, but also a materials designer.

For small deflections, the linear elastic analysis of anisotropic composite material structures requires the use of the equilibrium equations, strain-displacement relations, and compatibility equations, which remain the same whether the structure is composed of an isotropic material or an anisotropic composite material. However, it is very necessary to

drastically alter the stress-strain relations, also called the constitutive relations, to account for the anisotropy of the composite material structure.

In section 3.2 we will discuss about the methods to obtain the composite properties from the matrix and fiber properties, while in section 3.3 we will discussed about the analysis of the lamina or ply of the composite, an orthotropic material, which includes the background theory of stress-strain relations of the anisotropic to isotropic materials. Section 3.4 discuss the specific analysis of the orthotropic analysis of the laminate, and finally section 3.5 speaks about the failure criteria used for the modeling part, including, section 3.6, the Weibull statistics approach.

3.2. Methods to obtain Composite Elastic Properties from Fiber and Matrix Properties

There are several sets of equations that obtain the composite elastic properties from those of the fiber and matrix materials. These include those of Halpin-Tsai, Hashin, and Christensen. In 1980, Hahn codified certain results for fibers of circular cross section which are randomly distributed in a plane normal to the unidirectionally oriented fibers. For that case the composite is macroscopically, transversally isotropic, that is $( )_{12} = ( )_{13}$, $( )_{22} = ( )_{33}$ and $( )_{55} = ( )_{66}$, where in the parentheses the quantity could be E, G, or v; hence, the elastic properties involve only five independent constants, namely $( )_{11}$, $( )_{22}$, $( )_{12}$, $( )_{23}$ and $( )_{66}$.

For several of the elastic constants, Hahn states that they all have the same functional form:

$$P = \frac{(P_f \times V_f + \eta \times P_m \times V_m)}{(V_f + \eta \times V_m)} \tag{3.2.1}$$

Where for the elastic constant P, the P_f, P_m and η are given in Table 3.2.1 below, and where V_f and V_m are the volume fractions of the fibers and matrix respectively (and whose sum equal unity-no voids).

Table 3.2.1. Determination of Composite Properties from Fiber and Matrix Properties

Elastic Constant	P	P_f	P_m	n
E_{11}	E_{11}	E_{11f}	E_m	1
v_{12}	v_{12}	v_{12f}	v_m	1
G_{12}	$1/G_{12}$	$1/G_{12f}$	$1/G_m$	η_6

The expressions for E11 and v12 are called the Rule of Mixtures. The definition for η6 is given as follows:

$$\eta_6 = \frac{1 + G_m / G_{12\,f}}{2} \tag{3.2.2}$$

The transverse moduli of the composite, E22 = E33, are found from the following equation:

$$E22 = E33 = \frac{4 \times K_T \times G_{23}}{K_T + m \times G_{23}} \tag{3.2.3}$$

$$m = 1 + \frac{4 \times K_T \times v_{12}{}^2}{E_{11}} \tag{3.2.4}$$

Hahn notes that for most polymeric matrix structural composites, $G_m/G_f<0.05$. If that is the case then the η_6 parameter is approximately 0.5.

In a few instances only the weight fraction of the fiber, W_f, is known. In that case the volume fraction is obtained from the following equation, where Wm is the weight fraction of the matrix, and ρ_m and ρ_f are the respective densities.

$$V_f = \frac{\rho_m \times W_f}{\rho_m \times W_f + \rho_f \times W_m} \tag{3.2.5}$$

3.3. Analysis of an Orthotropic Lamina

Laminae (or plies) are combined with their fibers oriented in more than one direction to form a laminate. The plies are oriented according to the nature of the loads to be supported by the laminate. In order to determine the properties of the laminate, it is necessary to express the properties of individual plies in terms of a common coordinate system, which, for design purposes, is generally oriented along structural axes or boundaries.

Before discussing transformation of properties, the directional nature of the properties of a fiber composite will be examined further. From the standpoint of mechanics, unidirectional composites fit in the class of materials referred to as orthotropic. This section will develop an understanding of the behavior of orthotropic materials as compared with isotropic and generally anisotropic materials.

To begin, consider the definitions of isotropic and anisotropic:

• Isotropic: At a given point in a body the properties are independent of direction.

• Anisotropic: At a point, properties depend on direction.

Isotropic and anisotropic have very different meanings from homogeneous and inhomogeneous, which are defined as follows:

• Homogeneous: properties are uniformly distributed throughout a body; properties are not a function of position.

• Inhomogeneous: properties depend on position, e.g., (x, y, z).

Whether a fiber composite is considered homogeneous or inhomogeneous depends on whether it is being considered from a macroscopic or microscopic level. A macroscopic treatment considers properties of the composite, rather than its individual constituents. The composite properties are averaged over distances that are much greater than the separation between fibers. A microscopic point of view distinguishes between fiber and matrix and the interface between them. Whereas the macroscopic, mechanics of materials approach is generally sufficient for structural design, an understanding of microscopic effects is useful and often necessary.

3.3.1. Hooke's Law (Stress vs. Strain) for Materials – Anisotropic to Isotropic

If a uniaxial tensile load is applied to a specimen of isotropic material, an elongation will be produced in the loading direction. A reduction in specimen dimensions perpendicular to the loading direction will also be produced, and the relationship between axial and transverse deformations depends on Poisson's ratio. For the case of tensile loading, no shear distortion will be produced in an isotropic material. Likewise, for the isotropic material, a shear load will produce angular distortion but no changes in length of the sides. An anisotropic material behaves differently. Application of a tensile load to a

specimen of anisotropic material will produce angular distortions as well as length changes; a shear load also results in both length and angle changes. To understand the relationships between stress and strain for a fiber composite material, it is useful to begin with the general anisotropic material.

The stress-strain relation (Hooke's law) for a general anisotropic material:

$$\begin{Bmatrix} \sigma_1 \\ \sigma_2 \\ \sigma_3 \\ \sigma_4 \\ \sigma_5 \\ \sigma_6 \end{Bmatrix} = \begin{bmatrix} Q_{11} & Q_{12} & Q_{13} & Q_{14} & Q_{15} & Q_{16} \\ Q_{21} & Q_{22} & Q_{23} & Q_{24} & Q_{25} & Q_{26} \\ Q_{31} & Q_{32} & Q_{33} & Q_{34} & Q_{35} & Q_{36} \\ Q_{41} & Q_{42} & Q_{43} & Q_{44} & Q_{45} & Q_{46} \\ Q_{51} & Q_{52} & Q_{53} & Q_{54} & Q_{55} & Q_{56} \\ Q_{61} & Q_{62} & Q_{63} & Q_{64} & Q_{65} & Q_{66} \end{bmatrix} \begin{Bmatrix} \varepsilon_1 \\ \varepsilon_2 \\ \varepsilon_3 \\ \varepsilon_4 \\ \varepsilon_5 \\ \varepsilon_6 \end{Bmatrix} \qquad (3.3.1.1)$$

where [Q] is the stiffness matrix for the material. The coefficients Q_{ij} of the stiffness matrix are functions of the elastic constants of the material. An isotropic material has two independent elastic constants, Young's modulus E and Poisson's ratio ν. A third elastic constant, the shear modulus G can be uniquely determined for the other two.

In tensor notation $\sigma i = Cij\ \varepsilon j$ $i, j = 1, \ldots 6$

As seen in Equation (3.4.1.1), a general anisotropic material has 36 material constants, in this case written as stiffness coefficients C_{ij}.

Inverting Equation (3.4.1.1) gives the strain-stress relation is $\varepsilon i = Sij\ \sigma j$ i, j = 1, ..6

where Sij are compliance coefficients, and $[S] = [Q]^{-1}$.

Because of symmetry of the stiffness matrix, the indices are interchangeable:

$C_{ij} = C_{ji}$ and $S_{ij} = S_{ji}$

The number of independent coefficients is then reduced from 36 to 21.

Many materials exhibit symmetry in their elastic properties with respect to certain planes; that is, the elastic constants do not change when the direction of the axis perpendicular to the plane of symmetry is reversed. A single plane of symmetry reduces the number of independent elastic constants to 13. For example, suppose a material has some special direction aligned in (x1-x2-x3) coordinates. If there exists another coordinate system (x1′-x2′-x3) such that the difference cannot be distinguished by mechanical means, the x3 axis is called a material symmetry axis.

An orthotropic material exhibits symmetry of its elastic properties with respect to three orthogonal planes. The number of independent elastic constants is reduced to nine. If a uniaxial tensile force is applied to an orthotropic material along one of its orthotropic symmetry axes, no angular distortion will result. In other words normal stresses produce only normal strains and no shear strains. Application of a tensile force along an axis that is not one of the material's special orthotropic axes produces angular distortions, as illustrated in Figure 3.3.1.1. In other words, the material no longer behaves in an orthotropic manner.

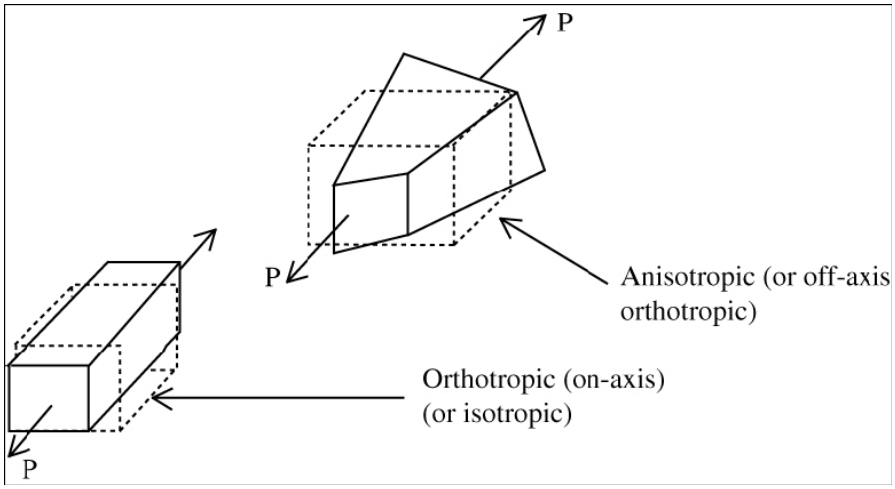

Figure 3.3.1.1 Application of tensile force along an orthotropic axis and a general axis in an orthotropic material.

The stress-strain law for an orthotropic material is

$$\begin{Bmatrix} \sigma_1 \\ \sigma_2 \\ \sigma_3 \\ \sigma_4 \\ \sigma_5 \\ \sigma_6 \end{Bmatrix} = \begin{bmatrix} Q_{11} & Q_{12} & Q_{13} & 0 & 0 & 0 \\ Q_{21} & Q_{22} & Q_{23} & 0 & 0 & 0 \\ Q_{31} & Q_{32} & Q_{33} & 0 & 0 & 0 \\ 0 & 0 & 0 & Q_{44} & 0 & 0 \\ 0 & 0 & 0 & 0 & Q_{55} & 0 \\ 0 & 0 & 0 & 0 & 0 & Q_{66} \end{bmatrix} \begin{Bmatrix} \varepsilon_1 \\ \varepsilon_2 \\ \varepsilon_3 \\ \varepsilon_4 \\ \varepsilon_5 \\ \varepsilon_6 \end{Bmatrix} \tag{3.3.1.2}$$

Which has 9 independent material constants. No interaction exists between shear stresses and normal strains or between normal stresses and shear strains. Remember that Equation (3.3.1.2) applies only for loads applied in direction parallel to the material's orthotropic axes. For loads applied along general directions, the zeros in Equation (3.3.1.2) will be replaced by nonzero coefficients that couple normal stresses and shear strains.

A unidirectional composite is a special type of orthotropic material, for it appears isotropic in planes perpendicular to the fiber direction. If the fibers are parallel to the 1-axis, then the material is isotropic in a 2-3 plane. Such a material is called transversely isotropic. Beginning with the orthotropic material whose stiffness coefficients are shown in Equation (3.3.1.2), the additional symmetry results in

$Q_{33} = Q_{22}$

$Q_{13} = Q_{12}$

$Q_{55} = Q_{66}$

The stress-strain relationship for a transversely isotropic material is given by

$$\begin{Bmatrix} \sigma_1 \\ \sigma_2 \\ \sigma_3 \\ \sigma_4 \\ \sigma_5 \\ \sigma_6 \end{Bmatrix} = \begin{bmatrix} Q_{11} & Q_{12} & Q_{12} & 0 & 0 & 0 \\ Q_{12} & Q_{22} & Q_{23} & 0 & 0 & 0 \\ Q_{12} & Q_{23} & Q_{22} & 0 & 0 & 0 \\ 0 & 0 & 0 & Q_{44} & 0 & 0 \\ 0 & 0 & 0 & 0 & Q_{55} & 0 \\ 0 & 0 & 0 & 0 & 0 & Q_{55} \end{bmatrix} \begin{Bmatrix} \varepsilon_1 \\ \varepsilon_2 \\ \varepsilon_3 \\ \varepsilon_4 \\ \varepsilon_5 \\ \varepsilon_6 \end{Bmatrix} \qquad (3.3.1.3)$$

Furthermore Q55 = 1/2 (C22 – C23), so that only five independent constants remain.

Now, for many problems involving fiber composites, especially those where the component thickness is small compared with other dimensions, the state of stress can be treated as two dimensional. For the state of plane stress, ignoring components in the 3-direction, the stress-strain relationship for an orthotropic material given by Equation (3.3.1.2) becomes

$$\begin{Bmatrix} \sigma_1 \\ \sigma_2 \\ \sigma_6 \end{Bmatrix} = \begin{bmatrix} Q_{11} & Q_{12} & 0 \\ Q_{12} & Q_{22} & 0 \\ 0 & 0 & Q_{66} \end{bmatrix} \begin{Bmatrix} \varepsilon_1 \\ \varepsilon_2 \\ \varepsilon_3 \end{Bmatrix} \tag{3.3.1.4}$$

Replacing σ_6, the shear stress in the 2-direction acting on a 1-plane (a plane with outward normal parallel to the 1-axis), with τ_{12}, and ε_6 by γ_{12} yields the form that is generally used.

$$\begin{Bmatrix} \sigma_1 \\ \sigma_2 \\ \tau_{12} \end{Bmatrix} = \begin{bmatrix} Q_{11} & Q_{12} & 0 \\ Q_{12} & Q_{22} & 0 \\ 0 & 0 & Q_{66} \end{bmatrix} \begin{Bmatrix} \varepsilon_1 \\ \varepsilon_2 \\ \gamma_{12} \end{Bmatrix} \tag{3.3.1.5}$$

3.3.2. Stress-Strain Relations for a Unidirectional Composite

The significance of the stiffness coefficients in Equation (3.3.1.5) and their relationship to the elastic constants can be most easily understood by considering how the engineering constants are determined in simple tests.

Beginning with a uniaxial tensile test, as in Figure 3.3.2.1, assuming that the load is applied in the 1-direction. Measurement of load and elongation allow calculation of Young's modulus E_1.

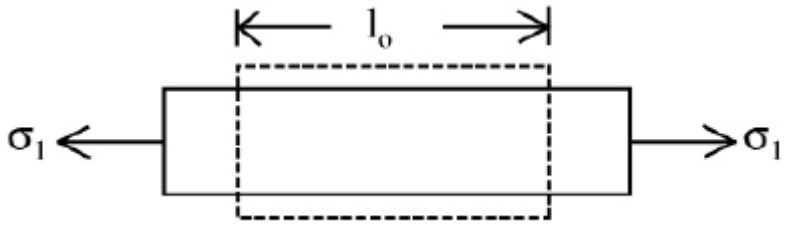

Figure 3.3.2.1 uniaxial tensile test

Transverse strain ε_2 is measured in order to determine Poisson's ratio ν_{12}.

$\nu_{12} = -\frac{\varepsilon_2}{\varepsilon_1}$ and the transverse strain is $\varepsilon_2 = -\frac{\nu_{12}}{E_1}\sigma_1$ (3.3.2.1)

A uniaxial tension test in the transverse direction permits determination of the transverse Young's modulus E_2.

$$\varepsilon_2 = \frac{\sigma_2}{E_2} \tag{3.3.2.2}$$

Measurement of strain in the 1-direction (90 degrees from the loading direction) allows calculation of the Poisson's ratio for transverse loading ν_{21}, also called the minor Poisson's ratio because it is less than ν_{12}.

$$\varepsilon_1 = -\nu_{21}\frac{\sigma_2}{E_2} = -\nu_{21}\varepsilon_2 \tag{3.3.2.3}$$

From a longitudinal shear test, as illustrated in Figure 3.4.2.2:

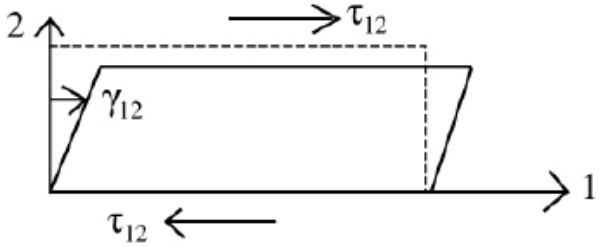

Figure 3.3.2.2 In-plane shear test.

In pure shear

$$\gamma_{12} = \frac{\tau_{12}}{G_{12}} \tag{3.3.2.4}$$

Superposition allows us to sum the effects for a general stress state (σ1, σ2, τ12):

$$\varepsilon_1 = \frac{1}{E_1}\sigma_1 - \frac{\nu_{21}}{E_2}\sigma_2$$

$$\varepsilon_2 = \frac{1}{E_2}\sigma_2 - \frac{\nu_{12}}{E_1}\sigma_1 \tag{3.3.2.5}$$

$$\gamma_{12} = \frac{1}{G_{12}}\tau_{12}$$

Expressing Equations (3.3.2.5) in matrix form, the strain-stress relation for a unidirectional composite is:

$$\begin{Bmatrix} \varepsilon_1 \\ \varepsilon_2 \\ \gamma_{12} \end{Bmatrix} = \begin{bmatrix} 1/E_1 & -\nu_{21}/E_2 & 0 \\ -\nu_{12}/E_1 & 1/E_2 & 0 \\ 0 & 0 & 1/G_{12} \end{bmatrix} \begin{Bmatrix} \sigma_1 \\ \sigma_2 \\ \tau_{12} \end{Bmatrix} \tag{3.3.2.6}$$

Finally, inverting the matrix equation (3.3.2.6) we will get the strain-stress relation:

$$\begin{Bmatrix} \sigma_1 \\ \sigma_2 \\ \tau_{12} \end{Bmatrix} = \begin{bmatrix} Q_{11} & Q_{12} & 0 \\ Q_{12} & Q_{22} & 0 \\ 0 & 0 & Q_{66} \end{bmatrix} \begin{Bmatrix} \varepsilon_1 \\ \varepsilon_2 \\ \gamma_{12} \end{Bmatrix} \tag{3.3.2.7}$$

Where the stiffness components:

$$Q_{11} = \frac{E_1}{1 - \nu_{12} \times \nu_{21}}$$

$$Q_{22} = \frac{E_2}{1 - \nu_{12} \times \nu_{21}} \qquad (3.3.2.8)$$

$$Q_{12} = \frac{\nu_{12} \times E_2}{1 - \nu_{12} \times \nu_{21}}$$

$$Q_{66} = G_{12}$$

Also, we know because of symmetry in material behavior:

$$\frac{\nu_{12}}{E_1} = \frac{\nu_{21}}{E_2} \qquad (3.3.2.9)$$

Therefore, a unidirectional composite, which is isotropic in the 2-3 plane, has four independent elastic constants and four independent stiffness coefficients.

3.3.3. Transformation of Stiffness

Knowing the stiffness of a unidirectional composite ply from measurable engineering constants, the next step is to determine how that stiffness varies with orientation.

The transformation of the stiffness of a lamina between an arbitrary orientation (x-y) and material coordinates (1-2) is illustrated in Figure 3.3.3.1.

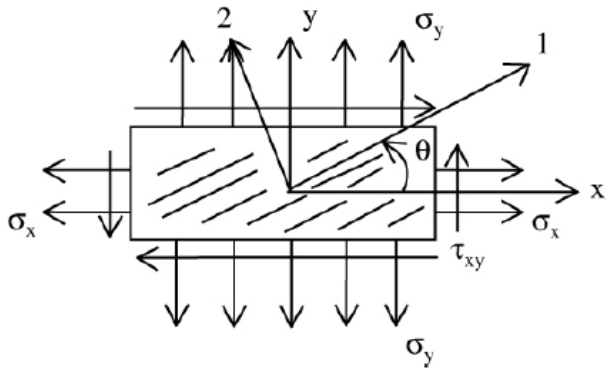

Figure 3.3.3.1. Material axes (1-2) oriented an angle θ from the global axes (x-y)

It is important to notice that the stress-strain relationships apply in material coordinates. Therefore, stress and strain can be transformed using equation (3.3.3.1), and the transformation matrix T shown on equation (3.3.3.2) in terms of θ (positive if it is going CCW from the x-axis to the 1-axis).

$$\begin{Bmatrix} \sigma_1 \\ \sigma_2 \\ \tau_{12} \end{Bmatrix} = [T] \begin{Bmatrix} \sigma_x \\ \sigma_y \\ \tau_{xy} \end{Bmatrix} \tag{3.3.3.1}$$

$$[T] = \begin{bmatrix} \cos^2\theta & \sin^2\theta & 2\sin\theta\cos\theta \\ \sin^2\theta & \cos^2\theta & -2\sin\theta\cos\theta \\ -\sin\theta\cos\theta & \sin\theta\cos\theta & \cos^2\theta - \sin^2\theta \end{bmatrix} \tag{3.3.3.2}$$

Now for strain the relation changes to equation (3.3.3.3).

$$\begin{Bmatrix} \varepsilon_1 \\ \varepsilon_2 \\ \gamma_{12}/2 \end{Bmatrix} = [T] \begin{Bmatrix} \varepsilon_x \\ \varepsilon_y \\ \gamma_{xy}/2 \end{Bmatrix} \tag{3.3.3.3}$$

In transformation of strain, the strain tensor is to be used, instead of the engineering strain. Therefore, γ_{xy} and γ_{12} are divided by 2 in equation (3.3.3.3). Now using the Reuter matrix, equation (3.3.3.4), those ½ factors will go away.

$$[R]=\begin{bmatrix}1 & 0 & 0\\ 0 & 1 & 0\\ 0 & 0 & 2\end{bmatrix} \tag{3.3.3.4}$$

Now, the strain can be transformed from global to material coordinates for subsequent calculations from strain using equation (3.3.3.5).

$$\begin{Bmatrix}\varepsilon_1\\ \varepsilon_2\\ \gamma_{12}\end{Bmatrix}=[R][T][R]^{-1}\begin{Bmatrix}\varepsilon_x\\ \varepsilon_y\\ \gamma_{xy}\end{Bmatrix} \tag{3.3.3.5}$$

Multiplying equation (3.3.3.5) by the stiffness matrix gives us the stress in material coordinates. Since we are interested in stresses and strains in the global system, the global stress-strain law is:

$$\begin{Bmatrix}\sigma_x\\ \sigma_y\\ \tau_{xy}\end{Bmatrix}=[T]^{-1}[Q][R][T][R]^{-1}\begin{Bmatrix}\varepsilon_x\\ \varepsilon_y\\ \gamma_{xy}\end{Bmatrix} \tag{3.3.3.6}$$

The global stress-strain relationship is written in terms of the transformed stiffness matrix as:

$$\begin{Bmatrix}\sigma_x\\ \sigma_y\\ \tau_{xy}\end{Bmatrix}=\begin{bmatrix}QT_{11} & QT_{12} & QT_{16}\\ QT_{12} & QT_{22} & QT_{26}\\ QT_{16} & QT_{26} & QT_{66}\end{bmatrix}\begin{Bmatrix}\varepsilon_x\\ \varepsilon_y\\ \gamma_{xy}\end{Bmatrix} \tag{3.3.3.7}$$

The coefficients of the transformed stiffness matrix are calculated using the transformation and the Reuter matrices. The equations derived from the matrices are the following:

$$QT_{11} = Q_{11}\cos^4\theta + Q_{22}\sin^4\theta + 2(Q_{12} + 2Q_{66})\sin^2\theta\cos^2\theta$$

$$QT_{22} = Q_{11}\sin^4\theta + Q_{22}\cos^4\theta + 2(Q_{12} + 2Q_{66})\sin^2\theta\cos^2\theta$$

$$QT_{12} = (Q_{11} + Q_{22} - 4Q_{66})\sin^2\theta\cos^2\theta + Q_{12}(\cos^4\theta + \sin^4\theta)$$

$$QT_{66} = (Q_{11} + Q_{22} - 2Q_{12} - 2Q_{66})\sin^2\theta\cos^2\theta + Q_{66}(\cos^4\theta + \sin^4\theta) \qquad (3.3.3.8)$$

$$QT_{16} = (Q_{11} - Q_{12} - 2Q_{66})\sin\theta\cos^3\theta - (Q_{22} - Q_{12} - 2Q_{66})\cos\theta\sin^3\theta$$

$$QT_{26} = (Q_{11} - Q_{12} - 2Q_{66})\sin^3\theta\cos\theta - (Q_{22} - Q_{12} - 2Q_{66})\cos^3\theta\sin\theta$$

Calculation of the transformed stiffness matrix using equations (3.3.3.8) will be a very important step in the laminate analysis that is presented in the next part, where the stiffness of all plies, expressed in a common coordinate system, will be combined to form the overall stiffness matrix of the laminate.

3.4. Laminate Analysis

A laminate consists of a number of layers (or plies) bonded together to act as an integral structural element. Made with fiber composites, each ply can contain unidirectional fibers or a bidimensional weave. The sequence of fiber orientations from layer to layer through the laminate is called ply orientation or stacking sequence.

A laminate is symmetric if the ply orientation and material stiffness are symmetric about the middle surface as the following example:

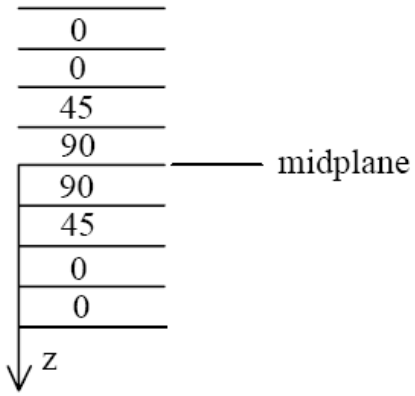

Figure 3.4.1. Symmetric laminate

Another consideration is that we need first to assume the following for the lamina:

- Each lamina of a laminate is a unidirectional composite.
- Each lamina is a homogenous orthotropic material (usually transversally isotropic).
- Because each lamina is very thin (typically less than 1mm), the analysis can be reduced to a plane-stress (two dimensional) problem.

3.4.1. Strain and Stress in a Laminate

Classical laminate theory assumes that all layers are perfectly bonded together, and the strains are continuous through the laminate thickness. In the absence of a moment (for a symmetric laminate) the strains in any given direction are equal, e.g., $(\varepsilon x)_k = (\varepsilon x)_{k+1}$. With applied moment, strains through the thickness can be related by the curvature, as in engineering beam theory.

Thin plate theory assumes that any line initially straight and normal to the mid-plane of the plate remains straight and normal to the mid-plane after extension and flexure, as shown in Figure 3.5.1.1 (This is equivalent to ignoring γ_{xz} and γ_{yx}.).

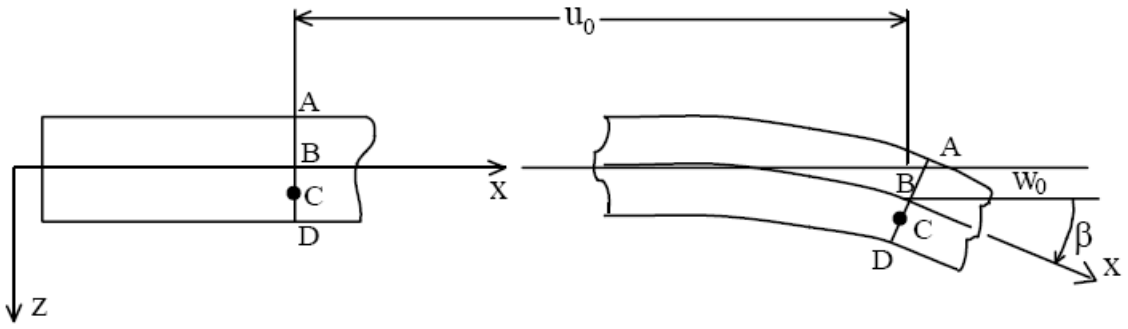

Figure 3.4.1.1. Bending of a laminate illustrating curvature of middle surface and displacement of point C

In figure 3.4.1.1, the line AD is trough the plate, normal to the middle surface, and intersecting the middle surface at B.

- u_o is the displacement of point B on the middle surface in the x-direction
- β is the slope of the middle surface
- z_c is the distance from B on the middle surface to C in the z-direction
- u_c is u_o-$z_c\beta$, displacement of C in the x-direction

Based on the assumptions of thin plate theory:

$$\beta = \frac{\partial w_0}{\partial x} \tag{3.4.1.1}$$

$$u_c = u_0 - z_c \frac{\partial w_0}{\partial x} \tag{3.4.1.2}$$

If v is the displacement in the y-direction:

$$v = v_0 - z\frac{\partial w_0}{\partial y}$$

$$\varepsilon_x = \frac{\partial u}{\partial x} = \frac{\partial u_0}{\partial x} - z\frac{\partial^2 w_0}{\partial x^2} \tag{3.4.1.3}$$

$$\varepsilon_y = \frac{\partial v}{\partial y} = \frac{\partial v_0}{\partial y} - z\frac{\partial^2 w_0}{\partial y^2}$$

$$\gamma_{xy} = \frac{\partial u}{\partial y} + \frac{\partial v}{\partial x} = \frac{\partial u_0}{\partial y} + \frac{\partial v_0}{\partial x} - z\frac{\partial^2 w_0}{\partial x \partial y}$$

Defining ε_x^0, ε_y^0, γ_{xy}^0 as the in-plane strain at the midplane:

$$\begin{Bmatrix} \varepsilon_x^{\,0} \\ \varepsilon_y^{\,0} \\ \gamma_{xy}^{\,0} \end{Bmatrix} = \begin{Bmatrix} \dfrac{\partial u_0}{\partial x} \\ \dfrac{\partial v_0}{\partial y} \\ \dfrac{\partial u_0}{\partial y} + \dfrac{\partial v_0}{\partial x} \end{Bmatrix} \tag{3.4.1.4}$$

Now, the strain at a point can be written as:

$$\begin{Bmatrix} \varepsilon_x \\ \varepsilon_y \\ \gamma_{xy} \end{Bmatrix} = \begin{Bmatrix} \varepsilon_x^{\,0} \\ \varepsilon_y^{\,0} \\ \gamma_{xy}^{\,0} \end{Bmatrix} = \begin{Bmatrix} k_x \\ k_y \\ k_{xy} \end{Bmatrix} \tag{3.4.1.5}$$

Where k_x, k_y and k_{xy} are the plate curvatures of the midplane surface, defined as:

$$\begin{Bmatrix} k_x \\ k_y \\ k_{xy} \end{Bmatrix} = \begin{Bmatrix} -\dfrac{\partial^2 w_0}{\partial x^2} \\ -\dfrac{\partial^2 w_0}{\partial y^2} \\ -2\dfrac{\partial^2 w_0}{\partial x \partial y} \end{Bmatrix} \tag{3.4.1.6}$$

Therefore, stress at a point in the k^{th} layer of laminate can be found from the stress-strain relation:

$$\begin{Bmatrix} \sigma_x^{\,k} \\ \sigma_y^{\,k} \\ \sigma_{xy}^{\,k} \end{Bmatrix} = \begin{bmatrix} QT_{11}^{\,k} & QT_{12}^{\,k} & QT_{16}^{\,k} \\ QT_{12}^{\,k} & QT_{22}^{\,k} & QT_{26}^{\,k} \\ QT_{16}^{\,k} & QT_{26}^{\,k} & QT_{66}^{\,k} \end{bmatrix} \left[\begin{Bmatrix} \varepsilon_x^{\,0} \\ \varepsilon_y^{\,0} \\ \gamma_{xy}^{\,0} \end{Bmatrix} + z \begin{Bmatrix} k_x \\ k_y \\ k_{xy} \end{Bmatrix} \right] \tag{3.4.1.7}$$

The strains in any direction vary linearly through the laminate, as shown in Figure 3.4.1.2. Stresses vary linearly through each ply but may be discontinuous at ply boundaries because of varying stiffness.

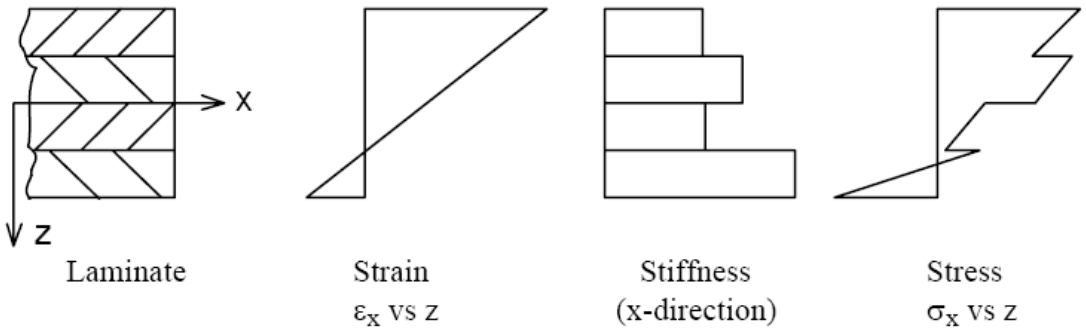

Figure 3.4.1.2. Variation of stress and strain through the thickness of a laminate

The stiffness matrix for the k^{th} layer is simply the off-axis stiffness obtained by transformation of unidirectional composite stiffness due to rotation (in plane) to orientation θ. The analysis of the off-axis stiffness for the plies was presented early in the chapter.

3.5. Failure Analysis

Failure criteria are needed to compare the actual state of stress with the failure stresses measured in the tests. Failure criteria can be developed for a unidirectional composite, considered from a macro mechanical point of view. Once failure criteria have been developed for individual plies, those criteria can be incorporated into a failure analysis procedure for a laminate.

Among the many failure criteria that have been developed for orthotropic materials, several have found application to continuous-fiber composites. Some are applicable only to specific loading conditions. We will only show in this section two simple and one interactive method.

3.5.1. Maximum Stress Criterion

Because of research in the forest products area, the Maximum Stress Theory was extended to orthotropic materials. It assumes that failure of a ply occurs when any of the stress components in the principal material directions (1-2) reaches its corresponding strength property. In other words, failure happens under any of the following conditions:

$\sigma_1 \geq S_{1T}$ $|\sigma_1| \geq S_{1C}$

$\sigma_2 \geq S_{2T}$ $|\sigma_2| \geq S_{2C}$

$\tau_{12} \geq S_{12}$

3.5.2. Maximum Strain Criterion

This theory states that failure occurs when the strain obtained along the principal material axes exceed their limiting values. In other words, failure happens under any of the following conditions:

$\varepsilon_1 \geq S_{1T}/E_1$ $|\varepsilon_1| \geq S_{1C}/E_1$

$\varepsilon_2 \geq S_{2T}/E_2$ $|\varepsilon_2| \geq S_{2C}/E_2$

$\gamma_{12} \geq S_{12}/G_{12}$

Both theories consider each component independently, ignoring any interaction. Each criterion must also be applied in the appropriate principal material direction. Actual failure stress measured in uniaxial tensile testing of off-axis specimens differ from the predictions of the criteria. Therefore, a more comprehensive failure criterion, which considers the interactions among stress component, is frequently used.

3.5.3. Interactive Failure Criterion – Tsai-Hill

Because rolled metals have slightly different properties in the roll direction than in the other two directions, R. Hill developed an extension of Von Mises-Hencky distortion energy theory as a yield criterion for orthotropic materials of the form:

$$F(\sigma_1 - \sigma_2)^2+G(\sigma_2 - \sigma_3)^2+H(\sigma_3 - \sigma_1)^2+2L(\tau_{12})^2+2M(\tau_{23})^2+2N(\tau_{31})^2=1 \qquad (3.5.3.1)$$

Where F, G, H, L, M, and N are functions of the yield strengths of the material.

S.W. Tsai related these constants to the failure strengths for a unidirectional composite. In his procedure, it is assumed that individual stresses are applied one at a time along principal material directions, as in the tests to measure strengths.

If only σ_1 acts on a body and the allowable stress in the 1-direction is S_1,

$$(F+H)\ S_1^2=1 \qquad F+H=1/\ S_1^2 \qquad (3.5.3.2)$$

If only σ_2 acts on a body and the strength is S_2,

$$(F+G)\ S_2^2=1 \qquad F+G=1/\ S_2^2 \qquad (3.5.3.3)$$

If only σ_3 acts on a body and the strength is S_3,

$$(G+H)\ S_3^2=1 \qquad G+H=1/\ S_3^2 \qquad (3.5.3.4)$$

Solving for F, G, H,

$$\begin{aligned} 2F&=1/\ S_1^2+1/\ S_2^2-1/\ S_3^2 \\ 2G&=1/\ S_3^2+1/\ S_2^2-1/\ S_1^2 \\ 2H&=1/\ S_1^2+1/\ S_1^2-1/\ S_2^2 \end{aligned} \qquad (3.5.3.5)$$

Following a similar procedure we can find L, M and N in the terms of the shear strengths:

$$2L=1/\ S_{12}^2 \qquad 2M=1/\ S_{23}^2 \qquad 2N=1/\ S_{31}^2 \qquad (3.5.3.6)$$

Now, in our case we can include the plane stress condition, in which unidirectional composites are normally characterized, where the only stress components are σ_1, σ_2, and τ_{12}. Setting the other components to zero we have the following equation, the Tsai-Hill criterion:

$$\frac{\sigma_1^2}{S_1^2}-\frac{\sigma_1\times\sigma_2}{S_1^2}+\frac{\sigma_2^2}{S_2^2}+\frac{\tau_{12}^2}{S_{12}^2}=1 \qquad (3.5.3.7)$$

3.6. Weibull Statistics

The classical way to view the strength of the materials or structures is a deterministic one. That is, a true strength, a single value that is characteristic of the material or structure, is supposed to exist. In experiments to determine this true strength, considerable scatter in the results is usually observed. As this is not considered to be a feature of the material or object itself, it is usually attributed to uncontrollable experimental variables. As a consequence, the second central moment of the experimental data, the standard deviation, is interpreted as indicating the success of standardizing the experimental set-up and procedures. Therefore, standard deviation can be considered to be an indicator of the quality of an experiment or testing method. The deterministic view has become much less popular in the technical sciences. If the deterministic view is valid, identical experiments performed on material specimens of different sizes should yield the same results for failure stress.

However, is been shown that fiber strength is a statistical quantity since it is governed by the propagation of pre-existing flaws or cracks in the fiber. Typically, statistical fiber strength distributions are measured directly by performing single-fiber tension tests on a collection of fibers at a common gage length L. In such a test, the fiber stress is uniform across the fiber cross-section and uniform along the length of the fiber within the gage section. The strength data obtained from such a test are usually characterized in terms of a Weibull probability distribution, wherein the cumulative probability of failure of a fiber of length L at stress σ is given by:

$$P_f(\sigma, L) = 1 - \exp\left[-\frac{L}{L_0} \times \left(\frac{\sigma}{\sigma_0} \right)^m \right] \tag{3.6.1}$$

Where σ_0 is the characteristic fiber strength at gage length L_0 and m is the Weibull modulus characterizing the spread in the distribution of strengths at any gage length.

Furthermore, in the case of having an interactive failure criterion, such as Tsai-Hill where the lamina could be oriented at a different position, as shown in Figure 3.6.1, the Weibull equation will change to the following:

$$P_f(TH, L) = 1 - \exp\left[-\frac{L}{L_0} \times \left(\frac{TH}{TH_0} \right)^m \right] \tag{3.6.2}$$

Where TH_0 is the characteristic Tsai-Hill value at gage length L_0 and m is the Weibull modulus characterizing the spread in the distribution of Tsai-Hill numbers at any gage length.

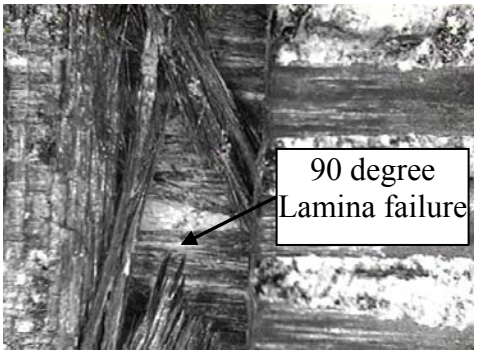

Figure 3.6.1. 90 degree lamina failure of a crossply CFE composite

Using this approach we can apply the Weibull statistics to a single analysis of the interactive failure, therefore increasing the accuracy of the model for multiple oriented laminates.

To calculate the Weibull modulus, two additional values must be computed, the natural logarithm of the stress and the natural logarithm of the natural logarithm of the following equation:

$$\frac{N+1}{N+1+i} \tag{3.6.3}$$

Where N is the total number of tests and *i* is the current test specimen. Therefore, there will be a corresponding relation for each test. The slope of the plot of the LN(stress) against the LN(LN(N+1/N+1+i)) will give us the Weibull modulus of the tests, as seen in Figure 3.6.2.

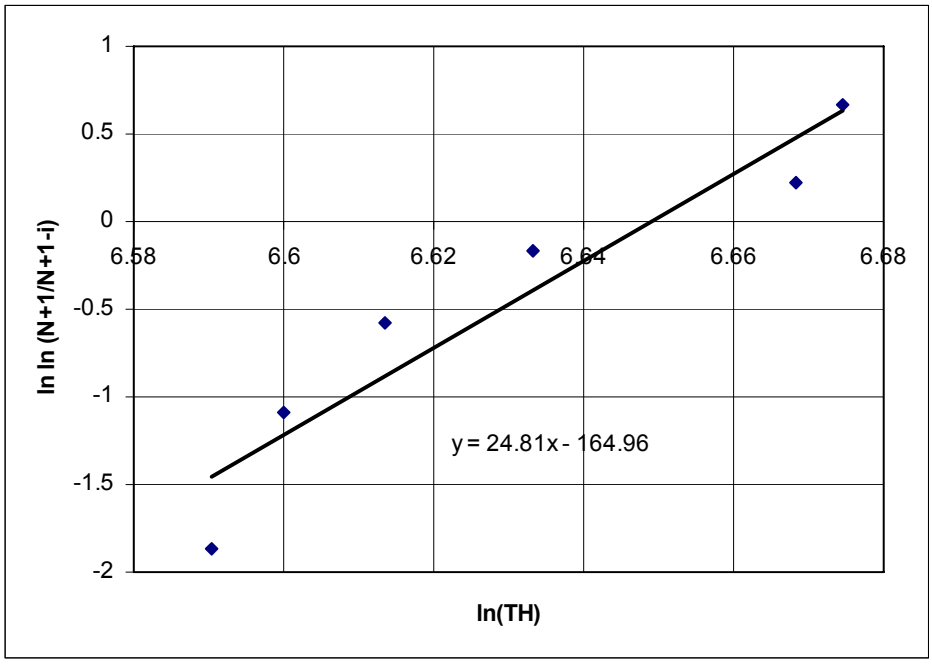

Figure 3.6.2. Weibull modulus determination

4. VALIDATION OF THE MATERIAL MODEL

4.1. Analytical Analysis and Algorithm for the Composite Model

Based on the orthotropic material behavior and the laminate theory, a computational analytical model was developed in several complexity phases. We can separate these phases in two types of laminate analysis: Unidirectional Laminates and Multidirectional Laminates. Under each category there are several assumptions and parameters involved (which will be explained in detail later in the section) that will govern the failure strength and the constitutive behavior of the laminate.

There are some assumptions taken in the algorithm such as:

1. Plane stress is assumed due to the thickness of the laminate in analysis, therefore σ_3, τ_{13}, and τ_{23} are zero and the stress-strain relation (constitutive behavior) will be reduced to:

$$\begin{Bmatrix} \varepsilon_1 \\ \varepsilon_2 \\ \gamma_{12} \end{Bmatrix} = \begin{bmatrix} 1/E_1 & -\nu_{21}/E_2 & 0 \\ -\nu_{12}/E_1 & 1/E_2 & 0 \\ 0 & 0 & 1/G_{12} \end{bmatrix} \begin{Bmatrix} \sigma_1 \\ \sigma_2 \\ \tau_{12} \end{Bmatrix} \tag{4.1.1}$$

2. Strain will be applied uniformly in the x-direction (ε_x global coordinates), and all layers or cells in the laminate will have the same amount of strain during the whole simulation, unless specified.
3. Strain in the y-direction (ε_y) and in-plane shear strain (γ_{xy}) will be minimized or ignored if necessary, by applying strain compensation or restrictions in the failure analysis.

4. Perfect bonding is assumed between the layers or cells, in other words there are no debonding or interlaminar shear defects or failures.
5. Any line straight and normal to the midplane of the laminate will remain straight and normal to the midplane after extension and flexure.

The simulation procedure, the common ground for both unidirectional and multidirectional approaches, is illustrated as following: (note: steps that need further explanation or are very different from one approach to the other will be explained in their respective sections)

1. Definition of the geometry (number of layers, cells, thickness, orientation of the lamina (if necessary), etc) for the composite laminate.
2. Definition of the composite material elastic properties (E_1, E_2, v_{12}, v_{21}, G_{12}) using any convenient method of section 3.2, where those properties are a function of the fiber and matrix properties.
3. Definition of the strength values for the specific failure criteria (S_{1T}, S_{2T}, S_{12}, etc.).
4. Calculation of the orthotropic stiffness matrix components according to the following equations:

$$Q_{11} = \frac{E_1}{1 - v_{12} \times v_{21}} \qquad Q_{22} = \frac{E_2}{1 - v_{12} \times v_{21}}$$

$$Q_{12} = \frac{v_{12} \times E_2}{1 - v_{12} \times v_{21}} \qquad Q_{66} = G_{12} \tag{4.1.2}$$

5. Transformation or reorientation of the stiffness matrix for each lamina, if necessary, using the angle given in step 1.
6. Assignation of the randomly statistical strength, or other related value, to each layer or cell; this step depends on the failure criteria. This statistical approach is based on the Weibull model for probability of failure detailed in section 3.6.
7. Incremental strain is applied, and the constitutive behavior of each lamina will calculate its respective stress level in global (x-y) coordinates.
8. If necessary, rotation of the stress tensor to the material (1-2) coordinates will be solved using the following transformation matrix:

$$[T]=\begin{bmatrix} \cos^2\theta & \sin^2\theta & 2\sin\theta\cos\theta \\ \sin^2\theta & \cos^2\theta & -2\sin\theta\cos\theta \\ -\sin\theta\cos\theta & \sin\theta\cos\theta & \cos^2\theta-\sin^2\theta \end{bmatrix} \tag{4.1.3}$$

9. According to the corresponding failure criteria and/or statistical criteria, the strength or failure value will be check and if failure occurs the layer or cell stiffness will be significantly reduced for the next step.
10. Depending on the complexity of the model, a load sharing rule will be applied on the neighbor lamina or cells. Equilibrium on the section will be maintained.
11. Border effects are related to the load sharing rule and will be taken into account only in the y-direction.
12. If failure occurs in the lamina or cells affected by the load sharing rule, they will follow the same procedure shown on step 10.

13. Accumulation of the stress for each lamina or cell, then we will return to step 7, adding the incremental strain and evaluate the laminate with the updated stiffness.

The following section will work on the specifics of each approach and the details of each of their models, going from the simplest to the more complex. Details of some of the steps in the algorithm will be further explained and some examples of the behavior will be shown.

4.1.1. Unidirectional Analysis Specific Considerations

Using the unidirectional approach we have three developed models, where each one is a sophistication of the previous model with an increase in the accuracy and the description of the experimental tests. As its name implies, since they are unidirectional laminates, steps 5 and 8 of the algorithm are not needed.

The first model is based on the Strength failure criterion mixed with the Weibull Statistics. It uses the Weibull failure probability function (equation (3.6.1)) to calculate the corresponding distribution of failure stresses, and a random distribution function to assign those stresses among the plies that compose the laminate. Failure of a layer will follow step 9 of the algorithm. No further considerations in the laminate were taken; therefore steps 10, 11 and 12 will not be used. As an example of the model behavior, a stress-strain plot is shown in Figure 4.1.1.1 and the corresponding Weibull function is plotted in Figure 4.1.1.2.

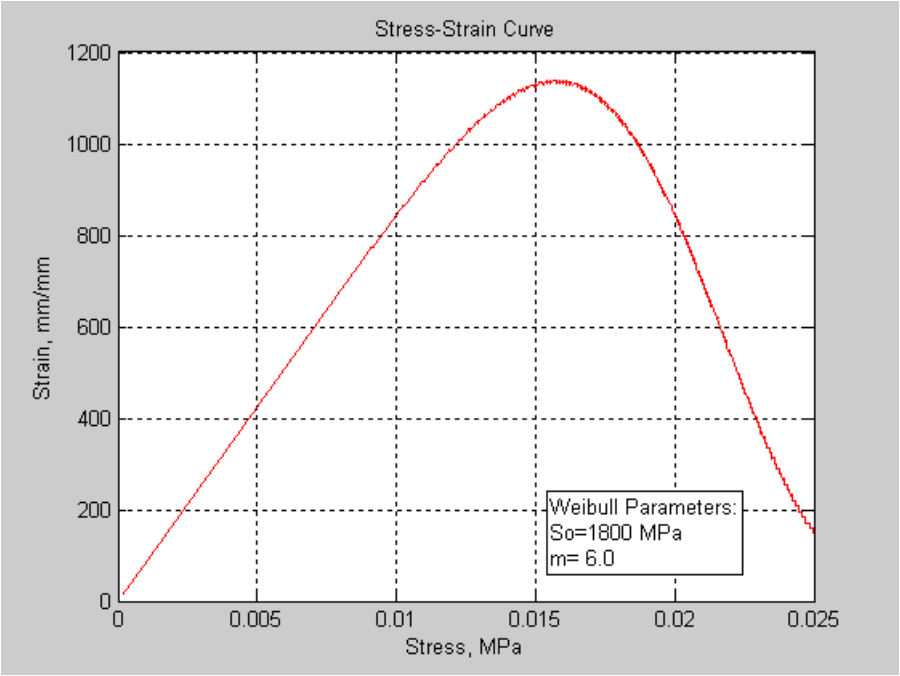

Figure 4.1.1.1. Stress-Strain plot for the Strength-Weibull model, material CF/E, Weibull values S_0 = 1800 MPa, m = 6.0

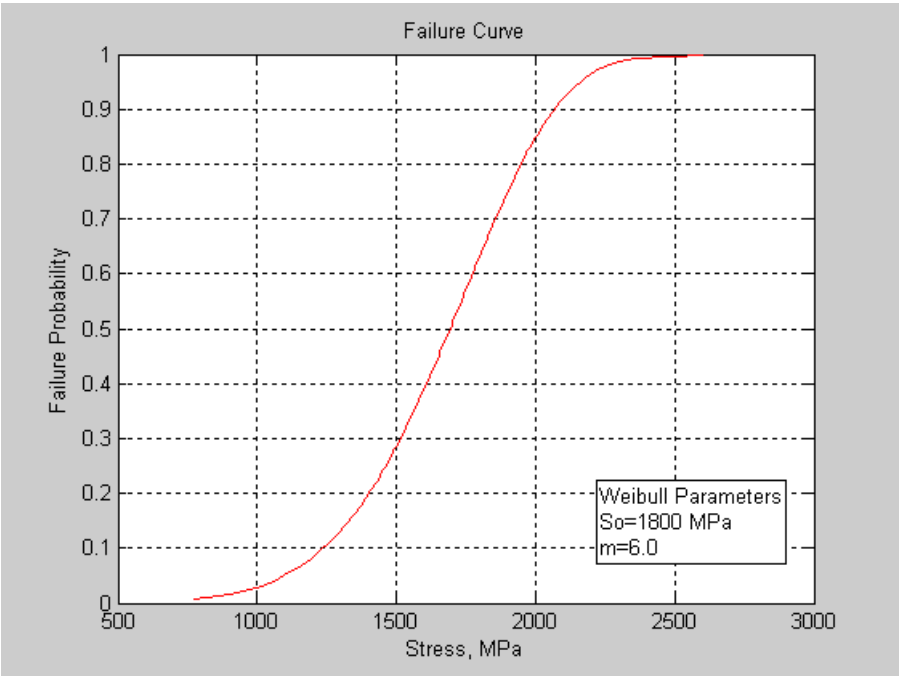

Figure 4.1.1.2. Weibull Distribution plot, Weibull values S_0 = 1800 MPa, m = 6.0

The second model additionally uses a simplified load sharing rule applied on steps 10, 11 and 12 of the algorithm. This rule specifies that once a failure happens, two layers above and two layers below will suffer an increase of the load, which will increase the chance of failure and the possibility of and accumulated failure region in the laminate. Border conditions were taken into account, if the failure happens near and/or at the edges (y-direction) the neighbor plies will have an additional increment in the load.

The typical laminate stress profile, where a load concentration happened, is shown on Figure 4.1.1.3. Also it can be seen in Figure 4.1.1.4 the effect of a load concentration failure on the stress-strain plot of CFE.

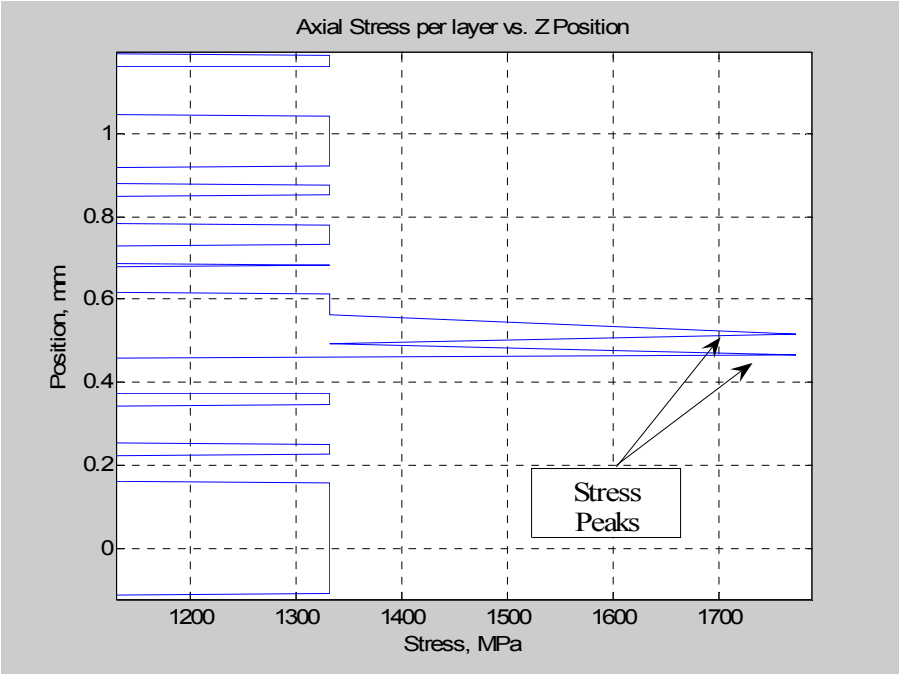

Figure 4.1.1.3. Detail of the laminate Stress profile with stress concentration effects, material CFE, Weibull values S_0 = 1800 MPa, m = 6.0

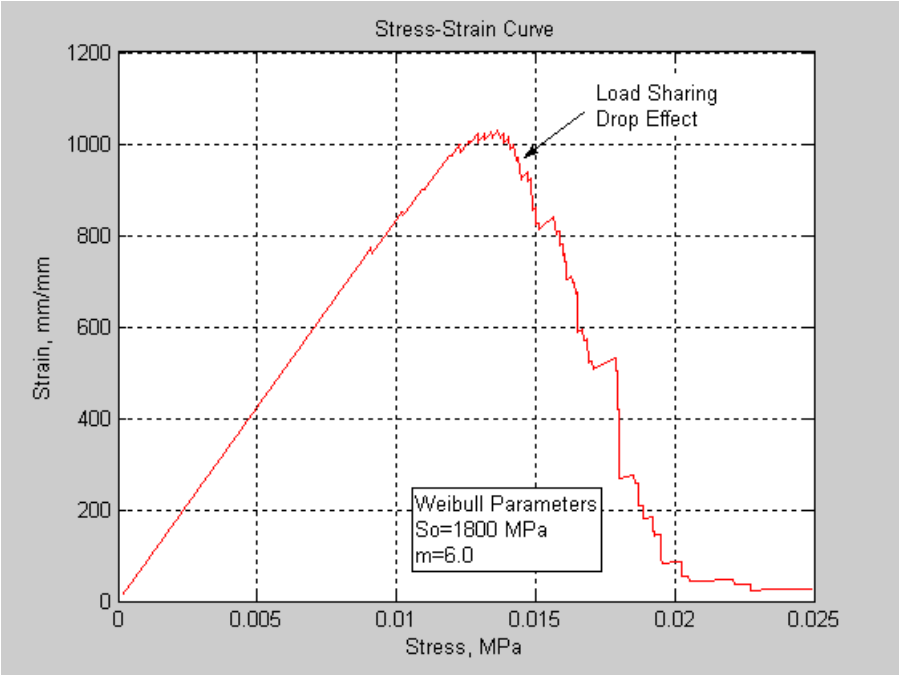

Figure 4.1.1.4. Stress-Strain plot for the Strength-Weibull-Load Sharing model, material CF/E, Weibull values S_0 = 1800 MPa, m = 6.0, note the accumulated load drops

The third model, most complex of all presented, is based on the same premises of the previous models, but with a different geometry concept. Instead of layers, this model uses cells, which together encompassed the whole laminate, making it a 2-D model. The unit cells are composed of matrix and fiber as shown on Figure 4.1.1.5. Additional assumptions were taken in order to simplify the model, these are as follows:

- Strain is the same for all the cells, there will not be an effect due to clamping in one side and the imposed displacement in the other.
- Each cell will have its own strength, that will be randomized and assign using the Weibull distribution.

- After failure, the load sharing rule will be only in the y direction (equilibrium), and the two x-direction cell neighbors' (1 to the left and 1 to the right) will suffer a load reduction that will be equilibrated in their respective y-direction cells.
- Border conditions in the x-direction borders, clamped and mobile side, will be reinforced to simplify the model; assuming a tri-axial state of stress will increase its strength significantly to avoid failue.
- Matrix will not fail until it reaches a maximum of 2.5% elongation according to experimental results, the entire load will be redistributed.
- The layer stress is the average of the stresses of the cells that composed it.

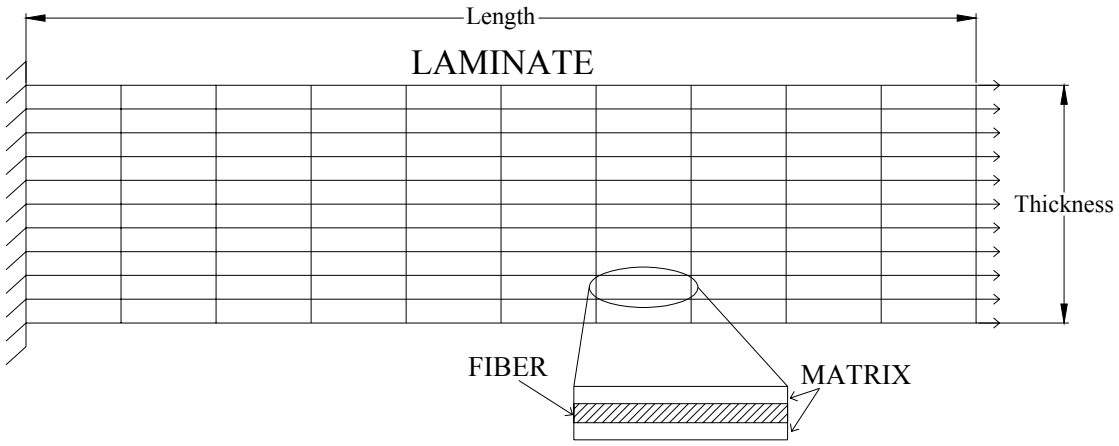

Figure 4.1.1.5. Unit Cell and Laminate Diagram for the Strength-Weibull-Load Sharing-2D Model.

Additionally, the stress-strain curve will be monitored at every important step with a graphic damage representation, as shown in Figure 4.1.1.6 for the whole stress-strain curve and on Figure 4.1.1.7 for several strain measures.

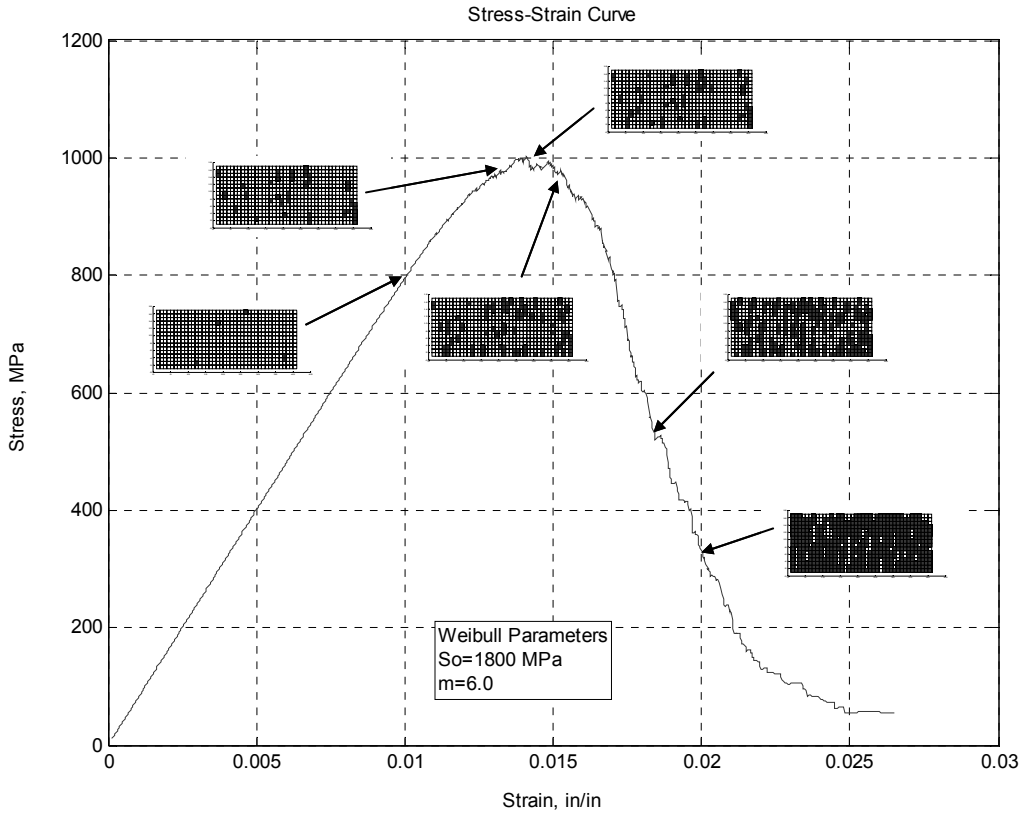

Figure 4.1.1.6. Stress-Strain Plot for the Strength-Weibull-Load Sharing-2D Model, material CFE, Weibull values S_0 = 1800 MPa, m = 6.0

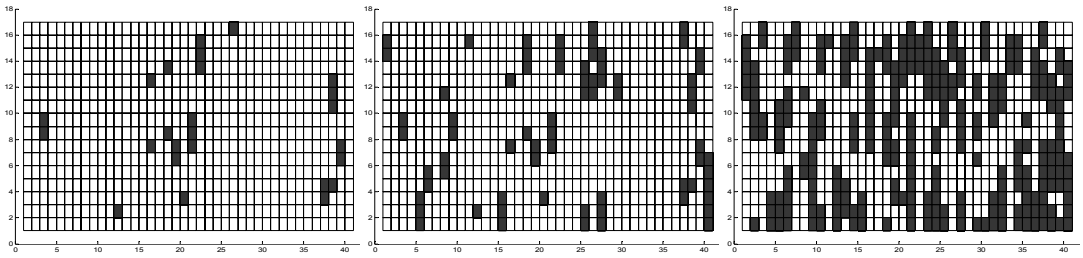

0.12% strain 0.14% strain 0.17% strain

Figure 4.1.1.7. Cell failure for several strain levels, Strength-Weibull-Load Sharing-2D Model

4.1.2. Multidirectional Analysis Specific Considerations

Using the multidirectional approach was more useful for the specific case of multiple orientation lamina or fabric composites. The approach we have three developed models, where each one is a sophistication of the previous model with an increase in the accuracy and the description of the experimental tests. As its name implies, since they are multidirectional laminates, steps 5 and 8 of the algorithm will be needed. All models will be using the Tsai-Hill interactive criterion, due to its accuracy and still simplicity in the tension test cases in comparison with the Tsai-Wu. Maximum Stress and Maximum Strain criteria were discarded for the complexity and inaccuracy that those criteria will pose for the multiple oriented plies.

The first model is based on the Tsai-Hill failure criterion alone, giving us a linear approach and an idea of the material strength when using multiple oriented layers. The model uses the Tsai-Hill interactive equation, displayed on (3.5.3.7), to calculate the laminate failure strength. There is no difference in the failure "Tsai-Hill value", therefore all plies will fail at the same time. Different orientation laminates Stress-Strain curves are shown in Figure 4.1.2.1.

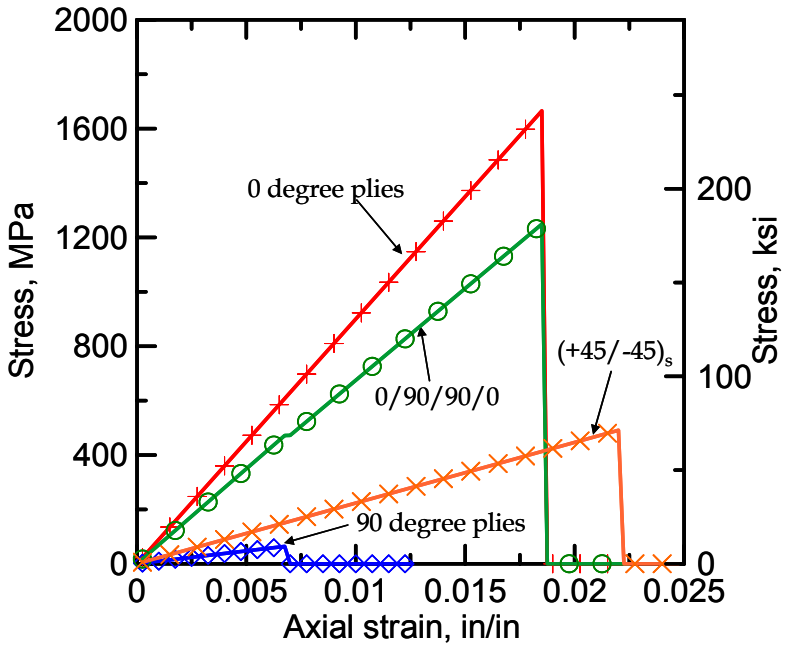

Figure 4.1.2.1. Stress--Strain Curves for Multiple Oriented Laminates in the Tsai-Hill model, Material CFE

The second model additionally uses a mix of the Tsai-Hill failure criterion and the Weibull failure probability function, similar to the unidirectional model with the difference that it uses the "Tsai-Hill value" instead of the lamina strength, as shown in equation (3.6.2). The model uses that equation to calculate the corresponding distribution of "Tsai-Hill values" and a random distribution of those values among the plies that compose the laminate. Failure of any ply will follow step 9 of the general algorithm. No further considerations were taken; therefore steps 10, 11 and 12 will not be used. As an example of the model behavior, several stress-strain curves for different laminate orientations are shown in Figure 4.1.2.2 and the corresponding Weibull function is plotted in Figure 4.1.2.3.

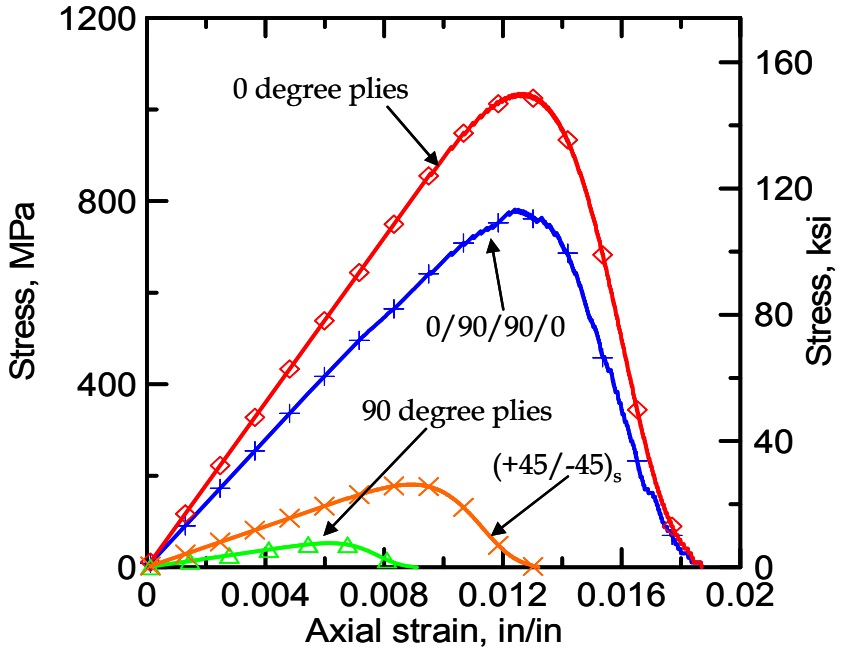

Figure 4.1.2.2. Stress-Strain Curves for Multiple Oriented Laminates in the Tsai-Hill-Weibull model, Material CFE, Weibull parameters TH_0= 0.75, m=5.0

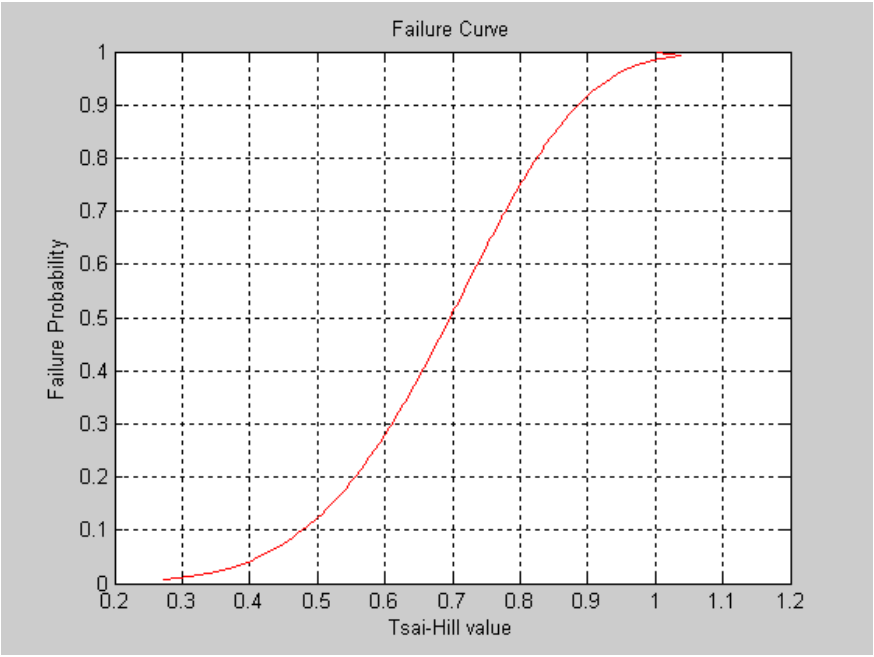

Figure 4.1.2.3. Weibull distribution plot, Weibull values TH_0= 0.75, m=5.0

The third model is based on the same premises of the previous two, but with the addition of a simplified load sharing rule, applied on steps 10, 11 and 12 of the general algorithm. The simplified rule specifies that when failure happens, two layers above and two layers below will suffer an increase of the load, which will increase the chance of failure and the possibility of an accumulated failure region in the laminate. The increased load will only be in the x-direction and its effect will be transformed to the material coordinates (1-2), if necessary, in order to find the Tsai-Hill value and evaluate the possible failure. Border conditions are also accounted, if the failures happen near or in the top or bottom border (y-direction) the involved plies will have an additional increase in the load. In the case of failure that are close to other failures the concentration effect will stack and increase the chance furthermore.

The random effect of the failures will be reflected in the stress-strain curve as shown in Figure 4.1.2.4. Multiple oriented laminates stress-strain curves are shown in Figure 4.1.2.5.

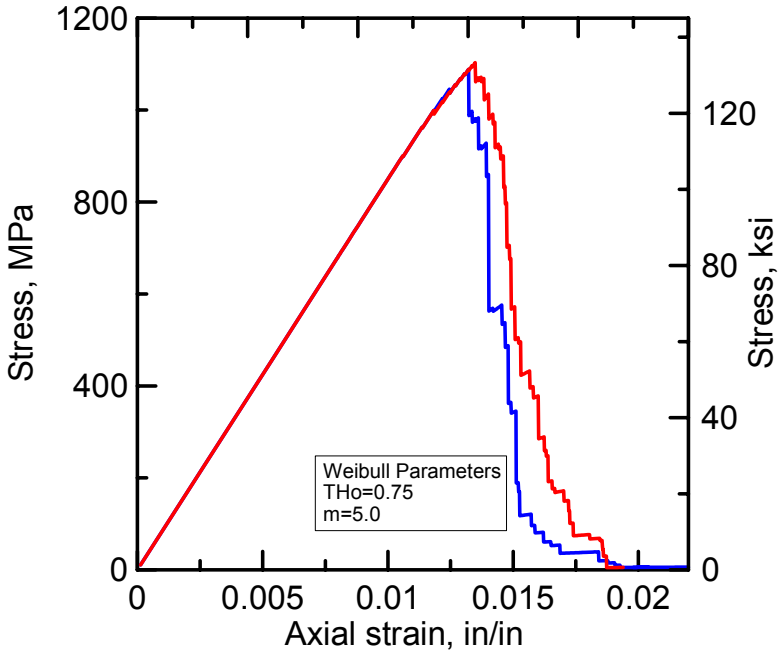

Figure 4.1.2.4. Two simulated 0 layer laminate tests with the same parameters, its differences due to the random failure value and the load concentration

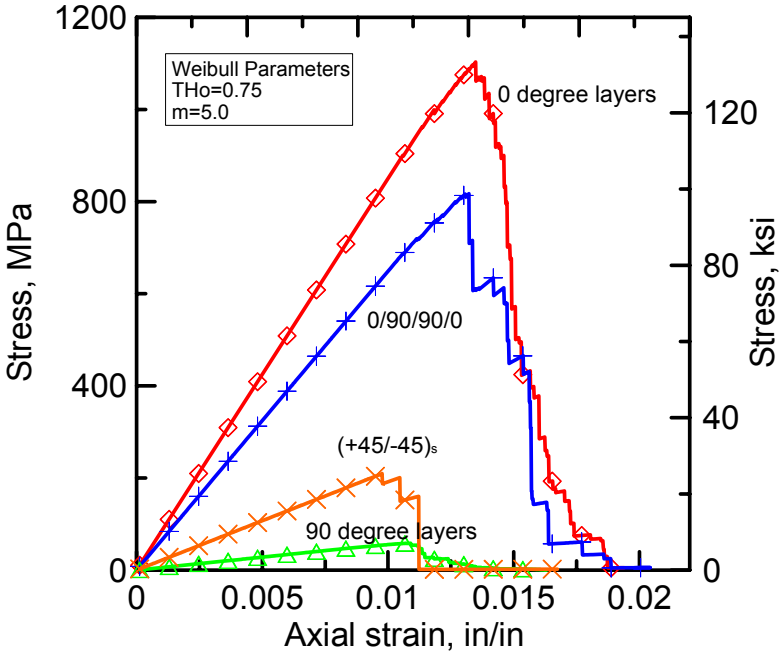

Figure 4.1.2.5. Stress-Strain Curves for Multiple Oriented Laminates in the Tsai-Hill-Weibull-Load Sharing model, Material CFE, Weibull parameters TH_0= 0.75, m=5.0

4.2. Weibull Parameters

An important part of the models was the Weibull function parameters. Those parameters are a statistical failure distribution that comes from the fundamental tests done on specific samples. For example, if we want to model the yarn behavior we need to use the failure distribution found on several tests done on single fibers, or smaller yarns. In the same fashion, if we want a fabric behavior we use the yarn test results in the distribution. Other options include using the same distribution of the tests to infer a Weibull distribution, in other words to get the Weibull parameters for a composite laminate, the use of a specific number of tests of the same composite laminate will be needed.

4.2.1. Weibull Parameters and Curve Fitting, Strength Criterion

The two parameter version of equation (3.6.1) is used to model the composite behavior. Those two parameters involved are the characteristic stress σ_0 (63.2% probability level) and the Weibull modulus m, both are shown in equation (4.2.1.1).

$$P_f(\sigma) = 1 - \exp\left[-\left(\frac{\sigma}{\sigma_0}\right)^m\right] \qquad (4.2.1.1)$$

Another set of tests evaluated at Arizona State University Structural Laboratory were the Kevlar® 49 fabric and yarn tensile tests. The yarn tests will be used to evaluate the Weibull parameters in order to evaluate the unidirectional model. The yarn tensile test results are shown in Table 4.2.1.1, but only the 17” length samples.

Table 4.2.1.1. Yarn tensile Tests for the 17” length Kevlar® 49 samples

Number	E (MPa)	Strength (MPa)	Strain
1	73006.46	1236.16	0.02
2	74120.05	1455.55	0.03
3	74790.52	1471.39	0.03
4	76422.67	1526	0.02
5	76827.5	1479.73	0.03
6	77162.63	1597.31	0.03
7	77380.4	1784.79	0.03
8	80878.48	1769.03	0.03
9	81335.05	1802.89	0.03
10	82475.12	1744.85	0.03

The Weibull analysis was made following the procedure on Section 3.6 (Chapter 3); being N = 10 the respective values were calculated and shown in Table 4.2.1.2.

Table 4.2.1.2. Weibull values for the determination of the parameter m

Number	ln(ln(N+1/N+1-i)	ln(stress)
1	-2.350618656	7.119765
2	-1.606090045	7.283139
3	-1.144278086	7.293963
4	-0.794106012	7.330405
5	-0.50065122	7.299615
6	-0.237676951	7.376076
7	0.011534137	7.487056
8	0.261812562	7.478187
9	0.533417353	7.497146
10	0.874591383	7.464424

The plot of ln(ln(N+1/N+1+i)) vs ln(stress) is plotted in Figure 4.2.1.1 and its slope is calculated to give the Weibull modulus (m) of 7.74.

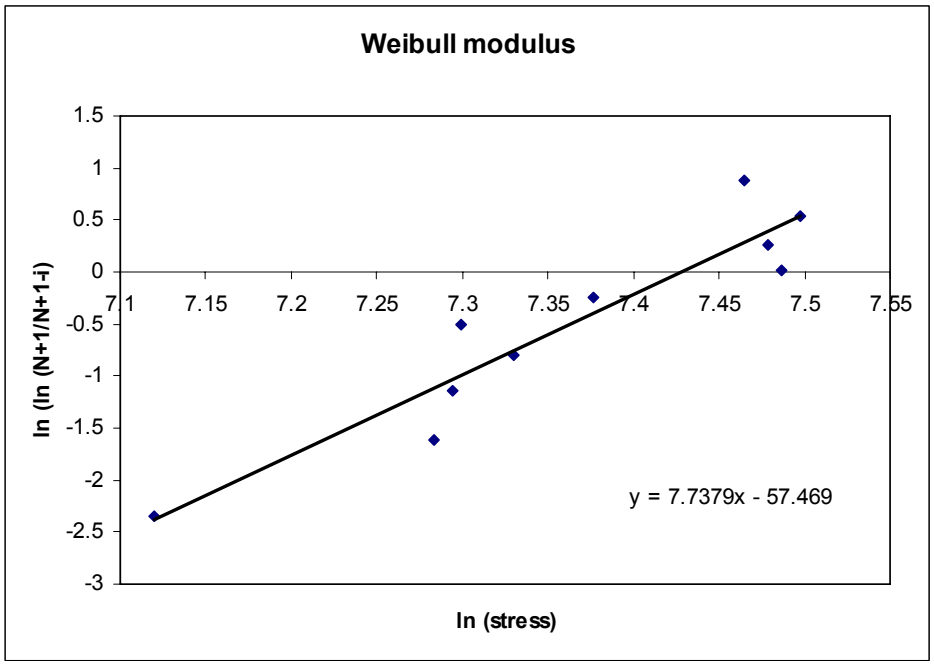

Figure 4.2.1.1. Weibull parameters plot to determine the modulus m

A developed Matlab code that employs the least squares approach to get the Weibull characteristic stress, found the value to be 1900 MPa; and with that characteristic stress calculated and the Weibull modulus of 7.74 the plot of the Weibull failure distribution is shown on Figure 4.2.1.2.

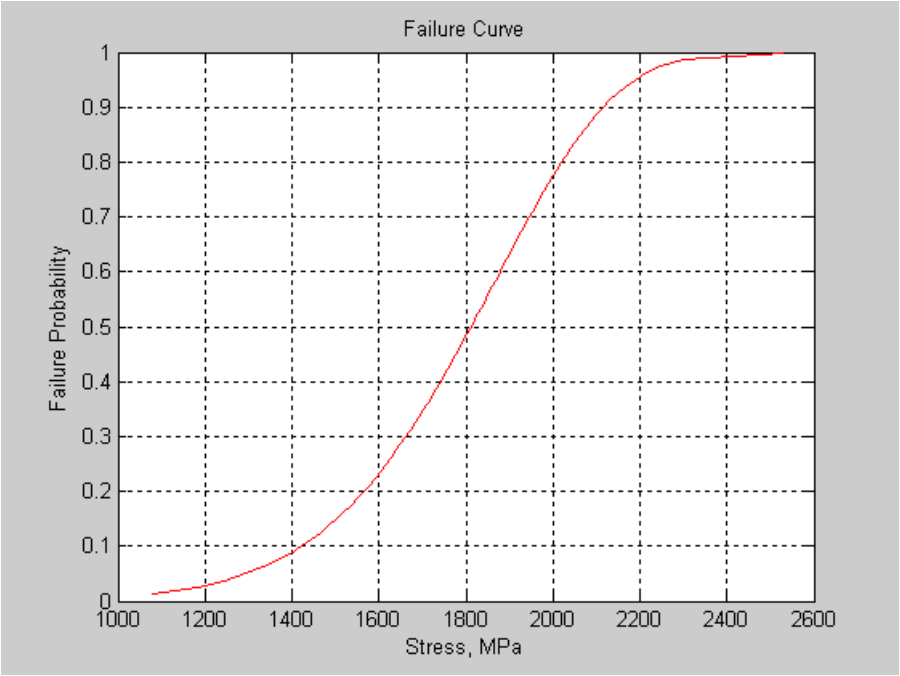

Figure 4.2.1.2. Weibull Failure Distribution for Kevlar® 49 yarn tensile tests

4.2.2. Weibull Parameters and Curve Fitting, Tsai-Hill Criterion

Several tests were effectuated on CFE composite laminates to determine its properties (Chapter 2) and those are used to determine the Weibull parameters in order to model the CFE composite behavior.

The two parameter version of equation (3.6.2) is used to model the composite behavior. The two parameters involved are the characteristic stress TH_0 and the Weibull modulus m, both are shown in equation (4.2.2.1).

$$P_f(TH) = 1 - \exp\left[-\left(\frac{TH}{TH_0}\right)^m\right] \qquad (4.2.2.1)$$

Using the data from chapter 2, 0_p / 90_t – 90_t / 0_p laminate (configuration C), a rough approximation was calculated to get the value of the average material direction's failure stresses (S_1, S_2) from the strength of the multiple oriented laminate. With those average values, an extrapolated distribution was created in order to define the Tsai-Hill failure value, giving it the value of 1 at the maximum failure stresses of all tests.

The S_{12} shear strength value was determined directly from the shear tests and for the sake of simplicity it was kept as a constant during the Tsai-Hill value calculation. Figure 4.2.2.1 shows the Tsai-Hill Failure plot for the fixed S_{12} value.

A detail of the extrapolated data is plotted in Table 4.2.2.1 showing the respective failure values and the Tsai-Hill value.

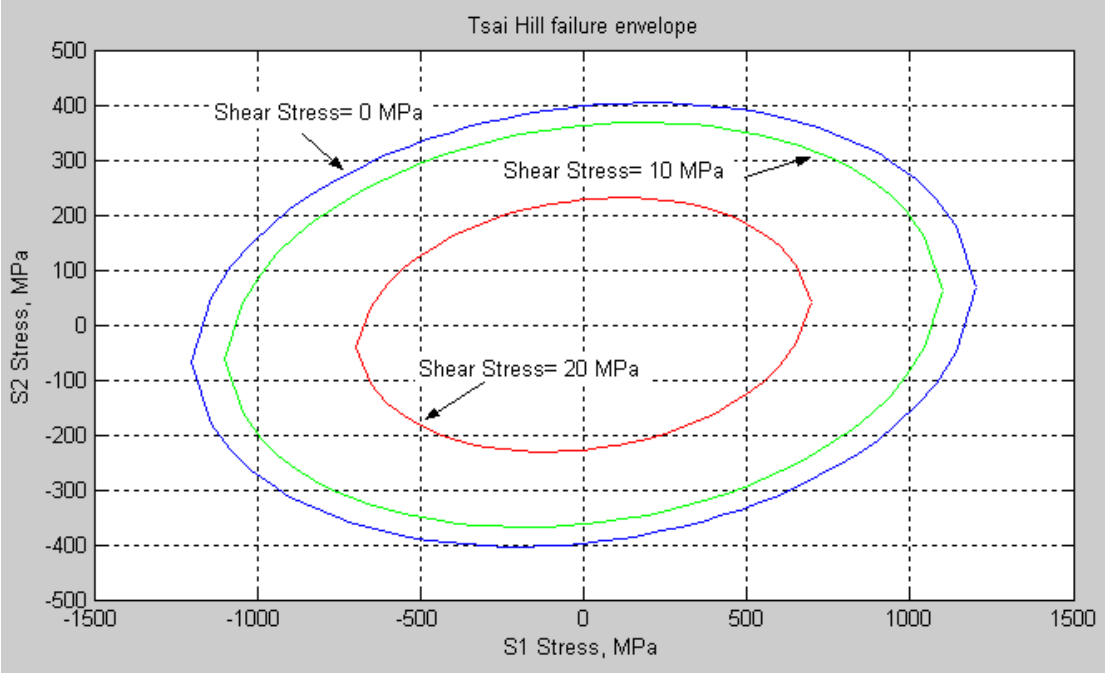

Figure 4.2.2.1. Tsai-Hill Failure Surfaces for several values of S_{12}

Table 4.2.2.1. Tsai-Hill values with their respective failure components

Strength	S1	S2	F1	F2	F12	TH
400	472	184	5.917E-07	5.165E-06	1.372E-03	0.26
420	495	193	5.917E-07	5.165E-06	1.372E-03	0.28
450	530	207	5.917E-07	5.165E-06	1.372E-03	0.32
500	590	230	5.917E-07	5.165E-06	1.372E-03	0.40
728	860	335	5.917E-07	5.165E-06	1.372E-03	0.85
735	868	338	5.917E-07	5.165E-06	1.372E-03	0.86
745	880	343	5.917E-07	5.165E-06	1.372E-03	0.89
760	897	350	5.917E-07	5.165E-06	1.372E-03	0.92
787	930	362	5.917E-07	5.165E-06	1.372E-03	0.99
792	935	365	5.917E-07	5.165E-06	1.372E-03	1.00

Using the data from Table 4.2.2.1 a linear failure probability was assembled, and with the data a Weibull fitting routine was applied to get the Weibull parameters. Those preliminary parameters are $TH_0 = 0.75$ and $m = 4.0$. With them as a starting point, the model will try to approach to the real stress-strain curve.

4.3. Simulation of Experimental Data

For the validation of the models, we selected several experimental cases that will apply to the specific model type or geometry. Such cases will include fabric experimental tests, multiple oriented composite laminate tests, and unidirectional composite laminate tests. One of these tests was taken from the literature, while the other two from actual tests done in the structural laboratory in Arizona State University.

4.3.1. Unidirectional Simplified Analytical Model Validation

Another set of tests evaluated at Arizona State University Structural Laboratory were the Kevlar® 49 fabrics tensile tests. A total of six tests were conducted in the warp direction. This warp direction test setup is shown in Figure 4.3.1.1.

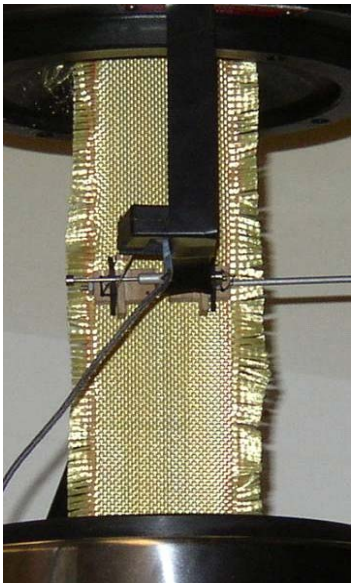

Figure 4.3.1.1. Uniaxial Tension test Setup for the warp direction of the fabric

Only the warp tensile test data was used to validate the model. Additional considerations in the model were taken:

- The low transversal interaction of the yarns made the Load Sharing rule avoidable.
- Poisson ratio effect could be denied, because the void space between the yarns allows the contraction without resistance or interaction between the yarns.
- The transversal young modulus (E_2) was denied since the lack of resistance in the transversal direction could cause sudden failure on the warp direction.

- The width will be considered as 2” and the thickness as 0.011” (equivalent values).

After all this considerations, the selected model was the **Strength-Weibull** model which has a similar behavior as the presented tests, Figure 4.3.1.2.

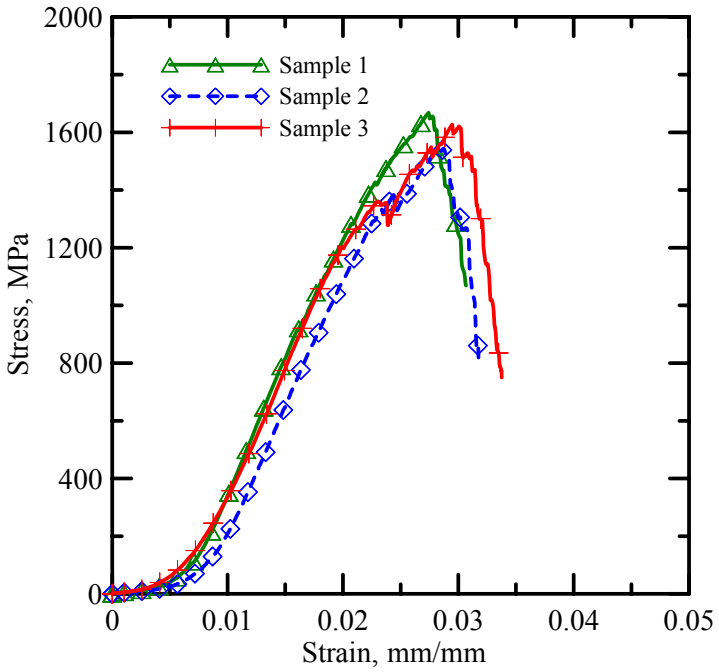

Figure 4.3.1.2. Kevlar® 49 warp direction uniaxial tensile stress-strain plots

The crimp region was ignored and the model was shifted closely to the initial elastic region. The Weibull parameters calculated before were used for the model and those values were: σ_0 = 1900 MPa and m = 7.74. In figure 4.3.1.3 the comparison, between these experimental tests and the simulation, is shown.

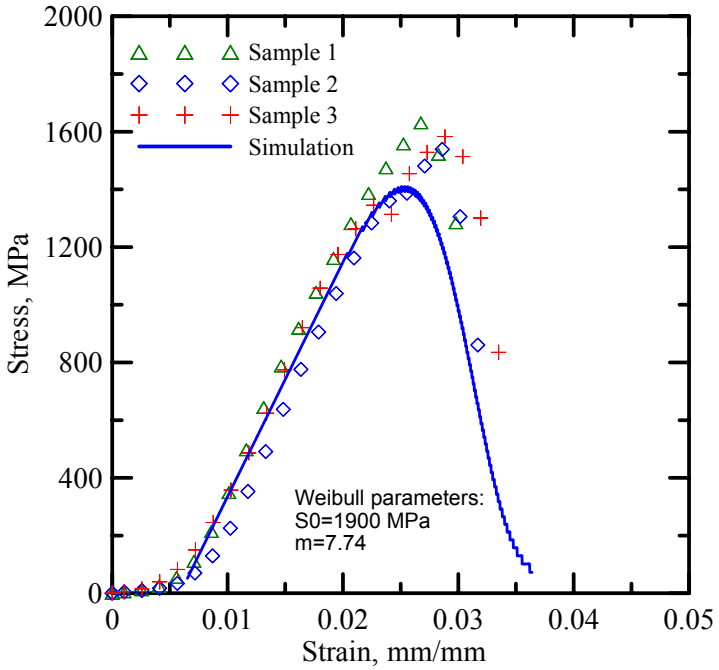

Figure 4.3.1.3. Kevlar® 49 warp direction uniaxial tensile tests and the simulation data

From the graph, there is an underestimation of the maximum stress value probably due the fact that we are neglecting any interaction of the warp yarns with the fill yarns and/or the crimp region effect. The elastic modulus was taken from the yarn tensile test data, as an average of the yarns that have 17" length. Therefore, the pre-peak behavior acted according to the experimental data. Post-peak behavior follows the tendency of progressive fiber damage and has the same slope as the experimental results. Several properties are shown, in Table 4.3.1.1, for the three experimental tests and the simulation, such as the strain at the peak stress, the strength, crimp strain, and respective errors. The error shown on the table is less than 10% of the experimental average for strength and strain at peak, the strength value is 2.375 standard deviation units below the average.

Table 4.3.1.1. Properties of the experimental and simulated Kevlar® 49 tests

Test Number	Strength MPa	Strain at peak mm/mm	Crimp strain mm/mm	Shifted strain peak
Sample 1	1668	0.027	0.007	0.02
Sample 2	1543	0.028	0.007	0.021
Sample 3	1626	0.029	0.007	0.022
Average	1612	0.028	0.007	0.021
St. Dv.	64	0	0	0
Simulation	1460	0.019	0	0.019
Error	**9.45**	**32.14**	**NA**	**9.52**

4.3.2. Unidirectional 2-D Analytical Model Validation

There is some publish experimental data on unidirectional tests on CFE composites and CF fiber bundles [Zhou Y. et al., 2006] that will be used to validate the Strength-Weibull-Load Sharing-2D model.

One type of carbon fibers (T700) with two types of matrices was investigated in the paper. The matrices used on the composite: neat epoxy and SiC nano-particle filled epoxy. The paper also evaluates the properties of the T700 CF bundles and finds the Weibull parameters for those bundles.

The statistical parameters of the fiber were obtained from tension tests of T700 fiber bundles. Three parameters were determined from the stress-strain experimental curves: Elastic modulus (E_1), tensile strength (σ_f), and failure strain (ε_f) and their average values are in Table 4.3.2.1 along with the epoxy matrices properties. The Weibull parameters for tensile strength of the carbon fibers were calculated and can also be seen in Table 4.3.2.1.

Table 4.3.2.1. T700 and matrices properties

Material	T700 CF	Neat Epoxy	Nano-phased epoxy
E_1(GPa)	210	2.45	3.32
G(GPa)	87.5	1.02	1.38
D(μm)	5	NA	NA
V_f(or V_m)(%)	49	51	51
m	**9.03**	NA	NA
σ_o(GPa)	**2.7**	NA	NA
σ_f(GPa)	NA	89	110
T(GPa)	NA	45	55

Figure 4.3.2.1 shows the experimental results of T700 CF and the simulation that used the Weibull modulus and the average properties previously mentioned. The characteristic strength was increased a small amount (**σ_o=2.9 GPa**) to compensate the length effect that is not included in the Weibull analysis subroutine of the model. The tensile stress-strain curve shows considerable amount of non-linearity. The specimen failed gradually after reaching the maximum stress due to the tensile strength distribution of fibers. The errors are tabulated in Table 4.3.2.2.

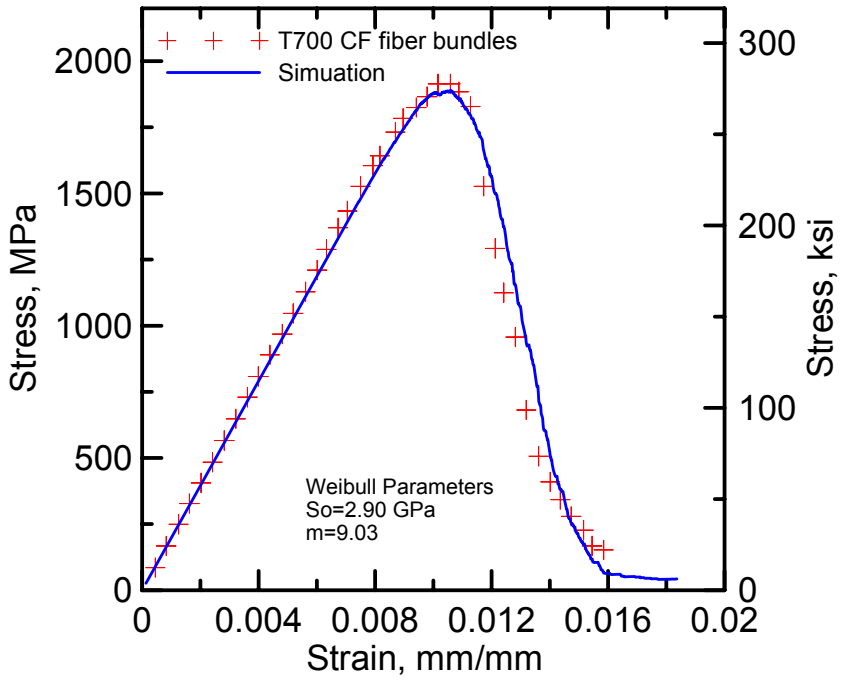

Figure 4.3.2.1. T700 CF bundles uniaxial tensile test and the simulation data

Table 4.3.2.2. Properties of the experimental and simulated CF bundles

Test Number	Strength MPa	Strain at peak mm/mm
Experimental	1914	0.0105
Simulation	1889	0.0106
Error (%)	**1.31**	**0.95**

Regarding the experimental tests on CF-epoxy matrices, no properties were given on the composite; therefore the model was implemented with a simple subroutine to get the composite properties from the components using the rule of mixtures to determine the values of E and G. Corrections on those values were made to adjust them to the experimental data. The analysis made on both composites is shown on Figure 4.3.2.2 and the errors and properties are shown in Table 4.3.2.3.

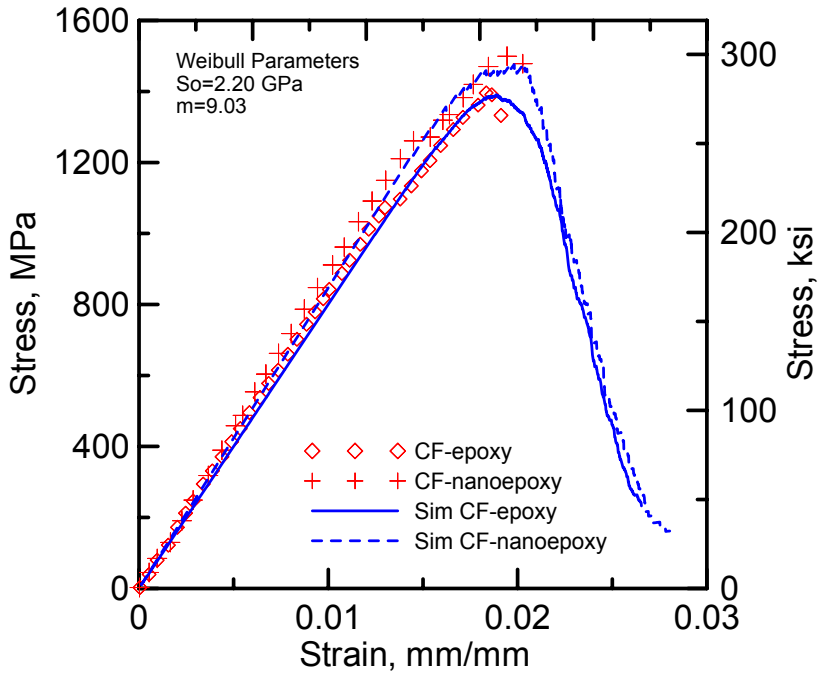

Figure 4.3.2.2. T700 CF composites uniaxial tensile tests and the simulated data

Table 4.3.2.3. Properties of the experimental and simulated CF composites

Test Number	Strength MPa	Strain at peak mm/mm
Experimental CF-Epoxy	1396	0.0185
Simulation CF-Epoxy	1390	0.0191
Error (%)	**0.43**	**-3.24**
Experimental CF-nano	1507	0.0201
Simulation CF-nano	1476	0.0198
Error (%)	**2.06**	**1.50**

From the graphs and tables, the model made a good approach to the real values, with the necessary adjustments to the Weibull characteristic strength. The elastic modulus calculated using the rule of mixtures was slightly higher than the experimental value probably due to the void content assumed in the rule of mixtures (initially zero), but after the correct adjustments the value was close to the experimental counterparts.

Pre-peak behavior acted according to the experimental data, but no information on the experimental post-peak behavior made the model unchecked in this region. The error levels shown on the table are less than 5% of the experimental data for strength and strain at peak, making the model trustworthy.

4.3.3. Multidirectional Simplified Analytical Model Validation

For the case of cross plied CFE laminate (tested and shown on Chapter 2), Figures 4.3.3.1 and 4.3.3.2 show the stress-strain response of the 0_p / 90_t – 90_t / 0_p (75% of the fibers/yarns are aligned in the 0˚ direction while the remaining are aligned in the 90˚ direction) and 0_t / 90_p – 90_p / 0_t (75% of the fibers/yarns are aligned in the 90˚ direction and the remaining 25% in the 0˚ direction) symmetrical laminates. The curves represent tensile stress-strain response in those laminates.

The final values used in the material model for the Weibull failure distribution were a characteristic Tsai- Hill value (TH_0) of 0.75 and a modulus (m) of 4.0. Regarding the material elastic properties, the value of the principal direction elastic modulus (E_1) was 85000 MPa, the major Poisson ratio (v_{12}) was 0.25, the transversal elastic modulus (E_2) was 6000 MPa, and the shear modulus (G_{12}) was 1800 MPa.

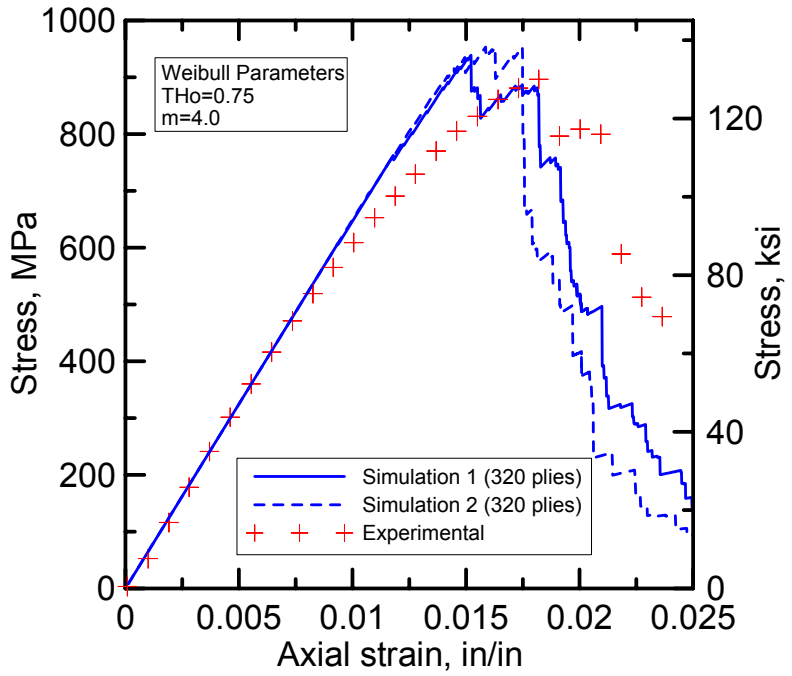

Figure 4.3.3.1. Two 0_p / 90_t – 90_t / 0_p laminate simulations with 320 plies compared to the experimental result of the same laminate configuration.

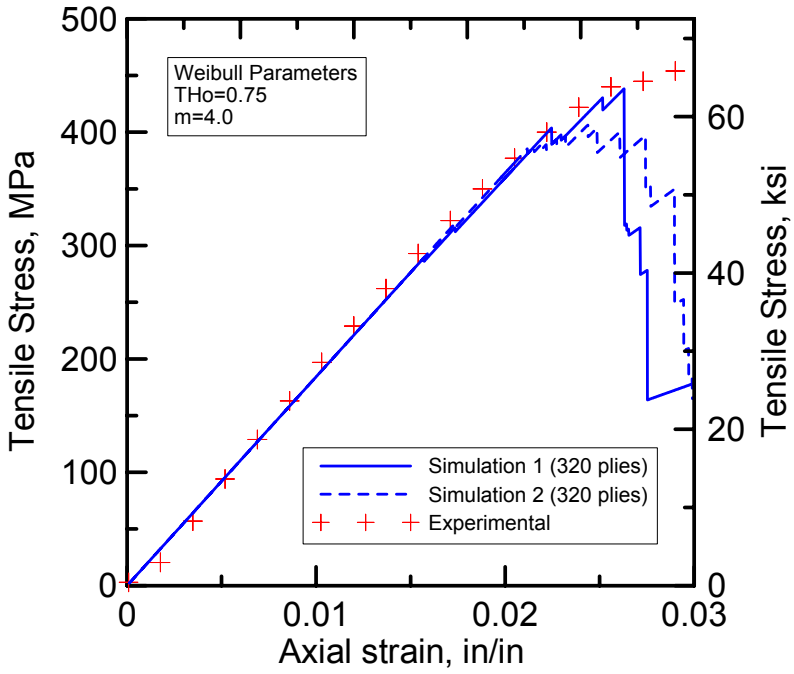

Figure 4.3.3.2. Two 0_t / 90_p – 90_p / 0_t laminate simulations with 320 plies compared to the experimental result of the same laminate configuration

From the graph, there is a small overestimation of the maximum stress value of the 0_p / 90_t – 90_t / 0_p, also the stiffness degradation is not as quickly as it is in the experiments, probably due the fact that we are using a wrong Weibull modulus and the data dispersion is greater than expected. The post-peak region behaves similarly to the experimental tests, with an accumulation of flaws that gives bigger load drops after the peak and a stress recovery after that. This behavior, due load sharing rules, simulates well the laminate configurations. The other laminate configuration simulation, 0_t / 90_p – 90_p / 0_t, shows a slightly lower strength value, while the pre-peak behavior followed the stiffness degradation quite well. Post-peak behavior is, for the experimental tests, a sudden failure, while the simulation still holds the stiffness degradation, but quicker compared to the other laminate configuration.

Several properties are shown, in Table 4.3.3.1, for the experimental tests and the simulations, such as the strain at the peak stress, the strength, initial stiffness degradation stress level, and respective errors.

Table 4.3.3.1. Properties of the experimental and simulated CFRP tests

Test Number	Strength MPa	Strain at peak mm/mm	Stress level at initial degradation
Laminate:	0_p / 90_t – 90_t / 0_p		
Experimental	902	0.018	400
Simulation 1	938	0.015	450
Simulation 2	954	0.016	480
Error (%)	**4.65**	**-16.13**	**13.98**
Laminate:	0_t / 90_p – 90_p / 0_t		
Experimental	458	0.029	380
Simulation 1	443	0.027	330
Simulation 2	409	0.025	315
Error (%)	**-7.51**	**-11.54**	**-17.83**

The error shown on the table for the 0_p / 90_t – 90_t / 0_p laminate is less than 5% of the experimental for strength (overestimation), while strain at the peak (underestimation) and the initial degradation stress (overestimation) have greater errors, probably due errors to determine the Weibull modulus or insufficient data for weaker tests.

For the 0_t / 90_p – 90_p / 0_t laminate the error in the strength is less than 10% of the experimental result (underestimation), while strain at the peak (underestimation) and the initial degradation stress (underestimation) have greater errors, especially the last one, probably due errors to determine the Weibull modulus or the underestimation of the 90˚ oriented plies strength.

5. FLEXURAL ANALYSIS OF A BEAM REINFORCED WITH CARBON FIBER-EPOXY LAMINATE

5.1. Introduction

The bonding of steel plates to reinforced concrete (RC) structures has been a popular method for strengthening deficient RC structures. But in recent years, there has been extensive research on the use of fiber-reinforced polymers (FRP) plates and/or sheets to replace steel plates in plate bonding. Also FRPs have also been used for column strengthening by external wrapping.

The common fibers used are carbon fibers, glass fibers and aramid fibers, whilst epoxy resins, polyester resins and vinylester resins are the common resins. Depending on the type of fibers used, FRP composites are classified as following: Carbon-Fiber-Reinforced-Polymer (CFRP); Glass-Fiber-Reinforced-Polymer (GFRP); and Aramid-Fiber-Reinforced-Polymer (AFRP). A useful general background on the composition of these materials and their mechanical properties can be found in ACI 440R.

The CFRP plate bonding was investigated at the Swiss Federal Laboratory for Material Testing and Research (EMPA) [Meier et al. 1993] where tests on RC beams strengthened with CFRP plates started in 1984. Being their main advantages the high strength-to-weight ratio and their high corrosion resistance. The former property leads to great ease in site handling, reducing labor cost and interruptions to existing services, while the latter ensures durable performance.

Pure uniform tension, compression and shear loadings must be individually applied to establish the fundamental strength and stiffness properties of a composite

material. A flexure test, bending of a beam, typically induces tensile, compressive and shear stresses simultaneously. Thus is not usually as a practical mean of determining the fundamental properties of a composite material. Nevertheless, flexure tests are popular, because of the simplicity of both specimen preparation and testing. Gripping of the specimen, the need of tabs, obtaining pure stress state, avoiding buckling, and most other concerns are out of question here.

5.2. Experimental Data

To determine the behavior of FRP reinforced concrete, several reinforced and unreinforced beams were tested at the Structural Laboratory at Arizona State University. Only CFRP samples were studied, and from those tests one and two fabric layer configurations were simulated. Figure 5.2.1 shows the typical equipment setup used for the tests. The CF fabrics used for the CFRP retrofit were provided by KPFF in a cross-ply configuration of stitched fabrics. The elemental properties of the CFRP were defined in Chapter 2.

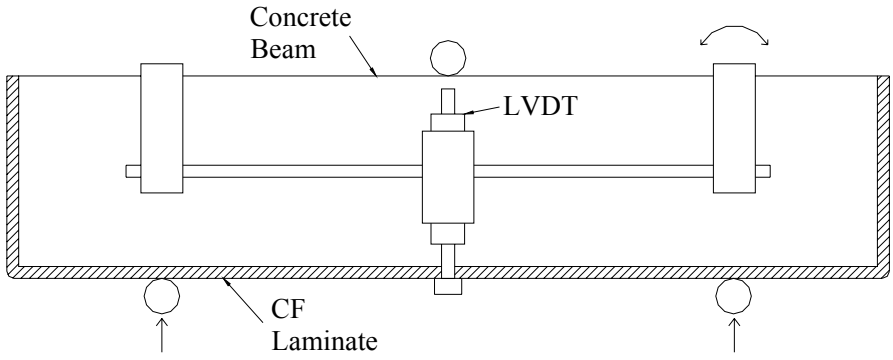

Figure 5.2.1. Setup of a CFRP reinforced concrete beam 3-point bending test

5.2.1. Equipment

- In accordance to ASTM E 4, an MTS servohydraulic testing machine with a capacity of 55 kips was used. All the testing procedures were developed using state of the art computer software. The test machine had the following characteristics:
- Testing machine heads: one stationary and one movable head.
- Drive mechanism: capable of imparting a controllable velocity with respect to the stationary head. The equipment was calibrated to 0.1% of the specifications by qualified and certified MTS technicians. All calibration files are on file in the Structural engineering laboratory.
- Load indicator: load range of interest of within +/- 0.1% of the indicated value.
- Three-point bending fixtures: Fixtures which are rotationally self-aligning to minimize unwanted stresses in the coupon.
- Strain indicating device: An electronic extensometer calibrated by certified technicians were used. The extensometer gage length had a range of 10 to 50 mm [0.5 to 2.0 in]. Extensometer used satisfied Practice E83, class B-1 requirements for the strain range and should be calibrated in accordance to the practice E83.
- All tests were conducted in nominal room temperature of 73°F. The temperature was maintained within +/-3˚C [+/-5˚F].

5.2.2. Testing Procedures

- Sampling: Concrete Beams were casted with the following dimensions: 4” x 4” x 18”, with a distance between supports of 12”and the tested was at 1 year.
- Retrofit: The CFRP laminates were added 35 days before the test, and pressure was applied to the samples during the curing time to increase the behavior of the beam.
- Speed of testing: nearly constant strain rate in the gage section, the strain rate was selected so as to produce failure within 1 to 10 min. For the constant head speed tests, the displacement rate was 2mm/min [0.05in/min].
- Transducer installation: A LVDT fixture was mounted on the sample to get an accurate measurement of the sample deflection.
- Throughout the duration of the test, the load versus strain (or transducer displacement) continuously at a frequency of 2 samples per second. During the test, any transition region or initial cracks were noted and the load, strain and mode of damage at such points were recorded.

5.2.3. Test Data

The three point bending tests results for the retrofitted beams are shown in Figure 5.2.3.1. The results are exclusive for the CFRP retrofitted samples, where 1 and 2 layers of CFRP reinforcement tests are shown.

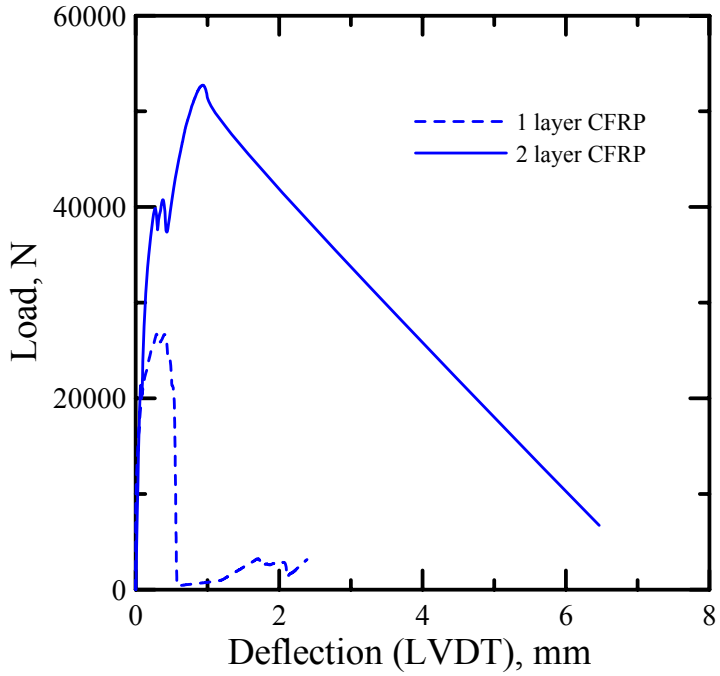

Figure 5.2.3.1. Load Deflection curves for 1 and 2 layers of CFRP retrofitted concrete beams

From the data can be inferred, the predominant failure mode observed for the CFRP retrofitted concrete beams consisted of shear cracks and debonding at the edges of the beam. The shear cracks can be seen in Figure 5.2.3.3 and 5.2.3.2, while the debonding can be observed in Figure 5.2.3.4.

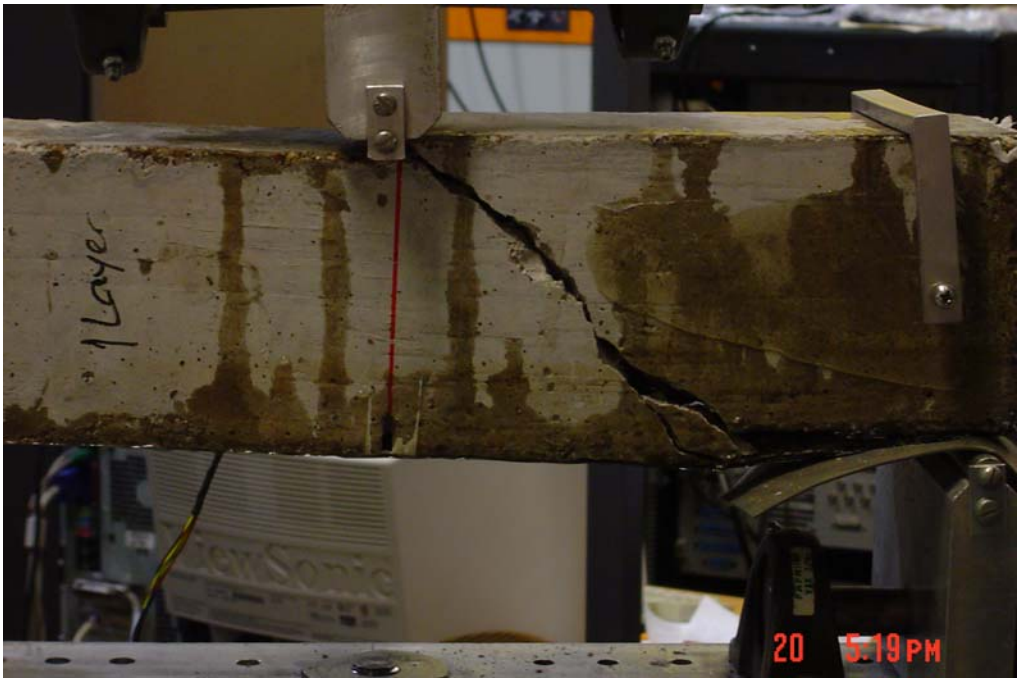

Figure 5.2.3.2. Failed CFRP 1 layer retrofitted sample

Figure 5.2.3.3. Failed CFRP 2 layers retrofitted sample

Figure 5.2.3.4. Debonding at the edges of the 2 layer CFRP reinforced concrete beam sample

5.3. Simulation and Validation

In this section the algorithm of the moment-curvature and load-deflection model is described. The validation is made using the pre-peak experimental data from the Concrete retrofitted with CFE laminates as shown in Figure 5.3.1.

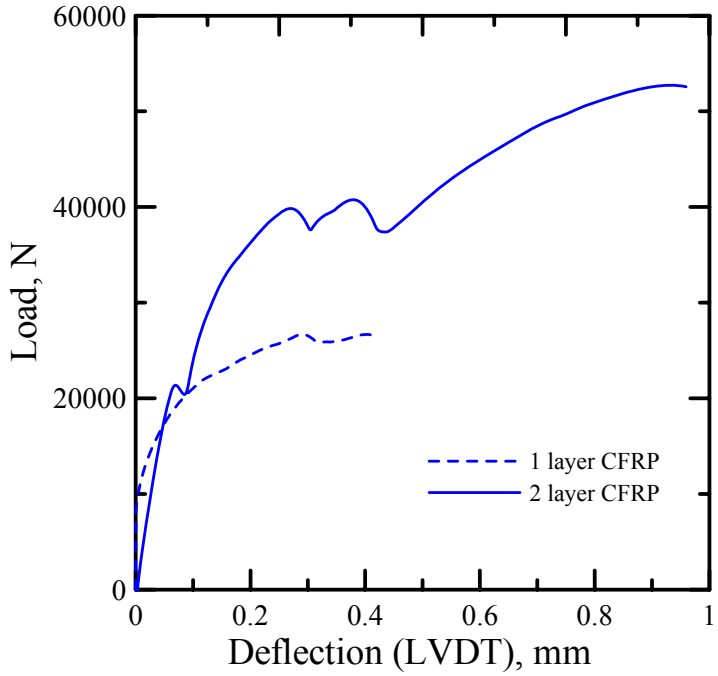

Figure 5.3.1. Load Deflection curves reduced to the pre-peak part

5.3.1. Algorithm of the Model

The simulation procedure is illustrated as following: (note: steps that need further explanation such as the material models will be explained in their respective section)

1. For concrete: input material geometry, beam width and depth, additionally some parameters of the constitutive behavior of the simplified material model.
2. For CFE composite: input material geometry (cross-sectional area), and parameters that will define the constitutive behavior of the simplified model.
3. Decomposition of the beam as several layers of concrete and the reinforcement, initialization of all parameters and properties, setup of the initial neutral axis location in the middle of the beam (middle layer).

4. Application of the first strain level at the top, giving the first values of the curvature, and with both of them (using beam theory) calculation of the strain at each layer of concrete and reinforcement.
5. Using the constitutive behavior of each material, the stress levels of each layer is calculated.
6. Knowing the areas and the stress levels, forces at each layer are calculated.
7. Equilibrium is measured, and if the equilibrium condition is not satisfied a relocation of the neutral axis is calculated according to the following conditions:

   If $\sum Fc > \sum Ft$ the neutral axis is shifted one layer up.

   If $\sum Fc < \sum Ft$ the neutral axis is shifted one layer down.
8. Repetition of steps 4 through 7 until equilibrium is close to be reached. Since the relocation of the neutral axis is discrete, when the equilibrium keep changing signs, at each iteration, that will mean that the neutral axis is located between those layers. Therefore, that situation will mark the position of the neutral axis.
9. Once the neutral axis position is found, the neutral axis parameter k, and the curvature is defined for this value.
10. The moment is calculated using the layer forces and their distances from the neutral axis.
11. Repetition of the steps 4 through 10 until the predetermined strain level.
12. The Moment-Curvature final plot is shown and specific points of the curve are collected.

13. With those Moment-Curvature points, the Load-Deflection bilinear curve is plotted according to the following equations [Soranakom and Mobasher, 2007]:

$$\delta_{bcr} = \frac{1}{12} L^2 \times \phi_{bcr} \tag{5.3.1.1}$$

$$\delta_u = \frac{L^2}{24 M_u{}^2} [(2M_u{}^2 - M_u M_{bcr} - M_{bcr}{}^2)\phi_u + (M_u{}^2 + M_u M_{bcr})\phi_{bcr}] \tag{5.3.1.2}$$

$$P_{bcr} = \frac{2M_{bcr}}{L/2} \tag{5.3.1.3}$$

$$P_u = \frac{2M_u}{L/2} \tag{5.3.1.4}$$

Where ***δ*** means deflection, ***M*** means moment, and the suffixes ***bcr*** and ***u*** mean cracking and ultimate respectively.

5.3.2. Materials Simplified Models

In this simulation two material models acting together as part of the beam were developed. The CFRP composite was developed using the experimental data gathered in Chapter 2 as a trilinear model, where each portion was well understood in Chapter 4.

The trilinear model is shown in Figure 5.3.2.1, there it can be seen the three parts of the model. In Chapter 4 the first part comprehends the linear elastic part and the initial cracks and failures that bring the decaying stiffness until the peak stress. This part was simplified and modeled as a perfectly elastic region with its stiffness reduced since it is a

linear fit of both elastic and initial failure regions. The second part, the strain-softening region, was introduced in Chapter 4 as a region were the failures were significantly numerous and the stiffness and capacity of the laminate were severely reduced, but not enough for total failure. The model also used a linear fit to approach the behavior. Finally, the third part, Chapter 4 described it as a quick decay of the remaining stiffness and capacity of the laminate, is modeled as the high slope failure of the laminate until it reaches a zero stress.

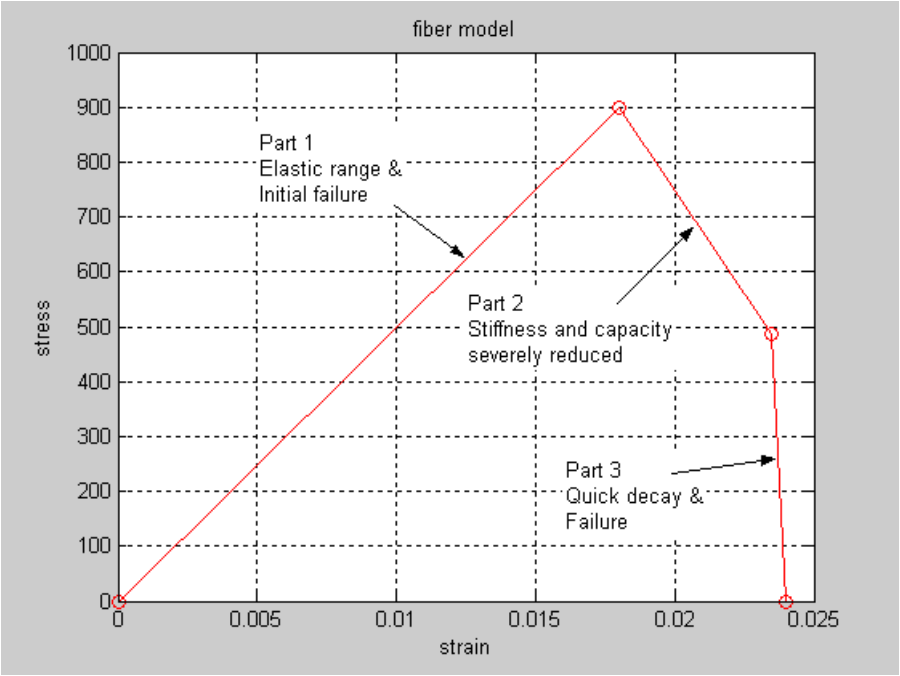

Figure 5.3.2.1. Simplified trilinear tension model for the CF laminate

The stress-strain relation for the concrete model, in the compression region, is characterized by the Hognestad parabola whereas the tension region is characterized by a trilinear model, as shown in Figure 5.3.2.2. The Hognestad parabola is defined using the strength value, the strain value at the peak, and the ultimate strain. The trilinear tension

model is defined by the tensile strength, the strain at the peak, the tensile strain at the post-peak and the ultimate strain.

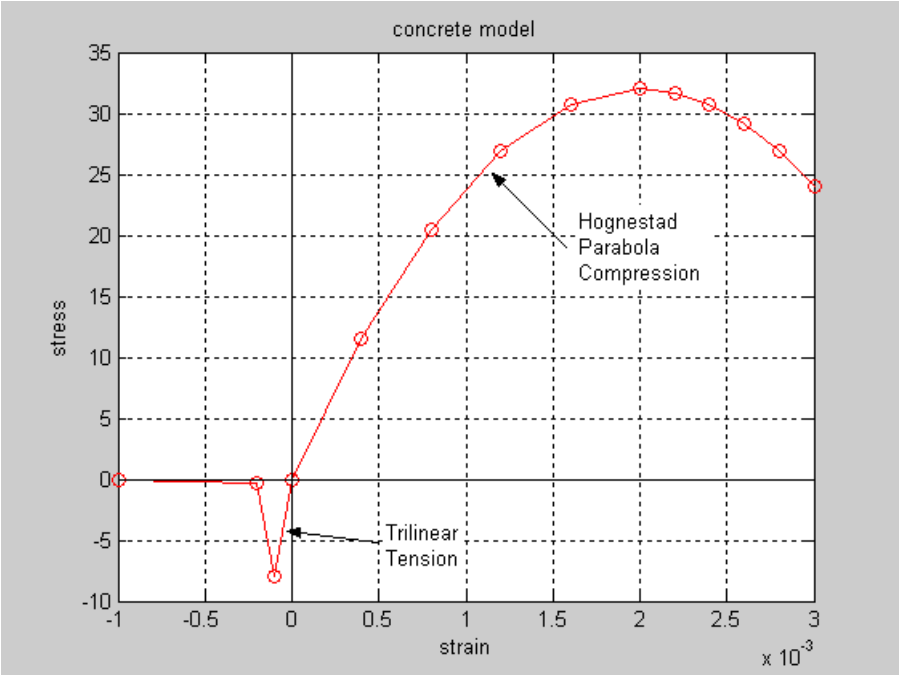

Figure 5.3.2.2. Concrete tension/compression model

5.3.3. Validation of the Model

For the validation of the model we reduced the experimental data to the pre-peak part as shown in Figure 5.3.1. The model will use the following values for the concrete constitutive behavior:

Number of concrete layers	= 1000
Width (mm)	= 102
Depth (mm)	= 102
Ultimate Compressive Strain	= 0.003
Strain at Peak Stress	= 0.002

Uniaxial Compressive Stress (MPa) = 32

Tensile Stress at first cracking = 0.0001

Uniaxial Tensile Strength (MPa) = 8

Tensile Strain at Post Peak = 0.0002

Residual Tensile Strain = 0.35

Ultimate Tensile Strain (strength=0) = 0.001

For the composite material the following values were applied to the constitutive behavior model (the values in parenthesis are for the 2 layer test):

Number of layers of CFE = 1

Area of the layer (mm^2) = 180 (360)

Location of the layer(s) (mm) = 102

Strain at peak Stress = 0.018

Strength (MPa) = 900

Post Peak Strain = 0.0235

Post peak Stress (MPa) = 487

Ultimate Strain (Stress=0) = 0.024

The results of the 1 layer CFE laminate retrofit is shown in Figure 5.3.3.1, while the 2 layer retrofit is shown in Figure 5.3.3.2. One of the assumptions of the model for the 2 layer configuration was that the two layers acted as a single layer with twice the area.

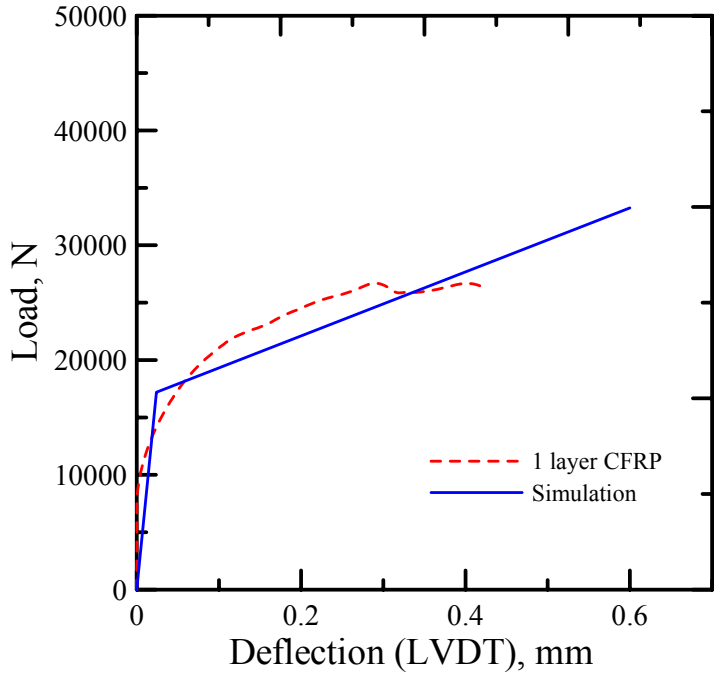

Figure 5.3.3.1. Concrete beam retrofitted with CFE laminates (1 layer)

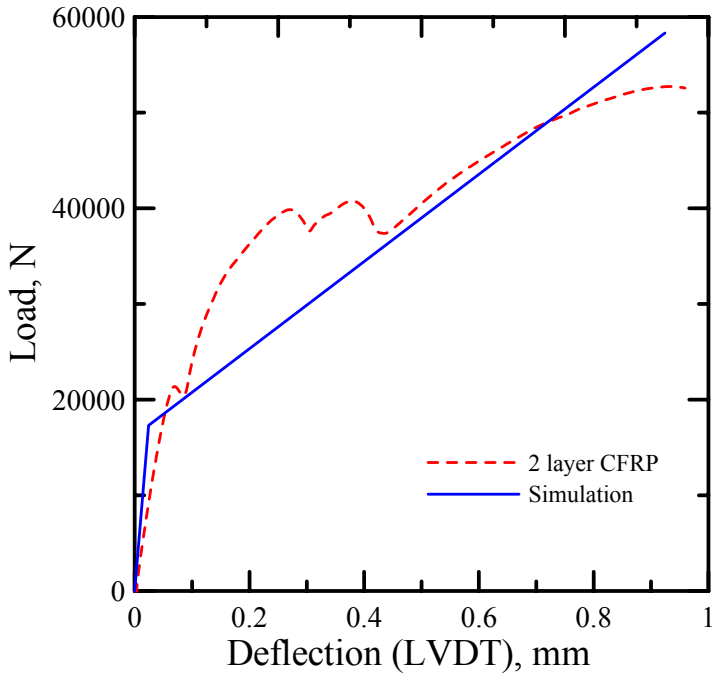

Figure 5.3.3.2. Concrete beam retrofitted with CFE laminates (2 layers)

The result of the simulation for the one layer retrofitted beam simulation gave greater values than the ones shown on Figure 3.3.3.1. Being the maximum load 46,702 N at a strain of 1 mm. Therefore, the plot will show a reduced version of the graph. The experimental mode of failure, for this configuration, is characterized by shear and before any visible damage on the CFE laminate happened, debonding between the concrete and the laminate occurred. That is reflected, in the plot, as a lower load capacity.

For the two layers retrofitted beam bilinear simulation, the values are close to the experimental results as shown in Table 3.3.3.1. The debonding between the CFE laminate and the concrete happened at a later stage giving the sample a better behavior.

Table 5.3.3.1. Properties of the experimental and simulated 3 point bending tests

Test	Load N	Deflection mm
Retrofit:	1 CFE layer	
Experimental	26700	0.45
Simulation 1	46702	1.00
Error (%)	**72**	**120**
Simulation 2	26850	0.45
Error (%)	**0.56**	**0.00**
Retrofit:	2 CFE layers	
Experimental	52730	0.94
Simulation	58316	0.93
Error (%)	**10.10**	**1.06**

For the two CFE layer retrofitted beam, the neutral axis factor (defined as the position of the neutral axis form the top divided by the depth of the beam) is shown in Figure 5.3.3.3 for several strain levels, while the displacement of it is shown on Figure

5.3.3.4. The constitutive behavior of the concrete is shown in the beam for several strain levels in Figure 5.3.3.5.

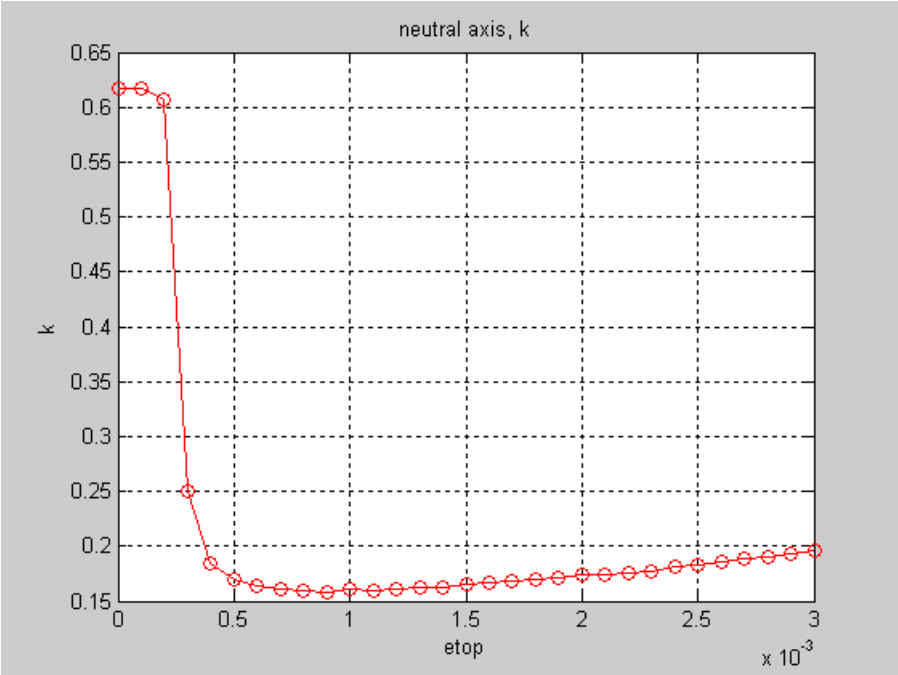

Figure 5.3.3.3. Neutral axis factor k for several strain levels

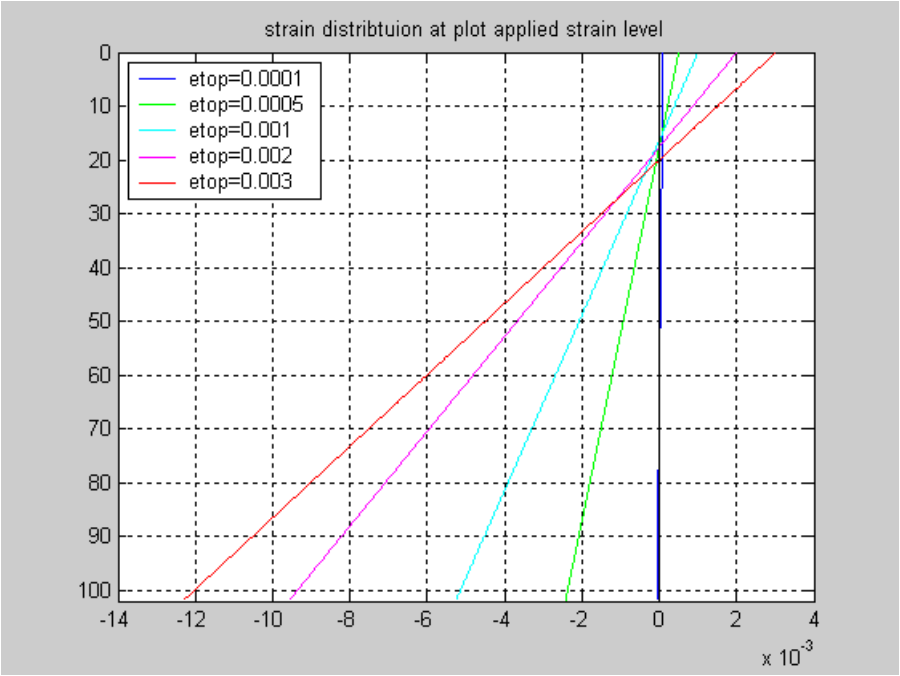

Figure 5.3.3.4. Neutral axis location in the 2 layer retrofitted beam

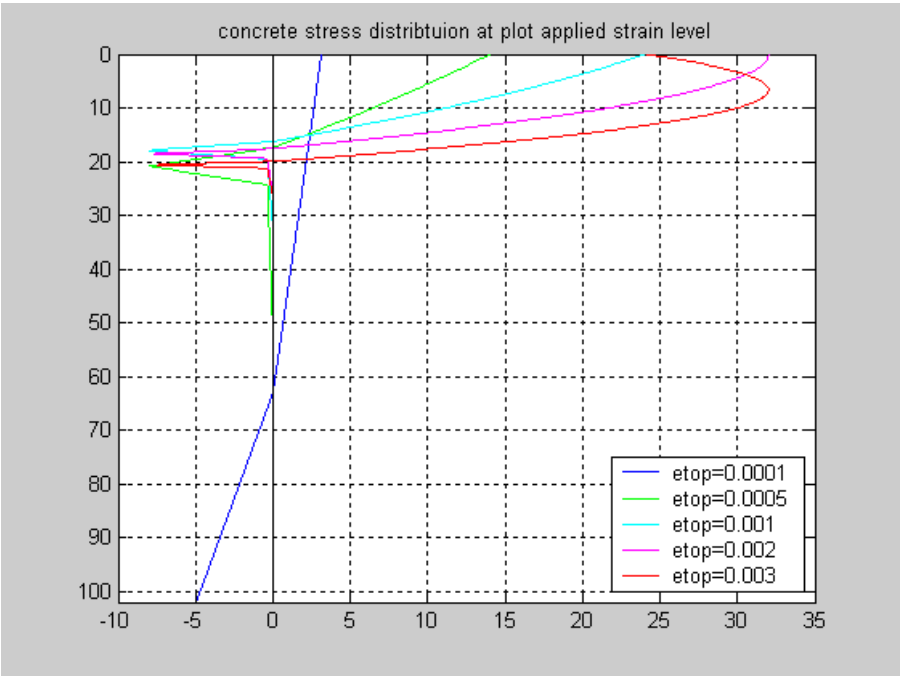

Figure 5.3.3.5. Stress-Strain Concrete curve for several strain levels

The moment curvature plot, shown in Figure 5.3.3.6, shows the deflection softening characteristic of samples with low post-peak tensile strength.

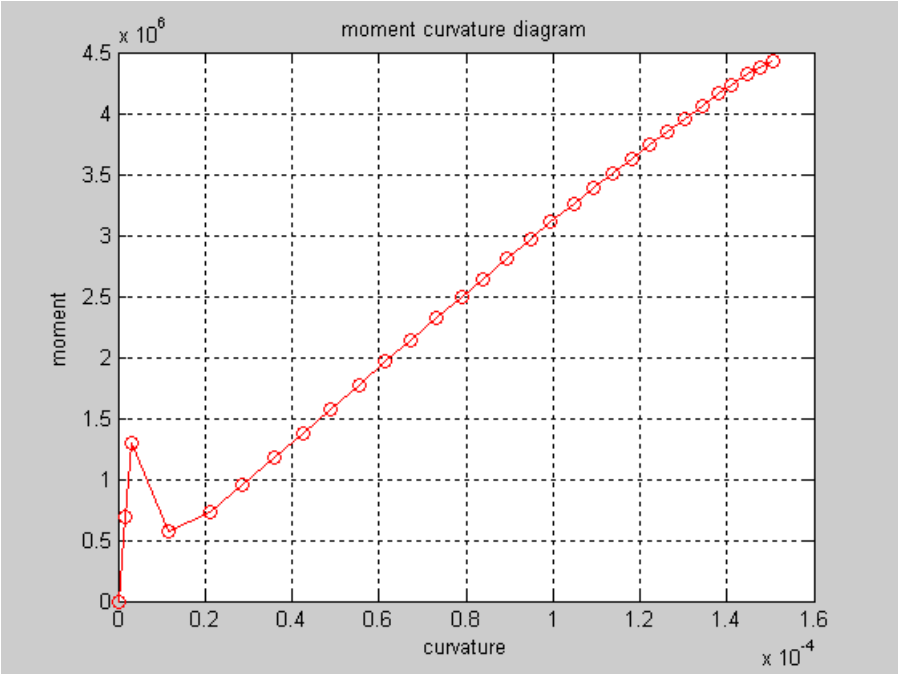

Figure 5.3.3.6. Moment-Curvature plot for the 2 CFE layer retrofitted beam

6. SUMMARY AND CONCLUDING REMARKS

The development of a material model to predict the behavior of carbon fiber composites and its application for reinforcing/retrofitting concrete beams was accomplished in this thesis. As shown on Chapter 4, the different scales of the model can be applied to different types of fibers and composite tests subjected to tensile loads.

The simulation of the reinforced concrete beams subjected to three point bending were developed using a bilinear model (load deflection curve) for one and two layers of retrofitted carbon fiber composites (CF using a trilinear model). The simulation can be carried for several different composites acting as an additional reinforcement for the concrete beam; the principal restriction of the model is that the reinforcement must be continuous along the beam length. Those reinforcements can also be taken as internal steel rebars or layers of cement AR glass composites, commonly used to this type of retrofit.

6.1. Experimental Results

The accuracy of the CFRP laminate tests, tension, compression and shear, depends mostly on the equality of the composite preparation, the damage on the fibers and the testing conditions.

Damage of the fibers is made during the manufacturing process, the handling of the fibers and the stitching process, therefore is something out of our control. The composite preparation depends on the manufacturing procedure, including environmental conditions (temperature, humidity, etc.), applied pressure on the finished laminate,

volume fraction control, void content, etc. Most of the samples tested were given to us directly from the field conditions, therefore control of those factors were also out of our reach. Some samples were manufactured in the laboratory to make a comparison on applied pressure effects, alignment of the principal direction yarns, etc. The most important being the applied pressure on the laminate during consolidation, since it has a direct effect on the void volume and the volume fractions of the composite. The testing conditions were the only factor that we really could manage well. We tried to keep the environmental conditions, gripping and clamping conditions, and general procedure as close as possible between tests to minimize effects from that factor.

All the samples came from very similar applied pressure conditions, lab errors also to the minimum; therefore the experimental characterization of those samples was with a medium to low variability. As seen on Chapter 2, the modulus errors were small, and the strength values were close, but their difference is better explained as part of the distribution of strength inherent in the fiber manufacturing conditions.

Errors were found on the composite manufacturing conditions. Flaws such as lack of impregnation, high void contents were not common, and those made a big difference on the results and therefore were taken out of the experimental analysis.

6.2. Validation Results

Depending on the specific conditions or the complexity several models were developed. The first division was to consider specific orientations, unidirectional or

multidirectional. Inside the unidirectional model classification, further classifications were taken such as the effects of load sharing and cell configuration for load distribution.

The first model, based solely on the Weibull strength distribution, works better with yarn tests, which do not have load interaction between the fibers that compose the yarn filaments. This assumption taken to model the behavior of Kevlar® 49 warp direction uniaxial tensile tests gave results with errors of 10%, due the fact that the interaction between warp and fill yarns was ignored. The friction that the geometric arrangement gives to the fabric and the restriction in the z-direction during loading must not be ignored for future studies. The model was later used to model the T700 CF yarns with a respectable accuracy of 1% error. For both validations the model gave an accurate behavior of the stress-strain curves.

The second model added the simplified load sharing rule, which means that applies better to composites, where the load can be transferred to other laminae. With proper considerations and a better understanding of the warp-fill yarn interaction this model can be used to predict with reasonable accuracy those tests.

And finally, the third model used a 2-D cell geometry to give a better interaction between the laminae and the possibility of the creation of transversal cracks due stress concentrations and load sharing rules. From the data in Chapter 4, you can see clearly the stages of the transversal crack formations. The prediction, based on yarn test data, for T700 CF and epoxy matrices gave an accuracy of around 2%. Post peak behavior could not be analyzed due the lack of data.

On the other side, the multidirectional models, three subsequent models were developed based on the Tsai-Hill criterion. The first model used the Tsai-Hill criterion alone to give instant failure values. The second model couples the Weibull distribution with the Tsai-Hill criterion to evaluate failure at a distribution of those Tsai-Hill values (below 1). Even using the random generation of the Tsai-Hill failure value, the behavior of the curve is unaltered from the laminate point of view. That means that for the same Weibull parameters and material properties, the stress-strain curve follows the same path for the laminate analysis. The random behavior for the laminate was truly introduced in the model update, third model, using the load sharing rule allowing sudden failures of other laminae, and reducing the stiffness and strength overall. This model was tested with the experimental data of Chapter 2 for two specific configurations giving good results for strength and general behavior. The sudden drop on the stiffness, in the elastic part, could not be mimicked by the model probably due some uncounted variables such as void content or a slight change in orientation of certain laminae. Another possible variable is that Tsai-Hill method over predicts the compression strength of the laminae, therefore allowing the laminate to carry additional load without failure.

6.3. Retrofitted Beam Results

Chapter 5 dealt with both experimental and analytical results of the retrofitted concrete beam tests. The experimental results failed under shear and debonding conditions. The simulation based on a very simplified composite model (trilinear model) based its failure criteria on material failure and the predictions were much higher

compared to the experimental data. The validation was adjusted later to the strain level were debonding occurred and the data was reasonable accurate. The behavior prediction, even if it was a bilinear load-deflection curve, was accurate. The model is prepared for using different materials, but the proper composite constitutive behavior must be used for each specific case.

6.4. Future Work

Cement base composites, brittle matrix, can be used in the 2-D cell model with some additional features, such as matrix cracking, pullout and bridging effects added for the individual cells.

The CFRP laminate tests could not provide with accurate Weibull values, therefore yarn tests would be mandatory for future characterization of the CF fabrics.

Pullout tests can be used as a base for getting the interaction values of the warp-fill yarns. Coupled with a strong knowledge of the interaction the unidirectional models can be improved to make an increase in the accuracy of the predicted values.

Experimental data for the three point bending retrofitted concrete beam tests is available for Cement-AR Glass and Cement-PE composites. Tensile modeling of those materials can be deduced and tested with available data in order to model the beam behavior and further the model validation and limitations.

7. REFERENCES

1. American Concrete Institute, *Building Code Requirements for Structural Concrete,* ACI 3: 18-99, 1999.

2. ASTM Standards, *Standard Test Method for Tensile Properties of Polymer Matrix Composite Materials D3039/D3039M-00*, ASTM International, West Conshocken, PA, 2000, www.astm.org.

3. ASTM Standards, *Standard Test Method for Tensile Properties of Plastics D638-03,* ASTM International, West Conshocken, PA, 2003, www.astm.org.

4. ASTM Standards, *Standard Test Method for Determining the Compressive Properties of Polymer Matrix Composite Laminates Using a Combined Loading Compression (CLC) Test Fixture D6641/D6641M-01,* ASTM International, West Conshocken, PA, 2001, www.astm.org.

5. ASTM Standards, *Standard Test Method for In-Plane Shear Response of Polymer Matrix Composite Materials by Tensile Test of a ±45° Laminate D3518/D3518M-94,* ASTM International, West Conshocken, PA, 1994, www.astm.org.

6. Carlsson, L.A., Pipes, R.B., *Experimental Characterization of Advanced Composite Materials*, Prentice-Hall Inc., Englewood Cliffs, New Jersey, 1986.

7. Cheng, T., Qiao, R., Xia, Y., "A Monte Carlo Simulation of Damage and Failure Process with Crack Saturation for Unidirectional Fiber Reinforced Ceramic Composites," *Composites Science and Technology* 2004, 64: 2251-2260.

8. Christensen, R.M., *Mechanics of Composite Materials*, John Wiley & Sons, Inc., New York, 1979.

9. Curtin, W.A., "Theory of Mechanical Properties of Ceramic-Matrix Composites," *Journal of the American Ceramic Society* 1991, 76: 2837-2845.

10. Curtin, W.A., "The "Though" to Brittle Transition in Brittle Matrix Composites," *Journal of Mechanics and Physics of Solids* 1993, 41: 217-245.

11. Curtin, W.A., Zhou, S.J., "Influence of Processing Damage on Performance of Fiber-Reinforced Composites," *Journal of Mechanics and Physics of Solids* 1995, 43: 343-363.

12. Curtin, W.A., Ahn, B.K., Takeda, N., "Modeling Brittle and Tough Stress-Strain Behavior in Unidirectional Ceramic Matrix Composites," *Acta Materialia* 1998, 46: 3409-3420.

13. Curtin, W.A., "Tensile Strength of Fiber-Reinforced Composites: III. Beyond the Traditional Weibull Model for Fiber Strength," *Journal of Composite Materials* 2007, 34: 1301-1331.

14. Daniel, I.M., "Failure of Composite Materials," *Strain* 2007, 43: 4-12.

15. Gao, Z., "Reliability of Composites Materials under General Plane Loadings," *Journal of Reinforced Plastics and Composites* 1993, 12: 430-456.

16. Gay, D., Hoa, S.V., Tsai, S.W., *Composite Materials, Design and applications,* CRC Press, New York, New York, 2003.

17. Hahn, H.T., "Simplified Formulas for Elastic Moduli of Unidirectional Continuous Fiber Composites," *Composites Technology Review* 1980, 3:5-7.

18. Harlow, D.G., Phoenix, S.L., "Probability Distribution for the Strength of Composite Materials 1: Two level bounds," *International Journal of Fracture* 1981, 17: 321-336.

19. Hinton, M.J., Kaddour, A.S., Soden, P.D., "A Comparison of the Predictive Capabilities of Current Failure Theories for Composite Laminates, judged against Experimental Evidence," *Composite Science and Technology* 2002, 62: 1725-1797.

20. Hollaway, L.C., Leeming, M.B., *Strengthening of Reinforced Concrete Structures - Using Externally-Bonded FRP Composites in Structural and Civil Engineering,* Woodhead Publishing, Cambridge, England, 1999.

21. Kasal, B., Leichti, R.J., "State of the Art in Multiaxial Phenomenological Failure Criteria for Wood Members," *Prog. Struct. Engng. Mater.* 2005, 7: 3-13.

22. Mallick, P.K., *Fiber Reinforced Composites, Materials, Manufacturing, and Design,* Marcel Dekker, Inc., New York, New York, 1993.

23. Miki, M., Murotsu, Y., Tanaka, T., Shao, S., "Reliability of Unidirectional Fibrous Composites," *AIAA Journal* 1990, 28: 1980-1986.

24. Mobasher, B., Li, C.Y., "Mechanical Properties of Hybrid Cement-Based Composites," *ACI Materials Journal* 1996, 93: 284-293.

25. Mobasher, B., Shah, S.P., "Test Parameters for Evaluating Toughness of Glass Fiber-Reinforced Concrete Panels," *ACI Materials Journal* 1989, 39: 547-555.

26. Naaman, A.E., Park, S.Y., Lopez, M.M., Till, R.D., "Parameters Influencing the Flexural Response of RC Beams Strengthened using CFRP Sheets," *FRPRCS-5*, University of Cambridge, UK, 2001, 5: 117-125.

27. Peebles, L.H., *CARBON FIBERS Formulation, Structure, and Properties,* CRC Press, New York, New York, 1995.

28. Phoenix, S.L., Smith, R.L., "A Comparison of Probabilistic Techniques for the Strength of Fibrous Materials under Local Load-Shear among Fibers," *International Journal of Solids Structures* 1983, 19: 479-496.

29. Soranakom, C., Mobasher, B., "Closed Form Solutions for Flexural Response of Fiber-Reinforced Concrete Beams," *Journal of Engineering Mechanics* 2007, 133: 933-941.

30. Swamy, R.N., Mukhopadhyaya, "Debonding of Carbon-Fiber-Reinforced Polymer Plate from Concrete Beams," *Structures and Buildings* 1999, 134: 301-317.

31. Teng, J.G., Chen, J.F., Smith, S.T., Lam, L., *FRP-strengthened RC Structures*, John Wiley & Sons, LTD, Chichester, West Sussex, England, 2002.

32. Turon, A., Costa, J., Maimi, P., Trias, D., Mayugo, J.A., "A Progressive Damage Model for Unidirectional Fiber-Reinforced Composites based on Fiber-Fragmentation. Part I Formulation," *Composites Science and Technology* 2005, 65: 2039-2048.

33. Vinson, J.R., Sierakowski, R.L., *The Behavior of Structures Composed of Composite Materials,* Kluwer Academic Publishers, Dordrecht, Netherlands, 2002.

34. Weibull, W., "The Phenomenon of Rupture in Solids," *Proc. Ing. Vetenskapsakad* 1939, Number 153.

35. Weibull, W., "A Statistical distribution function of wide applicability," *Journal of Applied Mechanics* 1951, 18: 293-297.

36. Whitney, J.M., Daniel, I.M., Pipes, R.B., *Experimental Mechanics of Fiber Reinforced Composite Materials,* Society for Experimental Mechanics, Englewood Cliffs, New Jersey, Prentice-Hall, 1984.

37. Xia, Z., Curtin, W.A., "Tough-To-Brittle Transitions in Ceramic-Matrix Composites with Increasing Interfacial Shear Stress," *Acta Materialia* 2000, 48: 4879-4892.

38. Yen, C., Jones, M.L., "Material Modeling for Cross-Ply Ceramic Matrix Laminates with Progressive Damages and Environmental Degradation," *MSC Technical Report, NASA Contract NAS3-27144*, 1997.

39. Zhou, Y., Baseer, M.A., Mahfuz, H., Jeelani, S., "Monte Carlo simulation on tensile failure process of unidirectional carbon fiber reinforced nano-phased epoxy," *Materials Science and Engineering* 2006, 420:63-71.

40. Zweben, C., Rosen, B.W., "A Statistical Theory of Materials Strength with Application to Composite Materials," *Journal of Mechanics and Physics of Solids* 1970, 18: 189-206.

APPENDIX A

CARBON FIBER EPOXY COMPOSITE LAMINATES EXPERIMENTAL TESTS

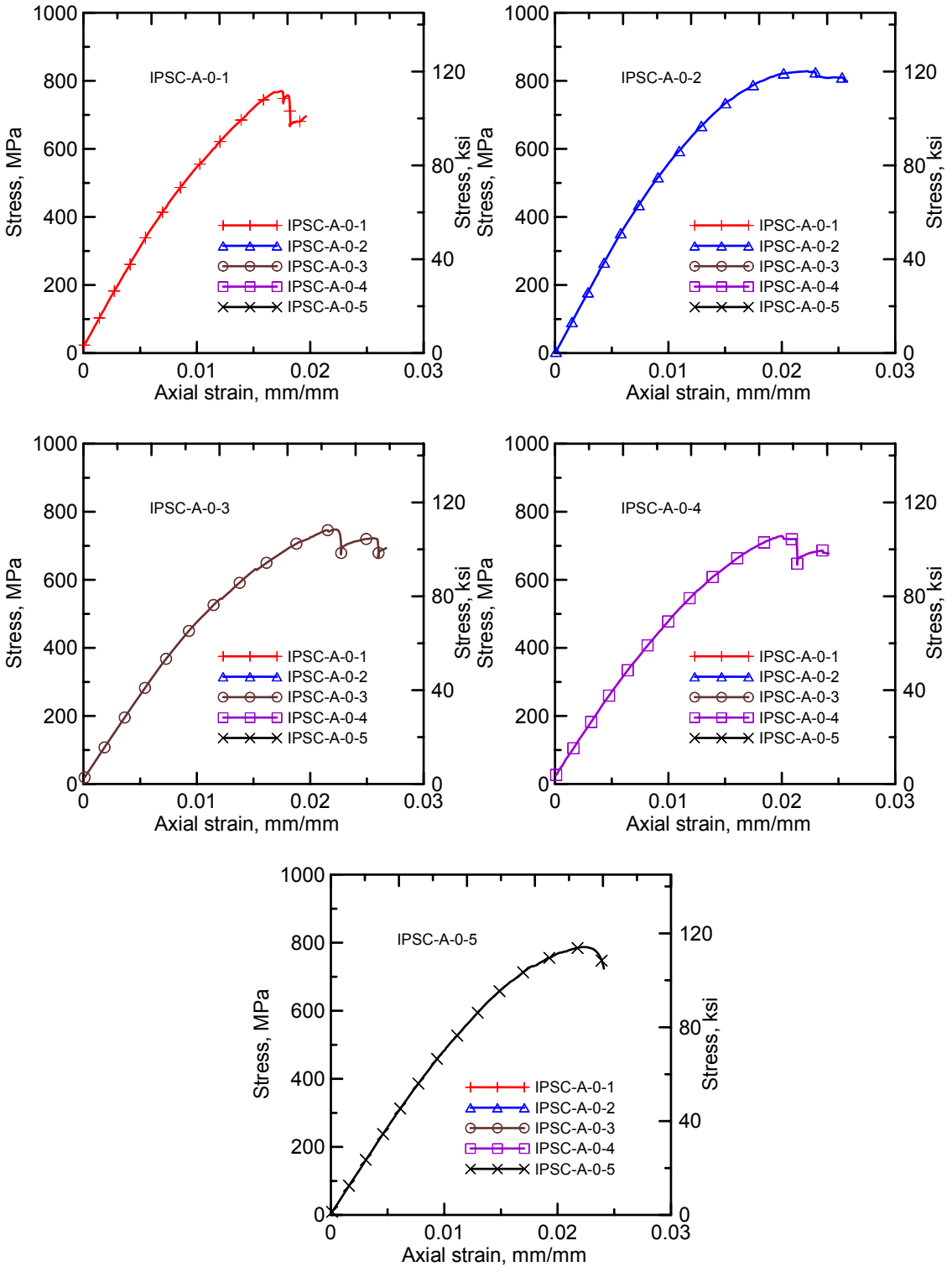

Figure A.1. CFRP configuration A tension tests

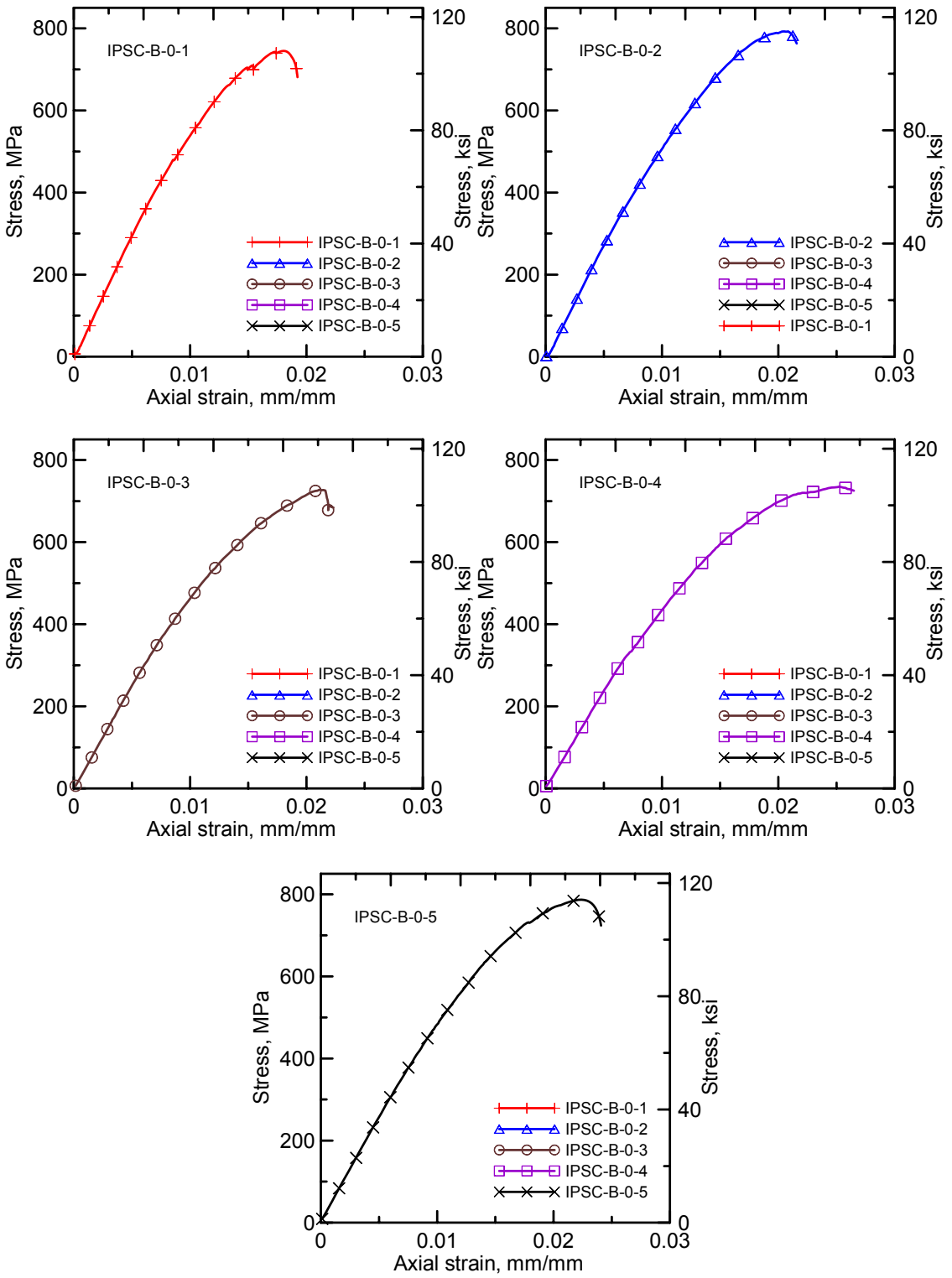

Figure A.2. CFRP configuration B tension tests

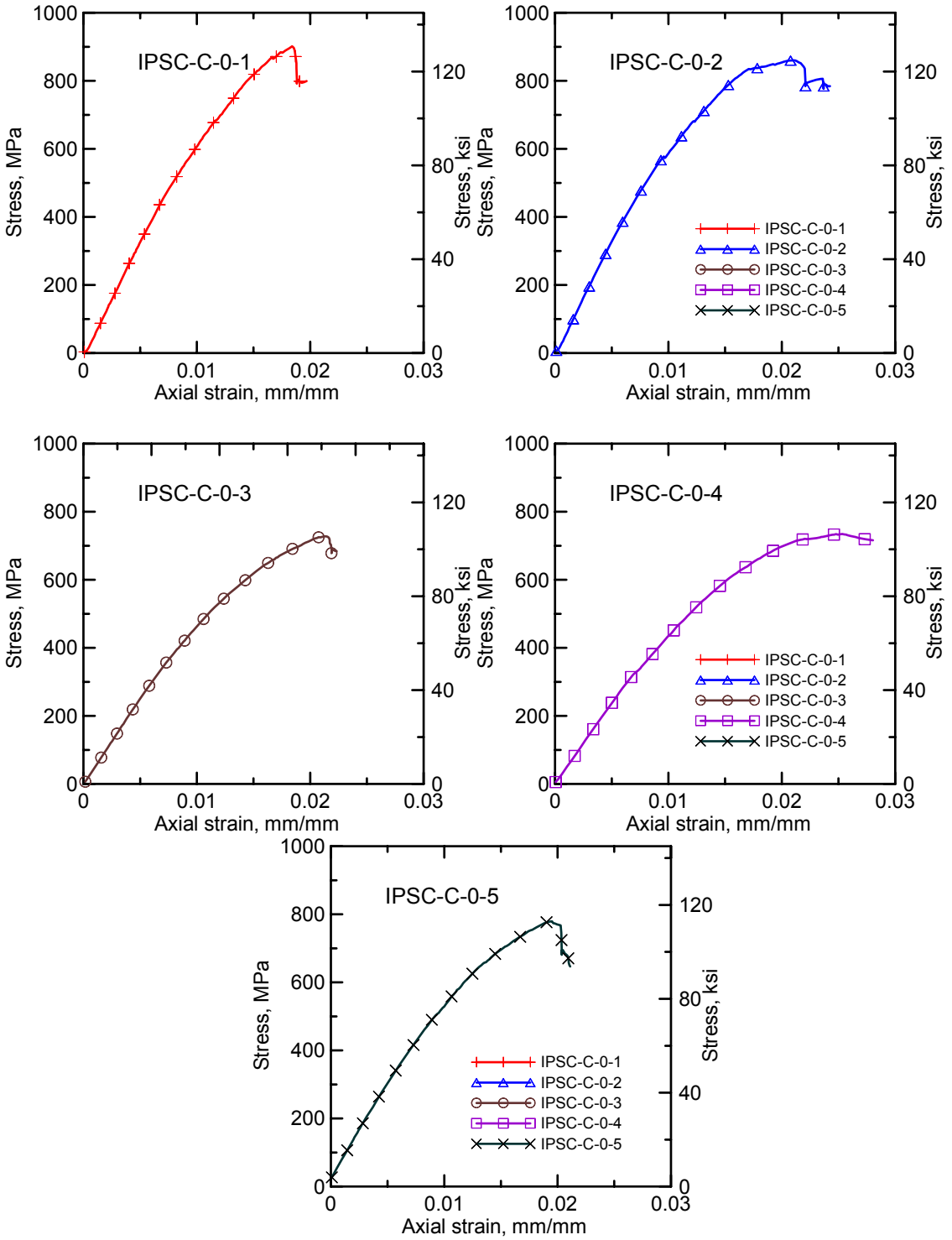

Figure A.3. CFRP configuration C tension tests

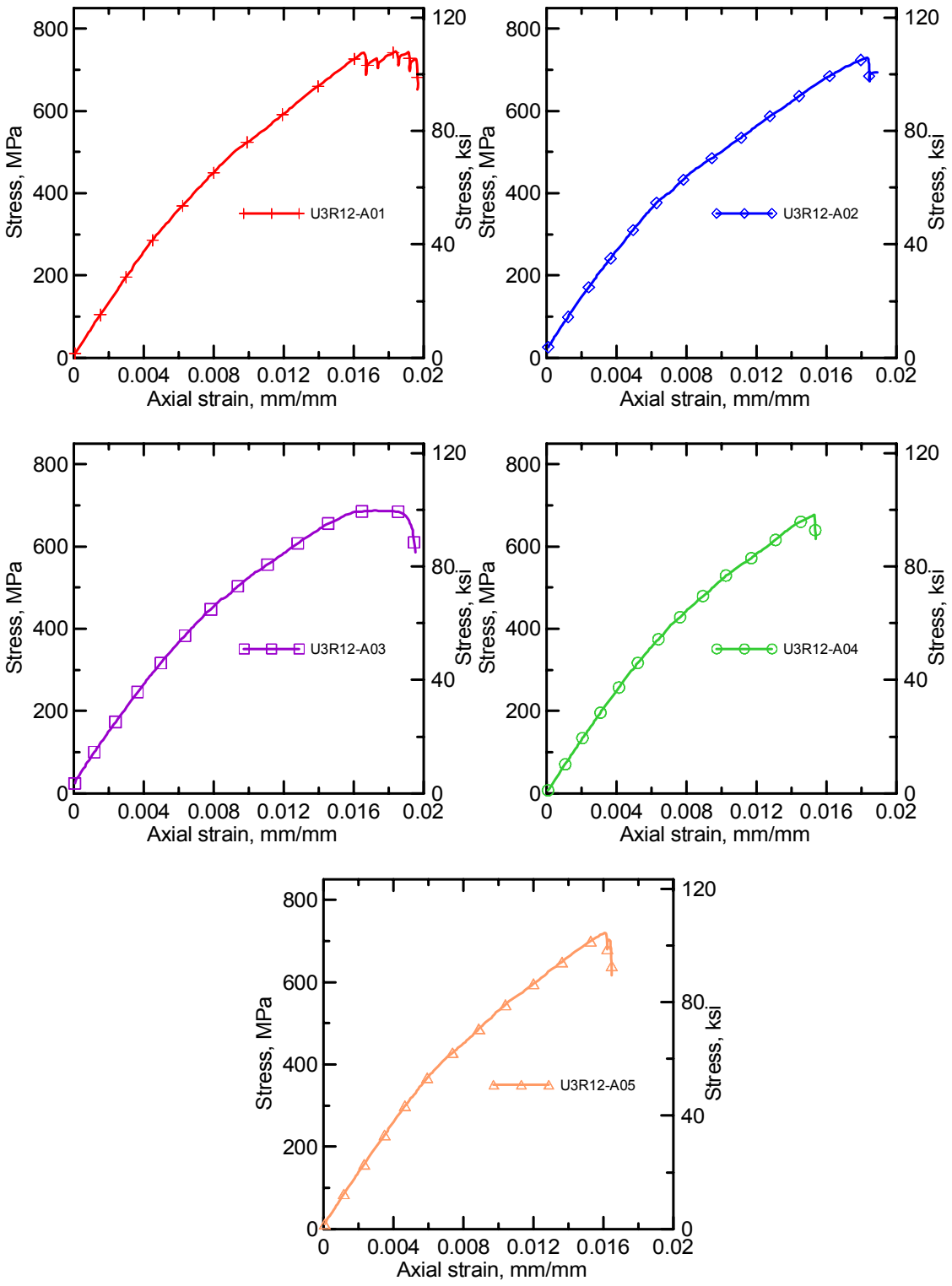

Figure A.4. CFRP configuration A tension tests

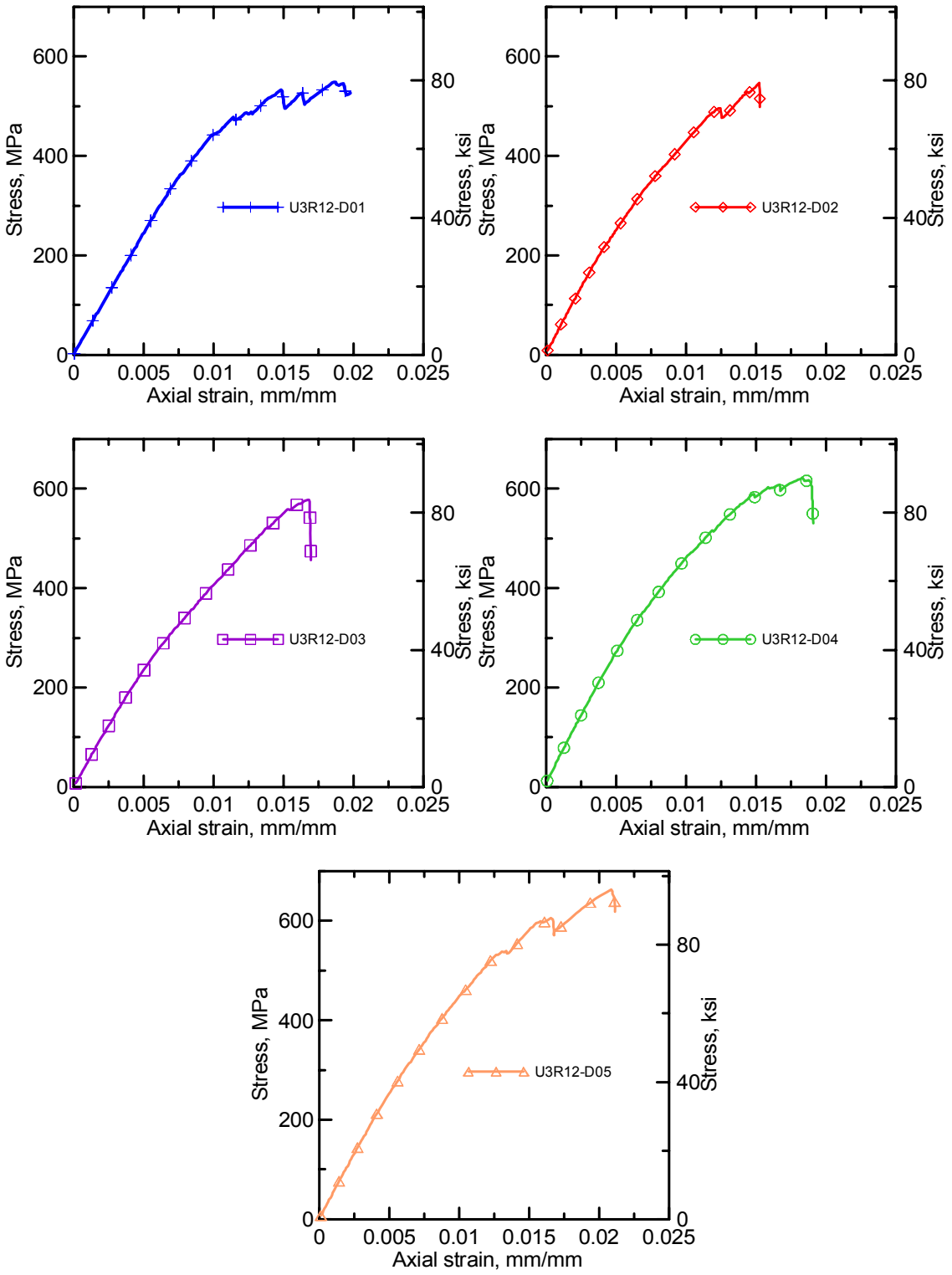

Figure A.5. CFRP configuration D tension tests

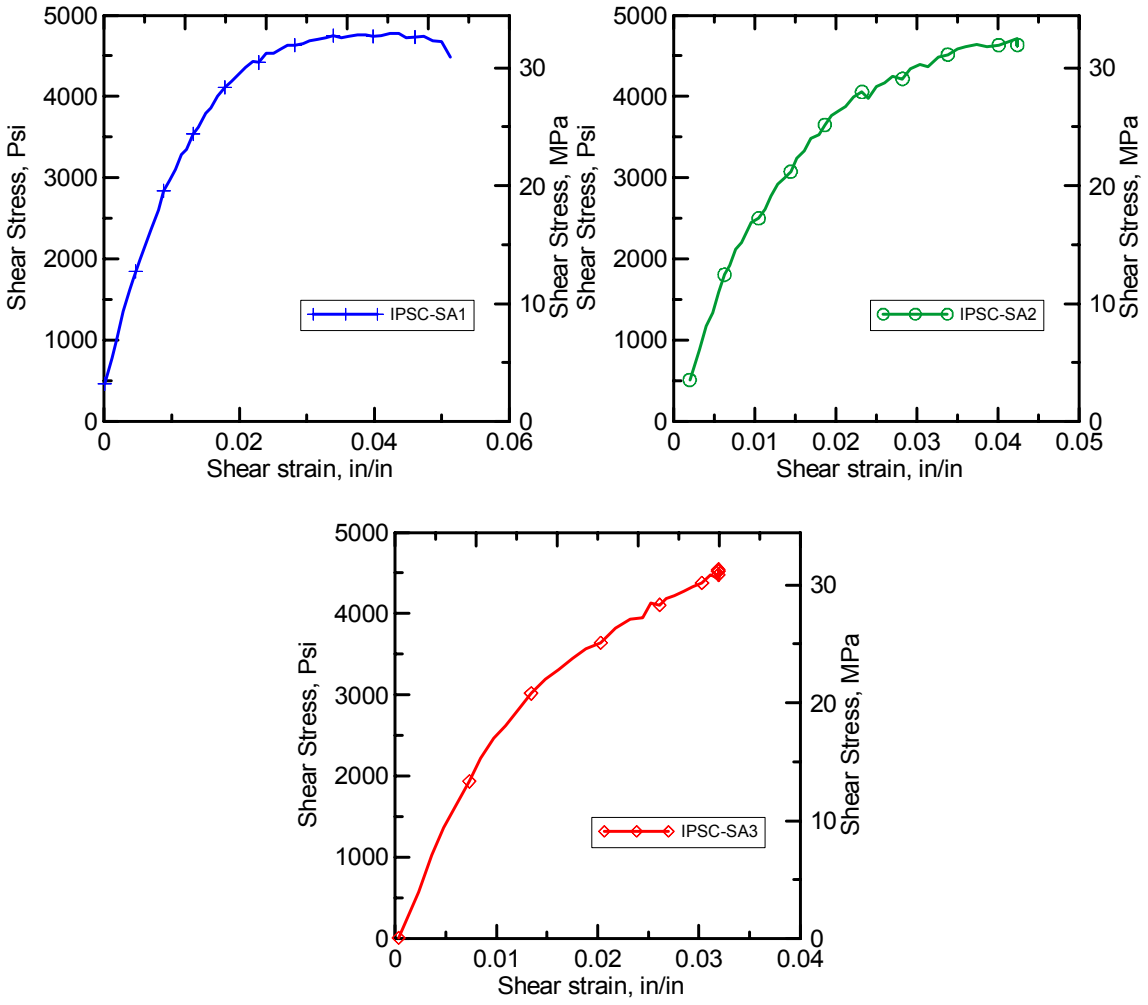

Figure A.6. CFRP configuration A shear tests

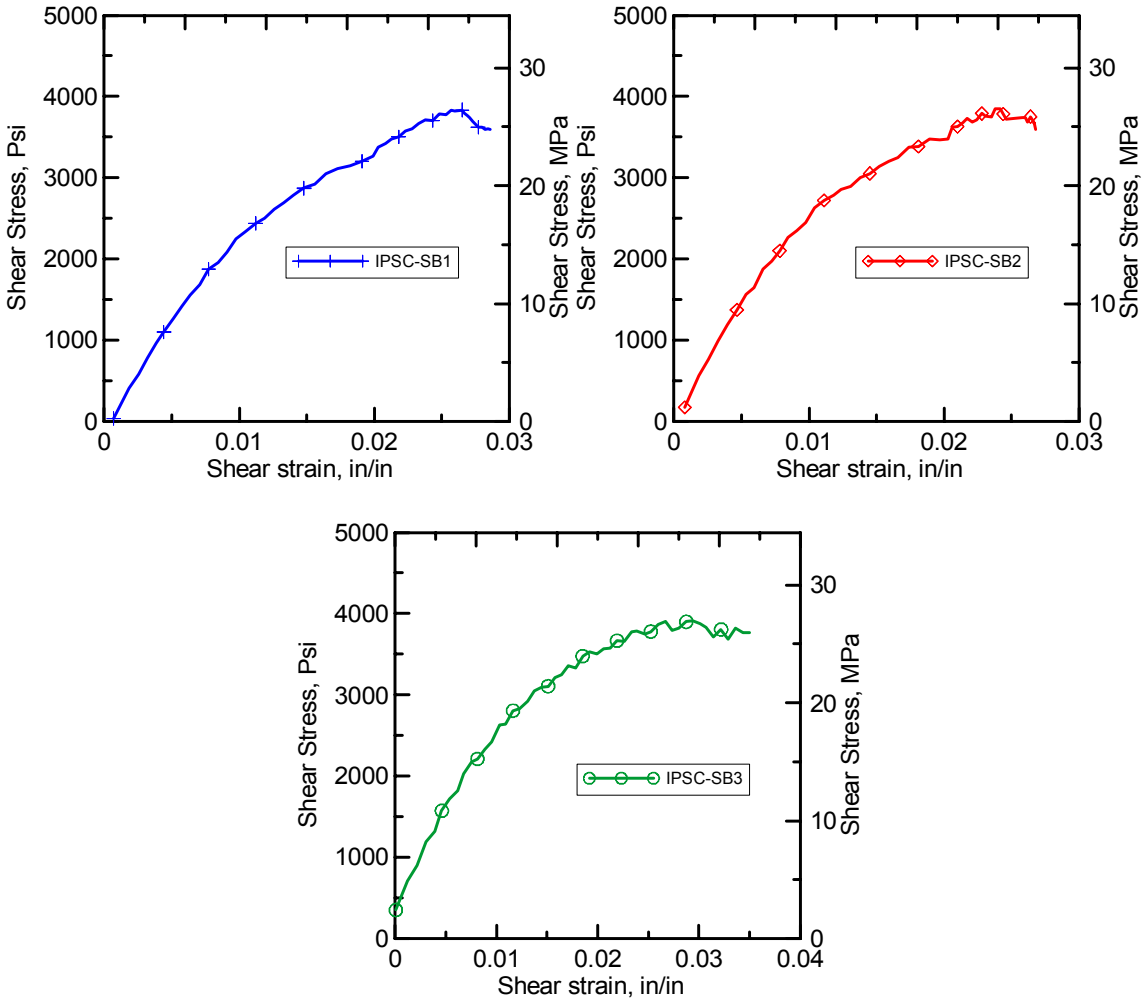

Figure A.7. CFRP configuration B shear tests

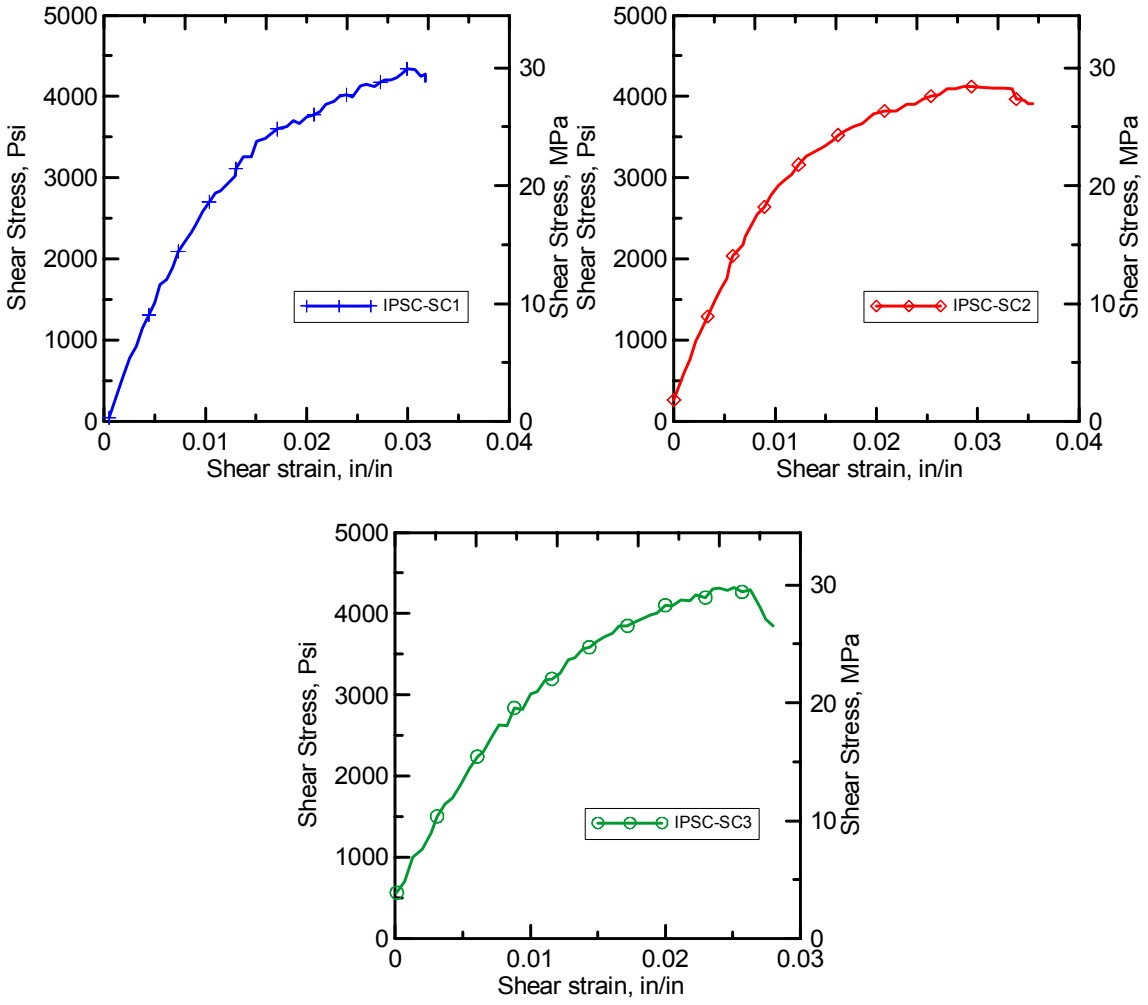

Figure A.8. CFRP configuration C shear tests

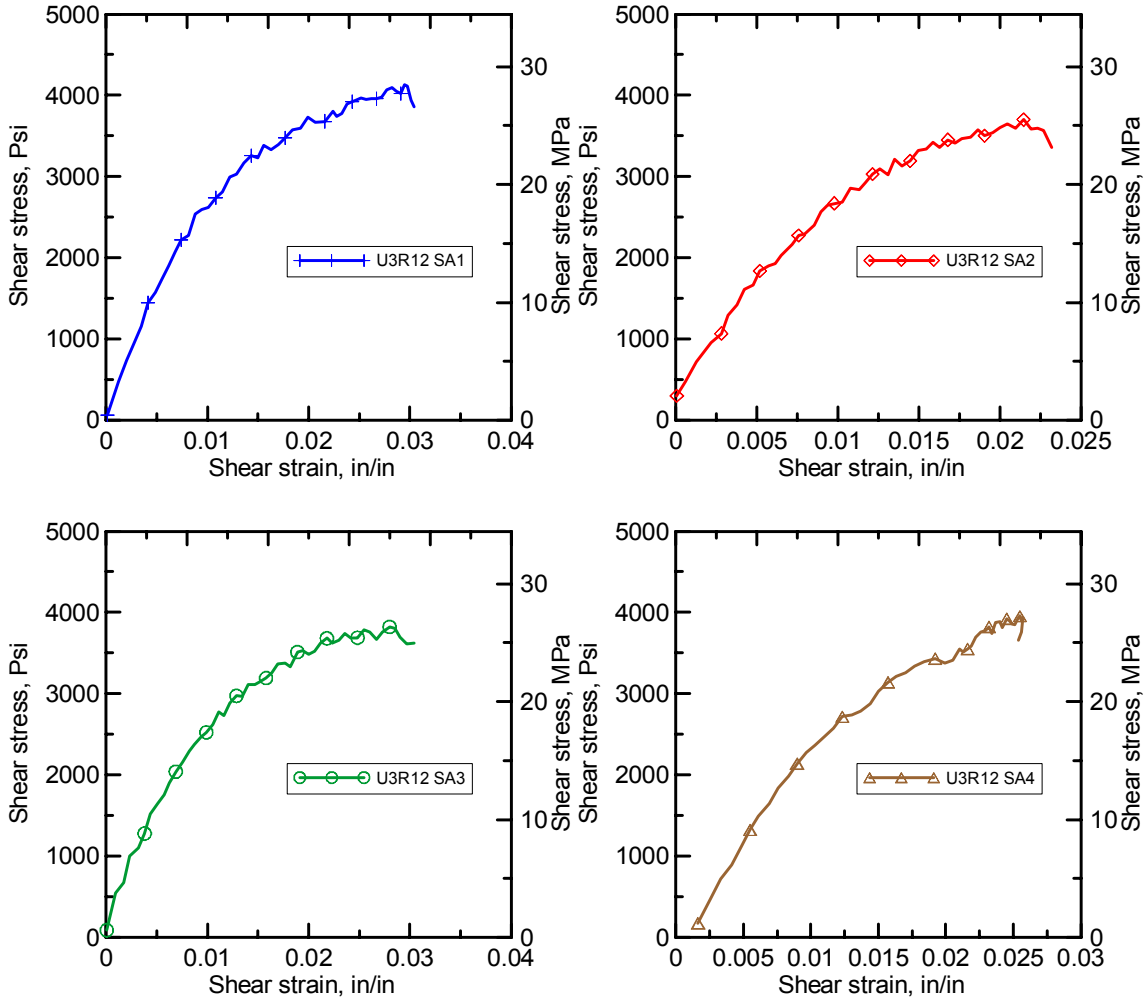

Figure A.9. CFRP configuration A shear tests

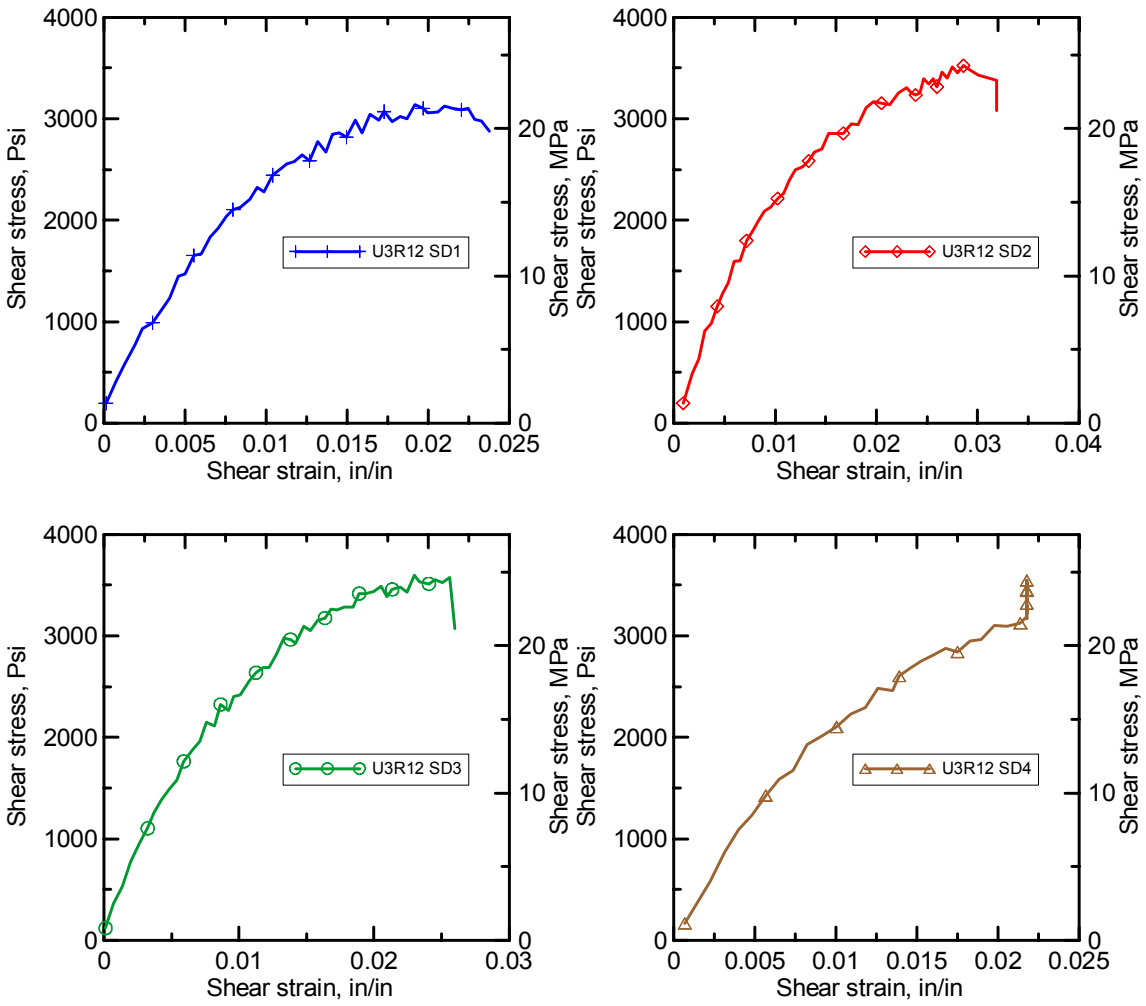

Figure A.10. CFRP configuration D shear tests

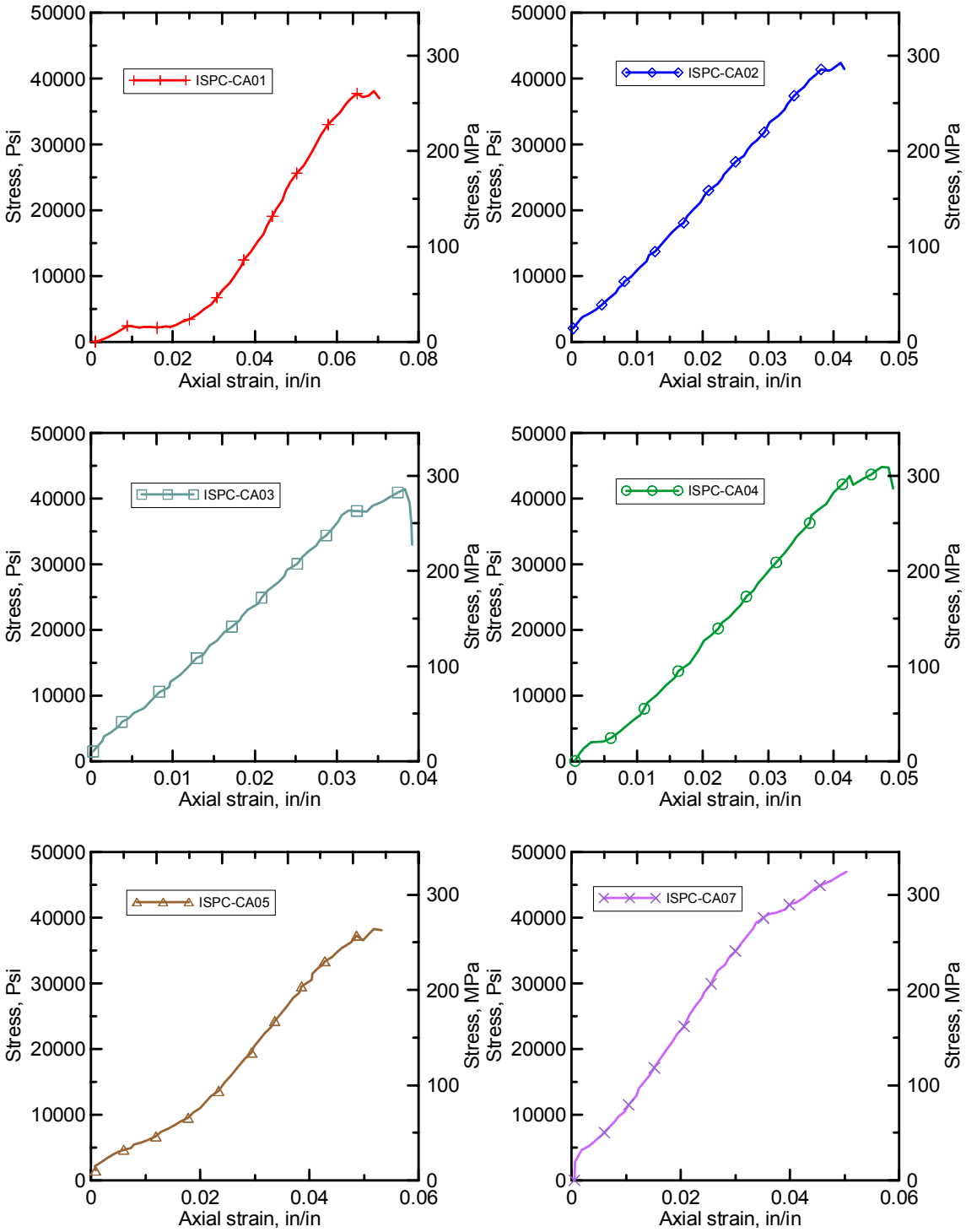

Figure A.11. CFRP configuration A compression tests

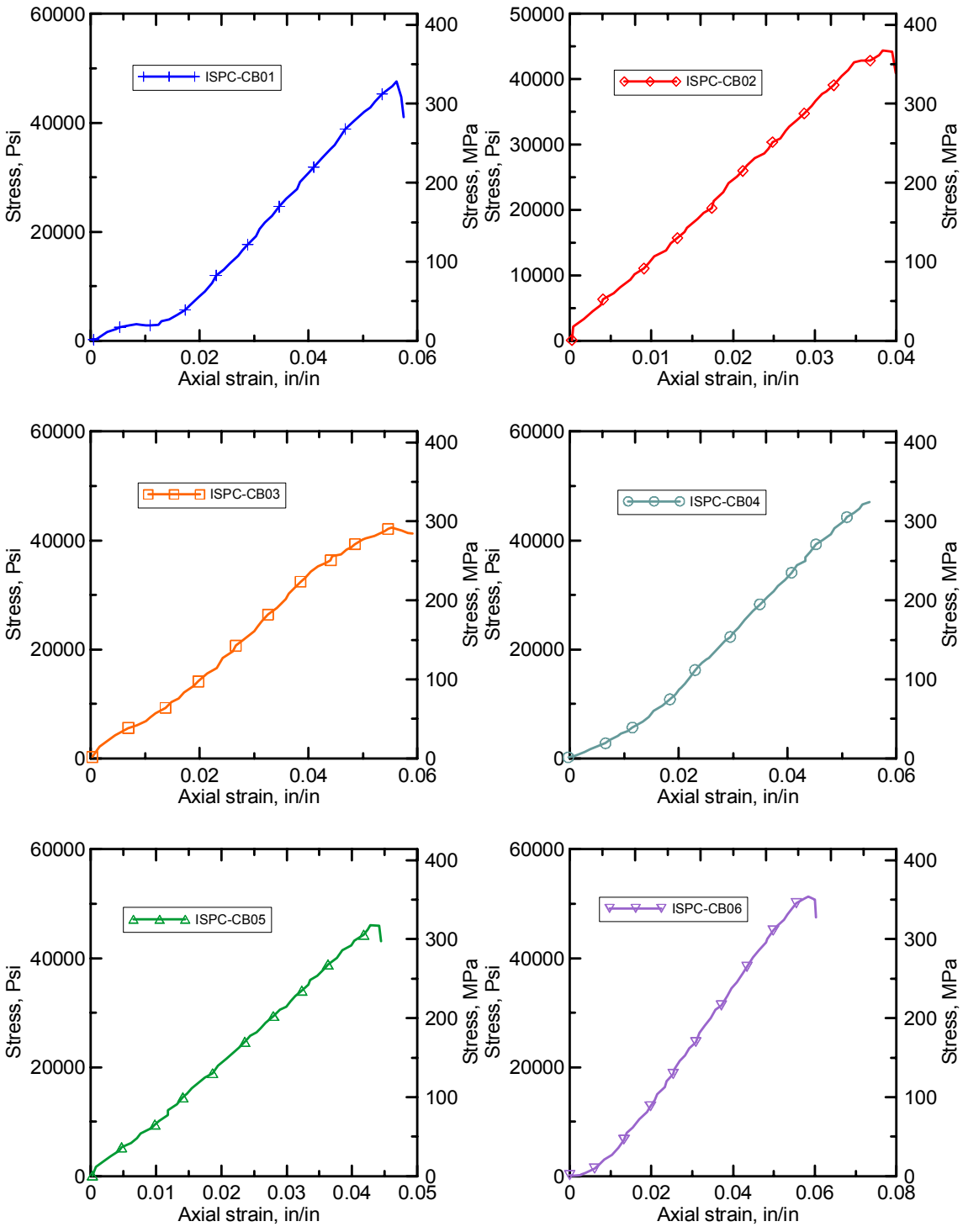

Figure A.12. CFRP configuration B compression tests

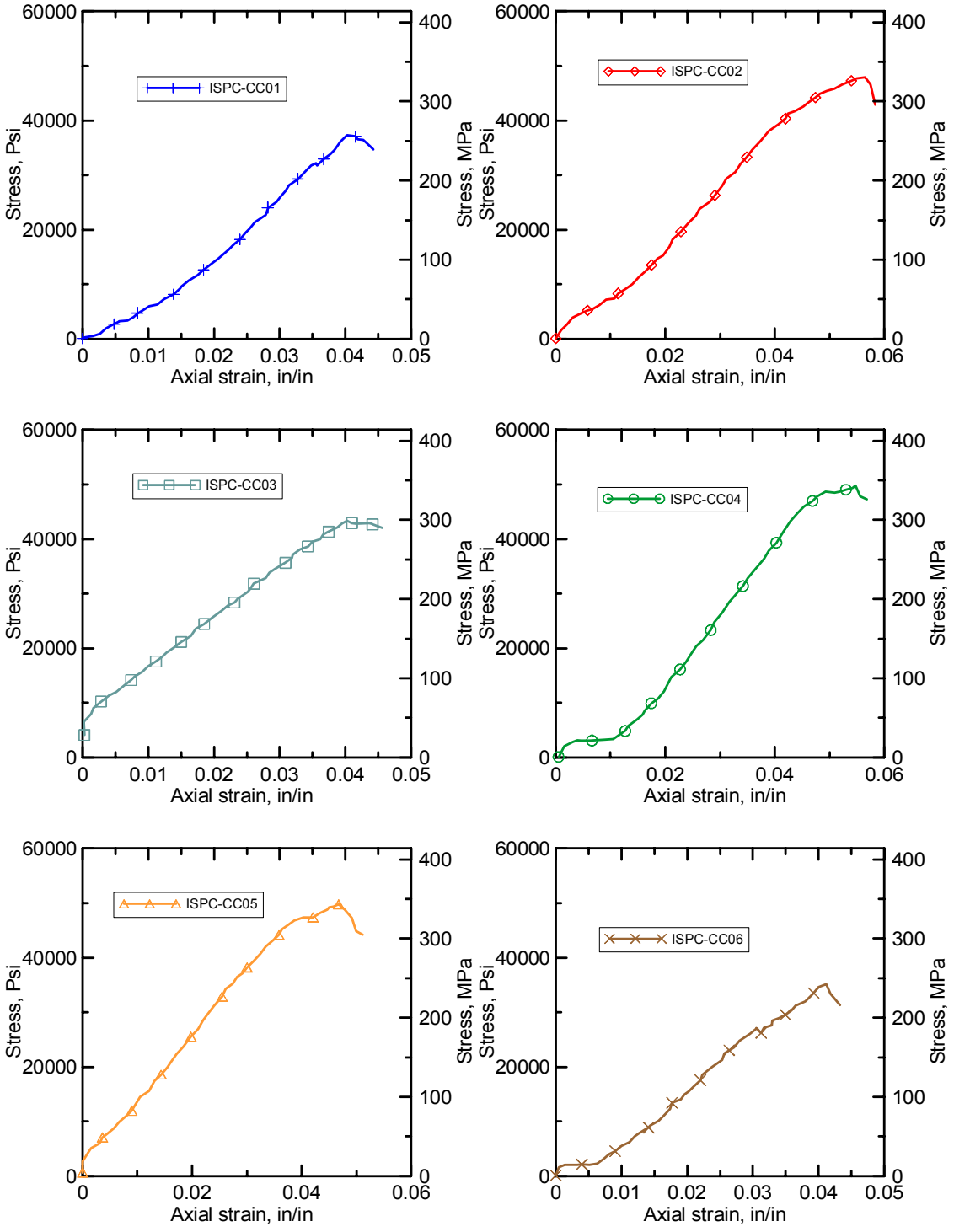

Figure A.13. CFRP configuration C compression tests

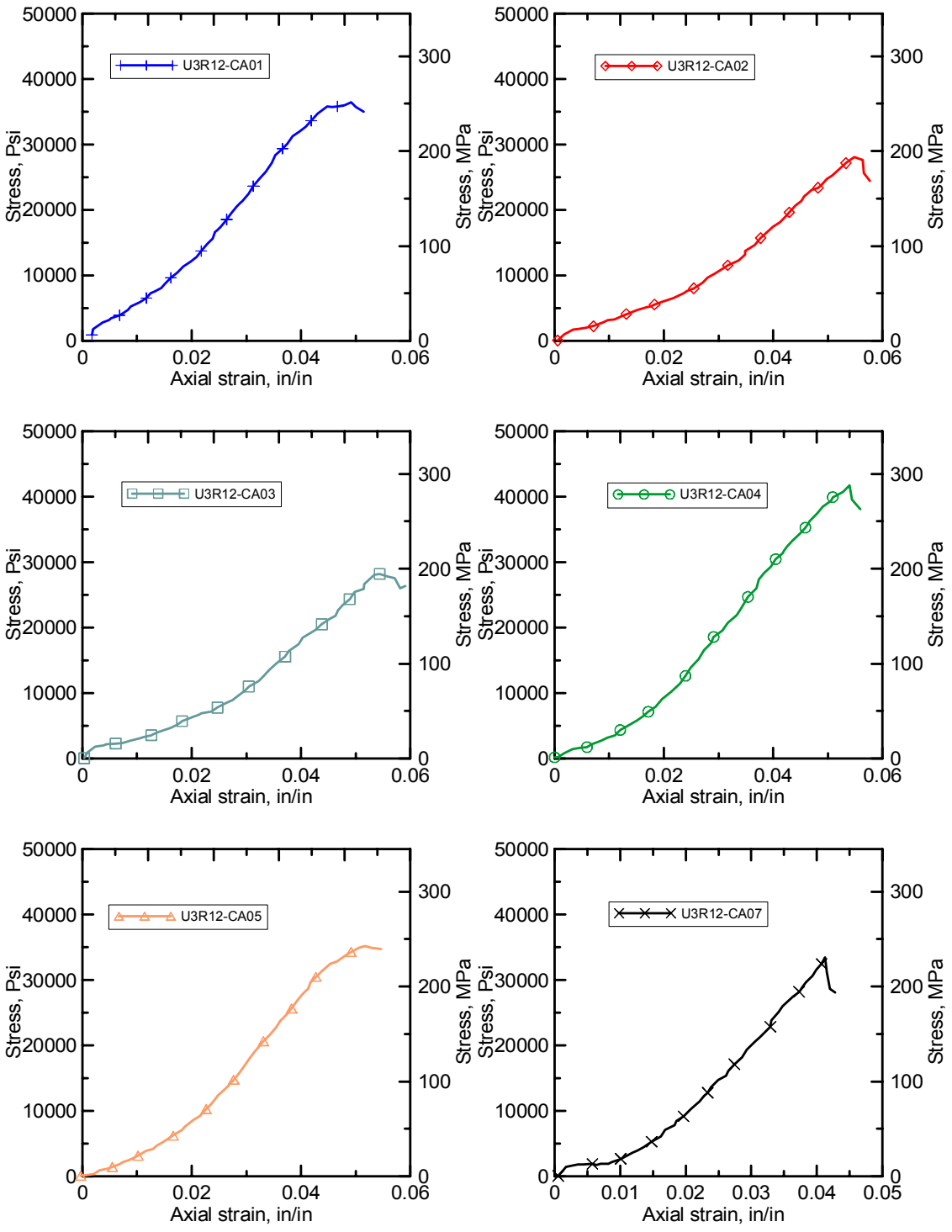

Figure A.14. CFRP configuration A compression tests

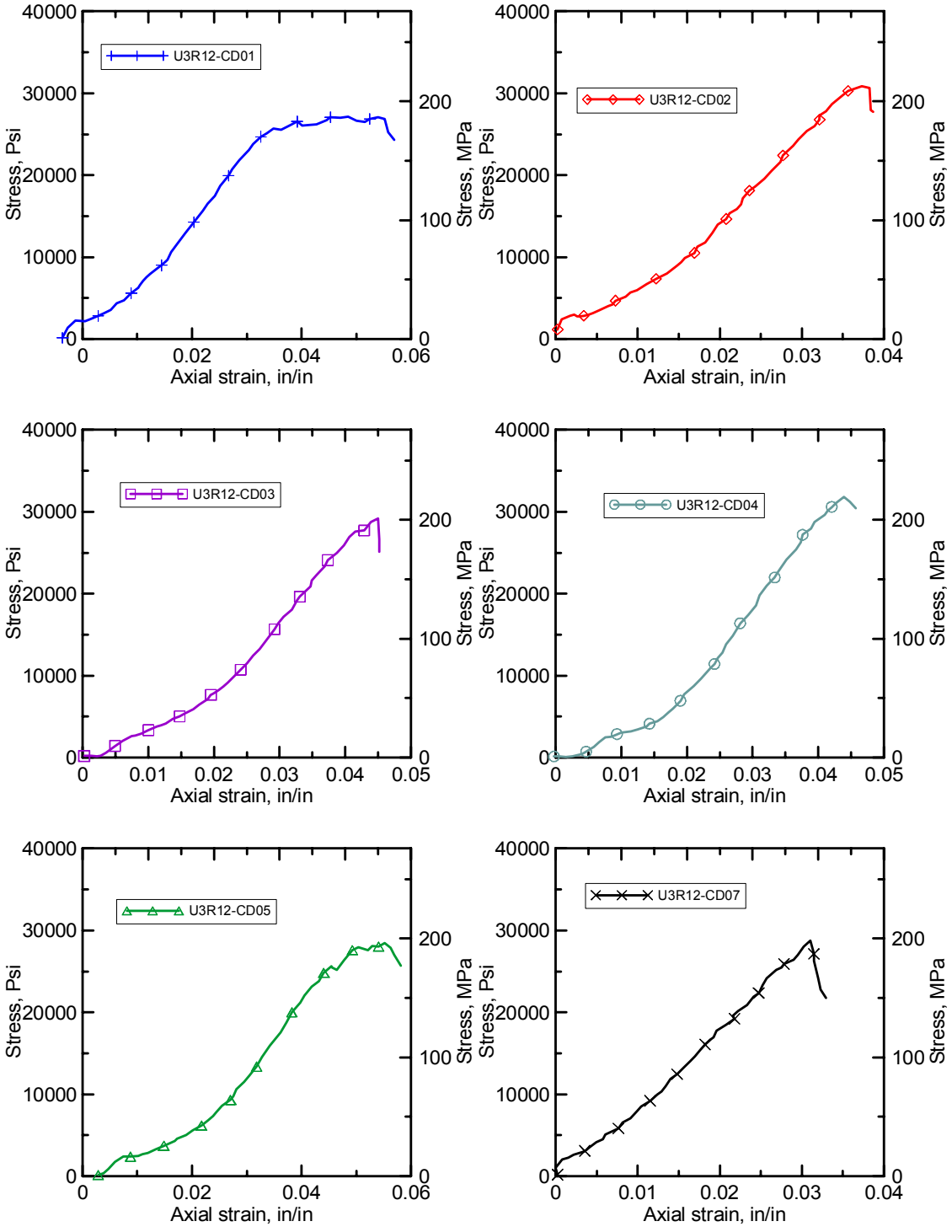

Figure A.15. CFRP configuration D compression tests